RL-TR-92-341
In-House Report
December 1992

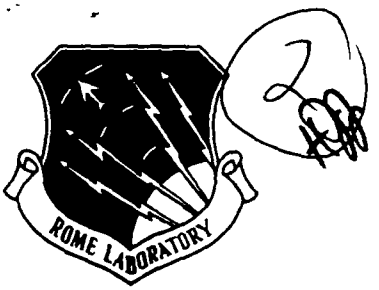

ADAPTIVE BEAMFORMING WITH IMPERFECT ARRAYS: PATTERN EFFECTS AND THEIR PARTIAL CORRECTION

Lars Emil Pettersson

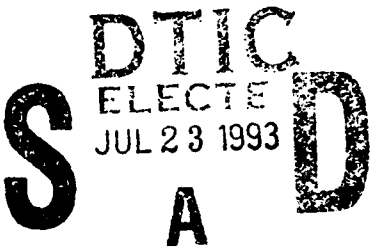

APPROVED FOR PUBLIC RELEASE; DISTRIBUTION UNLIMITED.

Rome Laboratory
Air Force Materiel Command
Griffiss Air Force Base, New York

This report has been reviewed by the Rome Laboratory Public Affairs Office (PA) and is releasable to the National Technical Information Service (NTIS). At NTIS it will be releasable to the general public, including foreign nations.

RL-TR-92-341 has been reviewed and is approved for publication.

APPROVED:

DANIEL J. JACAVANCO
Acting Chief
Antennas and Components Division
Electromagnetics and Reliability Directorate

APPROVED:

JOHN K. SCHINDLER
Director
Electromagnetics and Reliability Directorate

If your address has changed or if you wish to be removed from the Rome Laboratory mailing list, or if the addressee is no longer employed by your organization, please notify RL(ERAA) Hanscom AFB MA 01731-5000. This will assist us in maintaining a current mailing list.

Do not return copies of this report unless contractual obligations or notices on a specific document require that it be returned.

REPORT DOCUMENTATION PAGE

Form Approved
OMB No. 0704-0188

1. AGENCY USE ONLY (Leave blank)	2. REPORT DATE	3. REPORT TYPE AND DATES COVERED
	December 1992	In-House September 91-May 92

4. TITLE AND SUBTITLE
Adaptive Beamforming with Imperfect Arrays: Pattern Effects and Their Partial Correction

5. FUNDING NUMBERS
PR: 4600
TU: 14
WU: 01
PE: 62702F

6. AUTHOR(S)
Lars Pettersson

7. PERFORMING ORGANIZATION NAME(S) AND ADDRESS(ES)
Rome Laboratory (ERAA)
Hanscom AFB, MA 01731-5000

8. PERFORMING ORGANIZATION REPORT NUMBER
RL-TR-92-341

9. SPONSORING/MONITORING AGENCY NAME(S) AND ADDRESS(ES)
National Defence Research Establishment
Department of Information Technology
P.O. Box 1165
S-58111 Linkoping, Sweden

10. SPONSORING/MONITORING AGENCY REPORT NUMBER

11. SUPPLEMENTARY NOTES
Rome Laboratory Point of Contact: Hans Steyskal/ERAA/2052

12a. DISTRIBUTION/AVAILABILITY STATEMENT
Approved for public release;
Distribution Unlimited

12b. DISTRIBUTION CODE

13. ABSTRACT (Maximum 200 words)
The effects of various types of imperfections on the radiation pattern of adaptive antenna arrays, using the Applebaum and Frost algorithms, are investigated. The imperfections considered are nonuniform noise figures in the channels, gain and phase shift error, IQ imbalance, DC offset, finite number of samples when forming the covariance matrix, quantization of the signals and the weights and saturation of the signals. In particular the effects on the resulting sidelobe level, null depth, and gain are studied, and simulated results and analytical expressions for the expected pattern parameters are given. The effects of some methods to partly correct for the imperfections are also investigated. A method to obtain low sidelobe pattern when using the Frost algorithm is also discussed.

14. SUBJECT TERMS	15. NUMBER OF PAGES
Adaptive arrays, Digital beamforming, Error effects, Sampling effects, Error corrections	106
	16. PRICE CODE

17. SECURITY CLASSIFICATION OF REPORT	18. SECURITY CLASSIFICATION OF THIS PAGE	19. SECURITY CLASSIFICATION OF ABSTRACT	20. LIMITATION OF ABSTRACT
Unclassified	Unclassified	Unclassified	UL

Contents

1. INTRODUCTION 1

2. SOME BASIC RELATIONS 6

   2.1 Desired Signal Absent in the Covariance Matrix 7
   2.2 Desired Signal Present in the Covariance Matrix 10
   2.3 Eigenvalue Decomposition of the Covariance Matrix 13
   2.4 Methods of Correction 15

3. NONUNIFORM NOISE FIGURES 16

4. FROST'S ALGORITHM WITH TAPERED QUIESCENT WEIGHTS 21

5. GAIN AND PHASE SHIFT ERRORS 27

   5.1 Random Error Effects in the Applebaum Algorithm 27
   5.2 Random Error Effects in the Frost Algorithm 28
   5.3 Improvement of the Frost Algorithm 32
   5.4 Null Depth for the Frost Algorithm 34
   5.5 Effects of Pointing Error 38

6. ERRORS IN QUADRATURE SIGNAL GENERATION 38

   6.1 Error Effects on the Quiescent Patterns 40
   6.2 Pattern Effects for Nonzero Video Frequency 41
   6.3 Pattern Effects with Zero Video Frequency 45
   6.4 Pattern Effects for Identical Channels 48

7. DC OFFSET ERRORS 48

8. SAMPLED COVARIANCE MATRIX 52

8.1 SNIR as a Function of the Number of Samples 52
8.2 No Signal Incident on the Array 53
8.3 The Applebaum Case with One Jammer 60
8.4 The Frost Case with Desired Signal but No Jammer 63
8.5 The Frost Case with Desired Signal and Jammer 67
8.6 Effects of Steering Vector Projection 69
8.7 Pattern Parameters Versus the Number of Samples 70

9. SIGNAL QUANTIZATION 79

10. WEIGHT QUANTIZATION 80

11. SATURATION 83

12. CONCLUSIONS 87

REFERENCES 91

APPENDIX: ERROR INDUCED GAIN LOSS AND SIDELOBES 93

Illustrations

1. Adapted ——— , and Quiescent - - - -, Patterns for Configuration A. 4
2. Adapted ——— , and Quiescent - - - -, Patterns for Configuration B. 5
3. Simulated Patterns for Configuration B Using Applebaum's Algorithm. 18
4. Simulated Patterns for Configuration B Improved by Adding Artificial Noise and by Setting the Noise Eigenvalues to σ^2. 19
5. Simulated Pattern for Configuration A with Correction by Projecting the Steering Vector onto the Signal Subspace, and the Results for Uniform Noise Figures. 20
6. Adapted Patterns Using Frost's Algorithm, Configuration B. 22
7. Radiation Patterns for Configuration B. 26
8. Configuration A, Applebaum's Algorithm with 0.3 dB and 2° RMS Errors. 29
9. Configuration B. Same parameters as in Figure 8. 30
10. Configuration A, Frost's Algorithm. Same parameters as in Figure 8. 32
11. Configuration A, Frost's Algorithm with 0.3 dB and 2° RMS Errors. 35
12. Patterns for Configuration B, Using Frost's Algorithm. 36
13. Patterns for Configuration A, Using Frost's Algorithm. 39
14. Quiescent Patterns for Configuration B. 42
15. Adapted Patterns for Configuration B, Using Applebaum's Algorithm. 43
16. Adapted Patterns for Configuration A, $\omega \neq 0$, True and Image Frequencies. 44

17. Adapted Patterns for Configuration B, Applebaum's Algorithm. 46
18. Adapted Patterns for Configuration B, Frost's Algorithm. 47
19. Adapted Patterns for Configuration A, Applebaum's Algorithm. 49
20. Configuration B with DC-offset Errors, Using Applebaum's Algorithm. 51
21. Two, Normally Distributed, Simulated Sequences. 55
22. Adapted Patterns for Configuration B, Using Applebaum's Algorithm. 58
23. Configuration B, Applebaum's Algorithm. 59
24. Patterns for Configuration B, Using Applebaum's Algorithm. 61
25. Patterns for Configuration B, Using Applebaum's Algorithm. 64
26. Patterns for Configuration B, Using Frost's Algorithm. 67
27. Patterns for Configuration A, Using Frost's Algorithm, K=32. 71
28. Configuration B, K=32. 72
29. Configuration B. K=32. 73
30. Simulated and Calculated Aperture Efficiency for Configuration B as Functions of the Number of Samples. 74
31. Simulated and Calculated Sidelobe Level for Configuration B as Functions of the Number of Samples. 75
32. Simulated and Calculated Null Depth for Configuration B as Functions of the Number of Samples. 76
33. Simulated and Calculated SNIR for Configuration B as Functions of the Number of Samples. 77
34. Simulated Patterns for Configuration A, K=1024. 81
35. Effects of Weight Quantization on the Patterns. 82
36. Saturated Patterns, Configuration A, Applebaum's Algorithm, K = 4096 samples: ——— JNR = 70 dB, - - - JNR = 58 dB, ·-·-·- JNR = 55 dB. 85

List of Variables and Notations

$\mathbf{D}$	Diagonal matrix with the inverse of the quiescent weights
$\mathbf{e}$	Eigenvector of covariance matrix
G	Gain of the array
JNR	Jammer to noise ratio per channel
K	Number of time samples
N	Number of array elements
p_d, p_j	Incident desired signal and jammer power per channel
P_d, P_j	Total desired signal and jammer power ($P=N \cdot p$)
$\mathbf{s}_d$	Steering vector
$\mathbf{s}_d^p$	Projected steering vector
SNIR	Total signal to noise plus interference ratio
SNR	Signal to noise ratio per channel
$\mathbf{w}$,$\mathbf{w}_A$,$\mathbf{w}_F$,$\mathbf{w}_q$	Weight vectors: general, Applebaum, Frost and quiescent
$\mathbf{w}_D$	Vector with the elements of the diagonal matrix $\mathbf{D}^{-1}$
$\mathbf{x}$, $\mathbf{x}_d$, $\mathbf{x}_j$	Signal vector, desired signal vector, jammer vector
Δ	Error parameter
η_A	Aperture efficiency in main beam direction
$\eta(\theta)$	Aperture efficiency in direction θ
$\eta_0(\theta)$	Error free aperture efficiency
$\eta_q(\theta)$	Quiescent aperture efficiency
θ_d, θ_j	Angle of incidence of desired signal and jammer
λ	Eigenvalue of covariance matrix

σ^2	Thermal noise power, or noise variance, per channel
σ^2_{an}	Artificial noise power
σ_v	RMS noise voltage
$\Phi,\Phi_A,\Phi_F,\Phi_n$	Covariance matrix: general, Applebaum, Frost and noise
Φ_{an}	Artificially modified covariance matrix
$\tilde{\Phi}$	Sampled covariance matrix
$\hat{\cdot}$	Unit vector
$<\cdot>$	Mean value
$\cdot^T, \cdot^*, \cdot^+$	Transpose, complex conjugate and conjugate-transpose

Preface

This work was performed at Rome Laboratory during leave of absence from the National Defence Research Establishment (FOA) in Sweden which also provided financial support.

Adaptive Beamforming with Imperfect Arrays: Pattern Effects and Their Partial Correction

1. INTRODUCTION

This report considers adaptive beamforming[1,2,3] with arrays where some of the usual idealization assumptions are not valid. Specifically the digital, open loop, implementations (usually called sampled matrix inversion, SMI, or direct matrix inversion, DMI) of Applebaum's[4] "Maximum Signal to Noise plus Interference, SNIR, ratio" criterion and Frost's[5] "Constrained power minimization" criterion are

---

Received for publication 15 January 1993

[1] Compton, R.T., (1988), *Adaptive Antennas*, Prentice Hall.

[2] Hudson, J.E., (1981), *Adaptive Array Principles*, Peter Peregrinus.

[3] Monzingo, R. and Miller, T., (1980), *Introduction to Adaptive Arrays*, John Wiley & Sons.

[4] Applebaum, S.P., (1976), Adaptive arrays, *IEEE Trans. Antennas and Propagat.*, Sept., pp. 585-598.

[5] Frost, O.L., (1972), An algorithm for the linearly constrained adaptive processing, *Proc. IEEE*, Aug., pp. 926-935.

considered. The received signals in the channels are sampled, a covariance matrix is formed and inverted, or transformed by a similar operation, and multiplied with a steering vector giving an optimal channel weight vector.

Usually only the resulting SNIR is considered as a quality measure of the adaptation. However, especially in radar, it is also important to have a good pattern shape with low sidelobes and a narrow main beam to suppress reflected clutter and give good direction estimation.

In the following sections different types of errors in the antenna, which will affect the adaptive processes, are discussed and simulated results are shown. A narrowband antenna system is assumed. Methods for compensating for some of the errors are also discussed. The type of imperfections considered are inequality between the analog receiver modules (gain, phase shift, noise figure), errors in the conversion from the analog IF signal to complex baseband signal (IQ imbalance, DC-offset), errors in the conversion from analog to digital signals (signal quantization, DC-offset), errors when estimating the covariance matrix (sampling effects), and errors in dealing with the resulting weight vector (weight quantization). Also, the effect of saturation of the signal and the corresponding generation of intermodulation products and harmonics are considered.

A modification of Frost's algorithm for tapered quiescent weights is also discussed. This is not a correction of an error but the modification used is similar to the correction of some of the errors considered.

In the simulations in the following sections two basic configurations have been used with small variations in some cases. These basic configurations are:

A) Linear array with half wavelength spacing and $N = 16$ elements.
Desired signal at broadside, $\theta_d = 0^\circ$.
Uniform quiescent weights ($\sin x/x$ - type quiescent pattern).
Desired signal to noise ratio per channel, SNR = $p_d/\sigma^2 = 10$ dB.
One jammer close to the second sidelobe peak, $\theta_j = 18^\circ$.
Jammer to noise ratio per channel JNR = $p_j/\sigma^2 = 40$ dB.

B) Equal to configuration A) except for:
Quiescent weights tapered for 40 dB Chebyshev pattern, giving an aperture efficiency of, $\eta_A = 0.76$.

Jammer close to Chebyshev pattern sidelobe peak, $\theta_j = 20^\circ$.

The optimal gain, SNIR and null depth without any errors are:

A) Gain = 11.96 dB SNIR = 21.96 dB Null depth = -121.4 dB
B) Gain = 10.87 dB SNIR = 20.87 dB Null depth = -144.1 dB

All patterns in this report show the normalized array factor. No element patterns are included in the plots nor in the weight calculations.

Figures 1 and 2 show the optimal adapted patterns and the corresponding quiescent patterns.

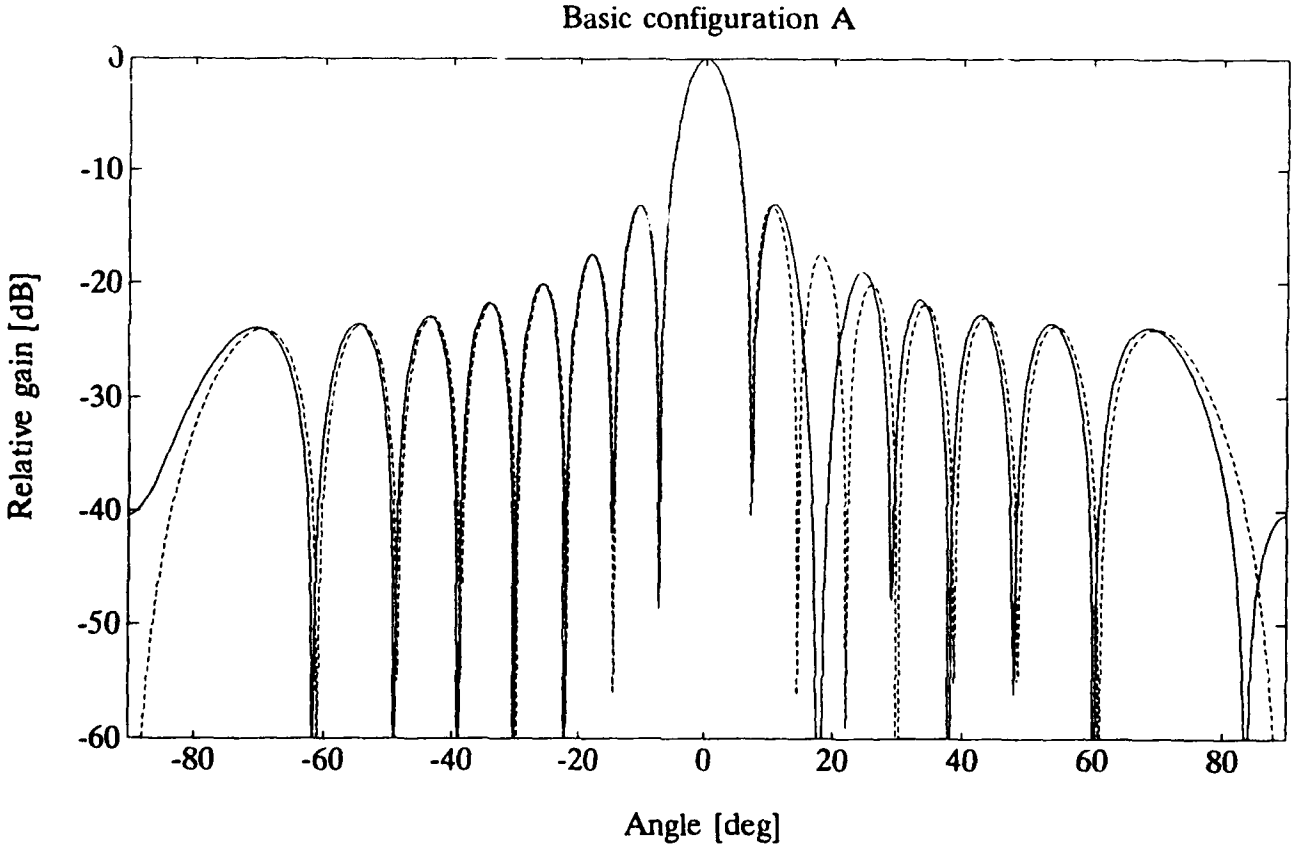

Figure 1. Adapted ——— , and Quiescent - - - -, Patterns for Configuration A.

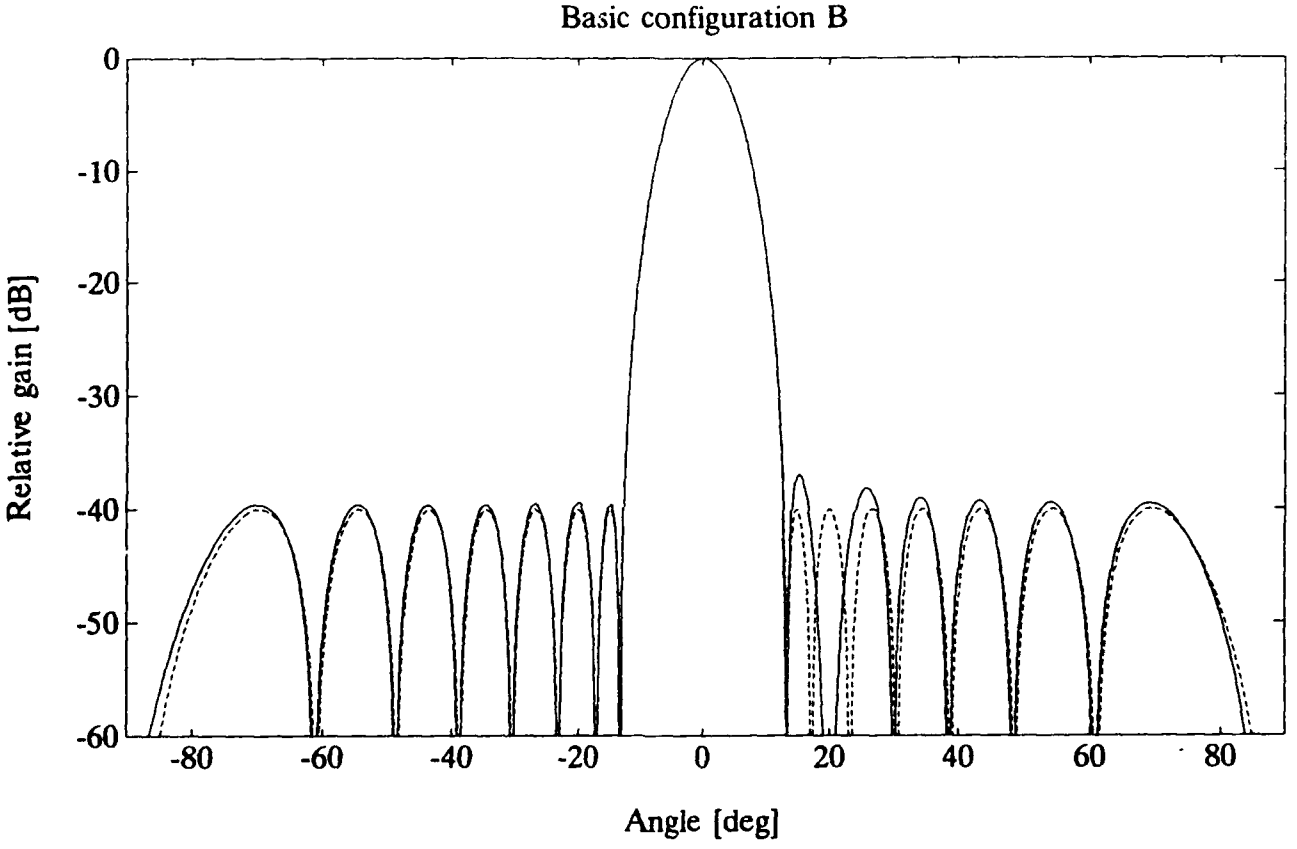

Figure 2. Adapted ——— , and Quiescent - - - -, Patterns for Configuration B.

2. SOME BASIC RELATIONS

In this section some equations to be used in the following sections are given.

Let $\mathbf{x}(t)$ be a vector of dimension N containing the total signals in the N channels of the antenna as a function of time. Also let $\mathbf{x}_n$, $\mathbf{x}_j$, and $\mathbf{x}_d$ be the separate signal vectors of thermal noise, jammers (interference), and the signal containing the desired information respectively, $\mathbf{x}(t) = \mathbf{x}_n + \mathbf{x}_j + \mathbf{x}_d$. The output signal of the array is: $s(t) = \mathbf{w}^T\mathbf{x}(t)$ where $\mathbf{w}$ is a vector containing the channel weight coefficients. (In this report, ^{T} indicates a transpose, * a complex conjugate, and $^+$ a conjugate transpose.) Applebaum[4] has shown that the maximum expected ratio of the desired signal to the interference plus noise, SNIR, in the output signal ($E\{\cdot\}$ represents the expectation value operator):

$$\max_{\mathbf{w}} E\left\{\frac{P_d}{P_j+P_n}\right\} = \max_{\mathbf{w}} E\left\{\frac{|\mathbf{w}^T\mathbf{x}'_d|^2}{|\mathbf{w}^T(\mathbf{x}_j+\mathbf{x}_n)|^2}\right\} \tag{2.1}$$

is obtained when the complex conjugate of the weight vector is given by:

$$\mathbf{w}^* \sim \Phi_A^{-1}\mathbf{s}_d \tag{2.2}$$

where $\mathbf{s}_d$ is the steering vector, which defines the desired signal $\mathbf{x}'_d$ as the part of $\mathbf{x}_d$ being parallel to $\mathbf{s}_d$, and where Φ_A is the covariance matrix of the interference plus noise:

$$\Phi_A = E\{(\mathbf{x}_j+\mathbf{x}_n)(\mathbf{x}_j+\mathbf{x}_n)^+\} \tag{2.3}$$

(Often the covariance matrix is defined as $\Phi = \Phi_A^*$.)
If the interference and noise are statistically independent:

$$\Phi_A = E\{\mathbf{x}_j\mathbf{x}_j^+\} + E\{\mathbf{x}_n\mathbf{x}_n^+\} \tag{2.4}$$

This Applebaum criterion can be used when the covariance matrix can be formed with the desired signal $\mathbf{x}_d$ either absent or very small, which is often true in

radar. Otherwise, Frost's criterion, in which (in its basic form) the total power is minimized subject to the constraint that the array sensitivity in the desired direction is constant, can be used.

$$\min_{w}\{|w^T x|\}:|w^T s_d|=\text{constant} \tag{2.5}$$

The solution for this is again:

$$w^* \sim \Phi_F^{-1} s_d \tag{2.6}$$

where Φ_F is now the total covariance matrix:

$$\Phi_F = E\{(x_d+x_j+x_n)(x_d+x_j+x_n)^*\} \tag{2.7}$$

In practice the expectation value of the covariance matrixes Φ_A and Φ_F is (assuming stationary signals) estimated by a time average so that, if $\mathbf{X}$ is the signal matrix of dimension $N \neq K$ with element (n,k) equal to the k^{th} sample in channel n, $\mathbf{X}=[x_1,x_2,...,x_K]$, we make the estimation:

$$\tilde{\Phi} = \frac{1}{K} XX^* \tag{2.8}$$

(The effect of this estimation for finite K is discussed in Section 8.)

Equations (2.2) and (2.6) may, as discussed below, be manipulated in different ways, useful for different purposes.

2.1 Desired Signal Absent in the Covariance Matrix

If, in this case, there are no jammers present, we get the quiescent Applebaum matrix and weights:

$$\Phi_{Aq} = \sigma^2 I \; ; \qquad w_q^* \sim s_d \tag{2.9}$$

where σ^2 is the noise power in each channel (assumed equal) and where $\mathbf{I}$ is the identity matrix. Thus s_d is identical to the complex conjugate of the quiescent

weights of the array, which are often chosen to give low sidelobes. This is desired in radar to keep clutter and other undesired off-mainbeam reflected signals low.

When there is only one narrowband jammer, uncorrelated with the noise, Eq. (2.4), the matrix inversion formula, [Reference 2, Appendix 1]:

$$(A+xx^{+})^{-1} = A^{-1} - \frac{A^{-1}xx^{+}A^{-1}}{1 + x^{+}A^{-1}x} \tag{2.10}$$

can be used to obtain:

$$\Phi_A^{-1} = \frac{1}{\sigma^2}\left[I - \frac{x_j x_j^{+}}{\sigma^2 + x_j^{+}x_j}\right] = \frac{1}{\sigma^2}\left[I - \frac{P_j \hat{x}_j \hat{x}_j^{+}}{\sigma^2 + P_j}\right] \tag{2.11}$$

where $\hat{}$ denotes a unit vector and P_j is the total jammer power $P_j = N \cdot p_j = x_j^{+} \cdot x_j$ where p_j is the jammer power per channel. The weights are then obtained from:

$$w_A^{*} = \Phi_A^{-1} s_d \sim \hat{s}_d - \hat{x}_j \frac{P_j}{\sigma^2 + P_j}(\hat{x}_j^{+}\hat{s}_d) \tag{2.12}$$

from which it is seen that the pattern is equal to the quiescent pattern minus a jammer cancellation beam with weights proportional to the jammer signals, constant amplitude and linear phase for a plane wave jammer.

The gain in the jammer direction relative to the gain in the signal direction becomes:

$$\text{Relative jammer gain} = \frac{|\hat{x}_j^{+} \cdot w^{*}|^2}{|\hat{x}_d^{+} \cdot w^{*}|^2}$$

$$= \frac{\eta_q(\theta_j)}{\eta_q(\theta_d)} \cdot \frac{1}{\left|1 + \frac{P_j}{\sigma^2}\left[1 - \frac{\hat{x}_d^{+}\hat{x}_j \hat{x}_j^{+}\hat{s}_d}{\hat{x}_d^{+}\hat{s}_d}\right]\right|^2} \tag{2.13}$$

where $\eta_q(\theta_j) = |\hat{\mathbf{x}}_j^+ \cdot \hat{\mathbf{s}}_d|^2$ and $\eta_q(\theta_d) = |\hat{\mathbf{x}}_d^+ \cdot \hat{\mathbf{s}}_d|^2$ are the quiescent pattern aperture efficiencies in the jammer and desired signal directions.

If $\hat{\mathbf{x}}_d = \hat{\mathbf{s}}_d$, $\eta_q(\theta_d) = 1$ and the last term in the denominator becomes:

$$\left. \frac{\hat{\mathbf{x}}_d^+ \hat{\mathbf{x}}_j \hat{\mathbf{x}}_j^+ \hat{\mathbf{s}}_d}{\hat{\mathbf{x}}_d^+ \hat{\mathbf{s}}_d} \right|_{\hat{\mathbf{x}}_d = \hat{\mathbf{s}}_d} = \eta_q(\theta_j) \tag{2.14}$$

If the jammer is in the sidelobe region this last term is small so that in the configurations in Section 1, where $P_j/\sigma^2 = 16 \times 10^4$, Eq. (2.13) gives a null depth of -104 dB relative to the quiescent value, $\eta_q(\theta_j)/\eta_q(\theta_d)$, in agreement with the simulations.

From Eq. (2.13) one can see the interesting fact that the received jammer power will decrease with increasing P_j due to an improved null depth. Since the signal gain, Eq. (2.15) below, will also decrease, the resulting SNIR will of course not increase.

The resulting gain in the desired signal direction, when there is one jammer present, becomes:

$$\text{Signal gain} = N \frac{|\hat{\mathbf{x}}_d^+ \cdot \mathbf{w}^*|^2}{|\mathbf{w}|^2}$$

$$= N\eta_q(\theta_d) \cdot \frac{\left| 1 + \frac{P_j}{\sigma^2} \left(1 - \frac{\hat{\mathbf{x}}_d^+ \hat{\mathbf{x}}_j \hat{\mathbf{x}}_j^+ \hat{\mathbf{s}}_d}{\hat{\mathbf{x}}_d^+ \hat{\mathbf{s}}_d} \right) \right|^2}{1 + \left[1 - \eta_q(\theta_j)\right] \frac{P_j}{\sigma^2} \left(\frac{P_j}{\sigma^2} + 2 \right)} \tag{2.15}$$

where, if $\hat{\mathbf{x}}_d = \hat{\mathbf{s}}_d$, Eq. (2.14) can be used to simplify the equation. For our basic configuration A this gives a gain decrease of 0.08 dB, in agreement with the simulations.

Sometimes the jammer vector $\mathbf{x}_j$ will have completely random components. In this case the algorithms will still try to nullify the jammer signal but the resulting

weight vector will get random components, $\mathbf{w}_A^* \sim \hat{\mathbf{s}}_d + \Delta\mathbf{w}_A^*$. The mean square error of the weights can be obtained from Eqs. (2.12) and (A.3). Eliminating the error term parallel to $\hat{\mathbf{s}}_d$, which will not give any sidelobe contribution (as later in Eq. (2.25)), gives the result:

$$\langle \Delta w_A^2 \rangle = \frac{1-1/N}{N}\left[\frac{P_j}{\sigma^2+P_j(1-1/N)}\right]^2 \approx \frac{1}{N}\left[\frac{P_j}{\sigma^2+P_j}\right]^2 \tag{2.16}$$

This will, for not too small N, give an average sidelobe level contribution from Eq. (A.6) of:

$$\text{Sidelobe level} = \frac{\langle \Delta w_A^2 \rangle}{N\ \eta_A} = \frac{\left[\frac{P_j}{\sigma^2+P_j}\right]^2}{N^2 \eta_A} \tag{2.17}$$

(*This assumes of course that there is no error in* $\hat{\mathbf{s}}_d$ itself that is correlated with Δw_A.) It can also be shown that, since $\langle \Delta w_A^2 \rangle$ is essentially proportional to the projection $|\hat{\mathbf{x}}_j^+ \hat{\mathbf{s}}_d|^2$, its standard deviation is, when $\mathbf{x}_j$ has normal distributed components, approximately equal to the expectation value itself.

2.2 Desired Signal Present in the Covariance Matrix

This is the Frost criterion, and with no jammer we get, using the inversion formula of Eq. (2.10):

$$\Phi_F^{-1} = \frac{1}{\sigma^2}\left[\mathbf{I} - \frac{\mathbf{x}_d \quad \mathbf{x}_d^+}{\sigma^2 + \mathbf{x}_d^+ \mathbf{x}_d}\right] = \frac{1}{\sigma^2}\left[\mathbf{I} - \frac{P_d \hat{\mathbf{x}}_d \hat{\mathbf{x}}_d^+}{\sigma^2 + P_d}\right] \tag{2.18}$$

$$\mathbf{w}_F^* = \Phi_F^{-1}\mathbf{s}_d \sim \hat{\mathbf{s}}_d - \hat{\mathbf{x}}_d \frac{P_d}{\sigma^2 + P_d}(\hat{\mathbf{x}}_d^+ \hat{\mathbf{s}}_d) \tag{2.19}$$

More generally, for uncorrelated narrowband signals:

$$\Phi_F = \Phi_A + x_d x_d^+ \tag{2.20}$$

and, using Eq. (2.10):

$$\Phi_F^{-1} = \Phi_A^{-1} - \frac{\Phi_A^{-1} x_d x_d^+ \Phi_A^{-1}}{1 + x_d^+ \Phi_A^{-1} x_d} \tag{2.21}$$

$$w_F^* \sim \Phi_A^{-1}[\hat{s}_d - \alpha \hat{x}_d] = w_A^* - \alpha \Phi_A^{-1} \hat{x}_d \tag{2.22}$$

where w_A^* is obtained using the normalized steering vector, $\hat{s}_d$, and where

$$\alpha = \frac{P_d \hat{x}_d^+ \Phi_A^{-1} \hat{s}_d}{1 + P_d \hat{x}_d^+ \Phi_A^{-1} \hat{x}_d} \tag{2.23}$$

is a scalar. Defining:

$$\alpha' = \frac{\alpha}{1 - \alpha(\hat{s}_d^+ \cdot \hat{x}_d)} = \frac{P_d \hat{x}_d^+ \Phi_A^{-1} \hat{s}_d}{1 + P_d \hat{x}_d^+ \Phi_A^{-1} \Delta \hat{x}_{d\perp}} \tag{2.24}$$

where $\Delta \hat{x}_{d\perp}$ is the part of the error vector $\hat{x}_d - \hat{s}_d$ that is perpendicular to $\hat{s}_d$, $\Delta \hat{x}_{d\perp} = \hat{x}_d - \hat{s}_d(\hat{s}_d^+ \cdot \hat{x}_d)$, we can also write:

$$w_F^* \sim \Phi_A^{-1}\left[\hat{s}_d - \alpha' \Delta \hat{x}_{d\perp}\right] = w_A^* - \alpha' \Phi_A^{-1} \Delta \hat{x}_{d\perp} \tag{2.25}$$

It is seen that $w_F \sim w_A$ if, and only if, x_d is parallel to s_d, ($\hat{x}_d = \hat{s}_d$). (The Frost case with $\hat{x}_d = \hat{s}_d$ is equivalent with the Applebaum case with $\hat{x}_j = \hat{x}_d = \hat{s}_d$ in which case Eq. (2.15) gives no signal gain decrease.)

Furthermore since α', Eq. (2.24), is often large, the Frost algorithm is in general much more sensitive to errors (when $\hat{x}_d \neq \hat{s}_d$) than Applebaum's algorithm. When P_d is very large the second term in the denominator of Eqs. (2.23) and (2.24) cannot be neglected and we get a completely error dominated pattern, independent of the signal power P_d.

Also when there are errors the quiescent Applebaum aperture efficiency, $\eta_q(\theta_d) = |\hat{\mathbf{x}}_d^+ \hat{\mathbf{s}}_d|^2$, will not be equal to one and the Frost gain in the signal direction, $\hat{\mathbf{x}}_d$, will then, according to Eq. (2.15) with $\hat{\mathbf{x}}_j = \hat{\mathbf{x}}_d \neq \hat{\mathbf{s}}_d$, decrease to:

$$\text{Signal gain} = N \frac{|\hat{\mathbf{x}}_d^+ \cdot \mathbf{w}^*|^2}{|\mathbf{w}|^2} = \frac{N \cdot \eta_q(\theta_d)}{1 + \Delta\eta_q \frac{P_d}{\sigma^2}\left[\frac{P_d}{\sigma^2} + 2\right]} \tag{2.26}$$

where $\Delta\eta_q = 1 - \eta_q(\theta_d)$.

As noted above, the Frost and Applebaum weights, and hence also the null depths, are identical when $\hat{\mathbf{x}}_d = \hat{\mathbf{s}}_d$. When this is not true, the jammer null depth, and also the null depths when there are more than one jammer, can be found by expressing the weight vector $\mathbf{w}$ in terms of the old weight vector $\mathbf{w}_0$. Thus if $\mathbf{w}_0$ is the weight vector, and Φ_0 the covariance matrix, for a specific jammer configuration, including the desired signal in the Frost case, the weights with one more jammer present can, using Eq. (2.10), be found from:

$$\mathbf{w}^* = \left[\mathbf{I} - \frac{P_j \Phi_0^{-1} \hat{\mathbf{x}}_j \hat{\mathbf{x}}_j^+}{1 + P_j \hat{\mathbf{x}}_j^+ \Phi_0^{-1} \hat{\mathbf{x}}_j}\right] \cdot \mathbf{w}_0^* \tag{2.27}$$

which again gives the old pattern plus a jammer cancellation beam.

For one jammer in the Frost case Φ_0 is the covariance matrix given by Eq. (2.18) and we get the jammer gain relative to the signal direction gain, equivalent to Eq. (2.13) for the Applebaum case:

$$\text{Relative jammer gain} = \frac{|\hat{\mathbf{x}}_j^+ \cdot \mathbf{w}^*|^2}{|\hat{\mathbf{x}}_d^+ \cdot \mathbf{w}^*|^2}$$

$$= \frac{\eta_q(\theta_j)}{\eta_q(\theta_d)} \cdot \frac{\left|1 + \frac{P_d}{\sigma^2} \frac{\hat{\mathbf{x}}_j^+ (\hat{\mathbf{s}}_d \hat{\mathbf{s}}_d^+ - \hat{\mathbf{x}}_d \hat{\mathbf{x}}_d^+) \hat{\mathbf{s}}_d}{\hat{\mathbf{x}}_j^+ \hat{\mathbf{s}}_d}\right|^2}{\left|1 + \frac{P_j}{\sigma^2} \frac{\hat{\mathbf{x}}_d^+ (\hat{\mathbf{s}}_d \hat{\mathbf{s}}_d^+ - \hat{\mathbf{x}}_j \hat{\mathbf{x}}_j^+) \hat{\mathbf{s}}_d}{\hat{\mathbf{x}}_d^+ \hat{\mathbf{s}}_d}\right|^2} \tag{2.28}$$

which differs from Eq. (2.13) only in the numerator containing the desired signal power P_d. Again we see that the Frost algorithm is quite sensitive to steering vector errors, $\hat{\mathbf{x}}_d \neq \hat{\mathbf{s}}_d$.

For more jammers the relative "jammer gain decrease" becomes, assuming $|\mathbf{w}| = |\mathbf{w}_0|$:

$$\text{Jammer gain decrease} \approx \frac{|\hat{\mathbf{x}}_j^+ \cdot \mathbf{w}^*|^2}{|\hat{\mathbf{x}}_j^+ \cdot \mathbf{w}_0^*|^2} = \frac{1}{[1 + P_j \hat{\mathbf{x}}_j^+ \Phi_0^{-1} \hat{\mathbf{x}}_j]^2} \tag{2.29}$$

which, for not too many strong jammers (when $\hat{\mathbf{x}}_j^+ \Phi_0^{-1} \hat{\mathbf{x}}_j$ may be small even when $\hat{\mathbf{x}}_j$ is not close to an old jammer), will still give a deep null, keeping the old ones.

2.3 Eigenvalue Decomposition of the Covariance Matrix

The properties of the covariance matrixes and weight vectors can also be analyzed in terms of eigenvalue decomposition. Since the covariance matrixes are Hermitian there exist N orthogonal eigenvectors $\mathbf{e}_1 \ldots \mathbf{e}_N$, forming a unitary matrix, $\mathbf{U} = [\mathbf{e}_1, \ldots, \mathbf{e}_N]$ *so that:*

$$\mathbf{U}\mathbf{U}^+ = \mathbf{U}^+\mathbf{U} = \mathbf{I} \tag{2.30}$$

$$\Phi = \mathbf{U} \cdot \Lambda \cdot \mathbf{U}^+ \tag{2.31}$$

$$\Phi^{-1} = \mathbf{U} \cdot \Lambda^{-1} \cdot \mathbf{U}^+ \tag{2.32}$$

where Λ is a diagonal matrix containing the eigenvalues, λ_i, of Φ. If there are M uncorrelated jammers, including the desired signal in Frost's case, and if all channels have identical noise, there will be N-M eigenvectors that are orthogonal to all signals present, called noise eigenvectors and spanning the noise subspace, and M eigenvectors corresponding to the signals, spanning the signal subspace.[6] (If the noise is not identical in each of the N channels the noise covariance matrix, Φ_n is not equal to $\sigma^2\mathbf{I}$ and the above statement is not strictly true. If Φ_n is known,

---

[6] Schmidt, R., (1986), Multiple emitter location and signal parameter estimation, *IEEE Trans. Antennas and Propagat.*, March, pp. 276-280.

however, the generalized eigenvalues and eigenvectors, obtained from $\Phi \mathbf{e}_i = \lambda_i \Phi_n \mathbf{e}_i$, *should be used.*[6]) *The noise eigenvalues are all, or should all be, equal to* σ^2.

As the jammers are in general not orthogonal, $\mathbf{x}_{jn}^{+}\mathbf{x}_{jm} \neq 0$, the eigenvectors are not identical to the jammer signal vectors, but if they are orthogonal the eigenvalues are $\lambda_J = P_J + \sigma^2$ and the jammer vectors are parallel to the eigenvectors. This is also approximately true if each jammer is in the sidelobe region of the desired signal and the other jammers.

Using the unitary property of the eigenvector matrix **U** and the fact that all noise eigenvalues are equal, we can write:

$$\Phi^{-1} = \mathbf{U}\Lambda^{-1}\mathbf{U}^{+} = \sum_{i=1}^{N} \lambda_i^{-1}\mathbf{e}_i\mathbf{e}_i^{+} \tag{2.33}$$

$$= \frac{1}{\sigma^2}\mathbf{I} + \sum_{i=1}^{M}\left(\frac{1}{\lambda_i} - \frac{1}{\sigma^2}\right)\mathbf{e}_i\mathbf{e}_i^{+} \tag{2.34}$$

$$\mathbf{w}^{*} \sim \mathbf{s}_d - \sum_{i=1}^{M}\left(1 - \frac{\sigma^2}{\lambda_i}\right)(\mathbf{e}_i^{+}\mathbf{s}_d)\mathbf{e}_i \tag{2.35}$$

which gives the quiescent pattern and signal eigenvector cancellation patterns.

Eq. (2.35) is equivalent to the method used by Gabriel[7], Eq. (3).
For one jammer in Applebaum's and no jammer in Frost's algorithm, $M = 1$ and $\lambda_1 = P_1 + \sigma^2$ and Eq. (2.35) is identical to Eqs. (2.12) and (2.19).

When the desired signal is present during adaptation one eigenvector, say $\mathbf{e}_M$, is approximately parallel to the steering vector $\mathbf{s}_d$, and term M in the sum will almost cancel the first term. In this case, using:

$$\mathbf{e}_M\mathbf{e}_M^{+} = \mathbf{I} - \sum_{i \neq M} \mathbf{e}_i\mathbf{e}_i^{+}$$

$$\Phi_F^{-1} = \sum_i \lambda_i^{-1}\mathbf{e}_i\mathbf{e}_i^{+} = \frac{1}{\lambda_M}\mathbf{I} + \sum_{i=1}^{M-1}\left(\frac{1}{\lambda_i} - \frac{1}{\lambda_M}\right)\mathbf{e}_i\mathbf{e}_i^{+} + \left(\frac{1}{\sigma^2} - \frac{1}{\lambda_M}\right)\sum_{i=M+1}^{N}\mathbf{e}_i\mathbf{e}_i^{+} \tag{2.36}$$

---

[7] Gabriel, W.F., (1986), Using estimation techniques in adaptive processing antenna systems, *IEEE Trans. Aerospace and Electronic Systems*, July, pp. 397-401.

$$\mathbf{w}_F^* \sim \mathbf{s}_d - \sum_{i=1}^{M-1} \left(1 - \frac{\lambda_M}{\lambda_i}\right)(\mathbf{e}_i^+ \mathbf{s}_d)\mathbf{e}_i + \left(\frac{\lambda_M}{\sigma^2} - 1\right) \sum_{i=M+1}^{N} (\mathbf{e}_i^+ \mathbf{s}_d)\mathbf{e}_i \tag{2.37}$$

or, denoting the error of $\mathbf{s}_d$ being orthogonal to $\mathbf{x}_d$ with $\Delta\mathbf{s}_d$.

$$\mathbf{w}_F^* \sim \mathbf{s}_d - \sum_{i=1}^{M-1} \left(1 - \frac{\lambda_M}{\lambda_i}\right)(\mathbf{e}_i^+ \mathbf{s}_d)\mathbf{e}_i + \left(\frac{\lambda_M}{\sigma^2} - 1\right)\left[\Delta\mathbf{s}_d - \sum_{i=1}^{M} (\mathbf{e}_i^+ \Delta\mathbf{s}_d)\mathbf{e}_i\right] \tag{2.38}$$

Since λ_i for $i < M$ is usually large, this is approximately equal to Eq. (2.35) except for the last term.

When P_d, and hence λ_M, is very large and $\Delta\mathbf{s}_d$ is nonzero the first term, $\mathbf{s}_d$, can be neglected and the pattern will become an error dominated pattern with jammer nulls.

2.4 Methods of Correction

Some of the errors discussed in the following sections can be partly corrected for by using essentially three different methods. These are also discussed more in the sections where they are used.

In both the Applebaum and Frost cases we know that all noise eigenvalues are, or should be for good patterns, equal to σ^2. However, this is not always true for real covariance matrixes. Therefore, one method for improvement is to identify the noise eigenvalues by their magnitude and set them to this value.

$$\lambda_{i,noise} \rightarrow \sigma^2 \tag{2.39}$$

This is equivalent to the method used by Gabriel.[7]

Another method to decrease the effects of errors in the covariance matrix is simply to make their relative magnitudes smaller by adding artificial noise to the covariance matrix,[7,8] forming an artificial matrix:

$$\Phi_{art} = \Phi + \sigma_{art}^2 \mathbf{I} \tag{2.40}$$

---

[8] Carlson, B.D., (1988), Covariance matrix estimation errors and diagonal loading in adaptive arrays, *IEEE Trans. Aerospace and Electronic Systems*, July, pp. 397-401.

Of course the noise is added in the covariance matrix only and not to the real signals. Since the error effects in the Frost algorithm are often functions of P_d/σ^2 this artificial noise will decrease these errors too.

In the Frost algorithm we often want the steering vector $\mathbf{s}_d$ to be parallel to the desired signal vector $\mathbf{x}_d$. Even if this vector cannot be directly found from the covariance matrix, it is, when all channels have identical noise (and approximately when the noise is nearly the same), contained in the signal subspace. Thus, modifying the steering vector by projecting it onto this signal subspace,:[9,10]

$$\mathbf{s}_d^p = \sum_{\substack{\text{signal} \\ \text{subspace}}} (\mathbf{e}_i^+ \mathbf{s}_d)\mathbf{e}_i \tag{2.41}$$

which is equivalent to setting the inverses of the eigenvalues in Eq. (2.33) equal to zero, will often give a big improvement.

3. NONUNIFORM NOISE FIGURES

When deriving many of the equations in Section 2 it was assumed that the noise in all channels was equal so that the noise part of the covariance matrix became the noise power times an identity matrix. If the noise figures in the channels are not equal this is not true but we get:

$$\Phi_n = \begin{bmatrix} \sigma_1^2 & & \mathbf{0} \\ & \sigma_2^2 & \\ \mathbf{0} & & \ddots \sigma_N^2 \end{bmatrix} \qquad \Phi_n^{-1} = \begin{bmatrix} 1/\sigma_1^2 & & \mathbf{0} \\ & 1/\sigma_2^2 & \\ \mathbf{0} & & \ddots 1/\sigma_N^2 \end{bmatrix} \tag{3.1}$$

So that, if $\sigma_i^2 = \sigma^2 \pm \Delta\sigma^2$ where $\Delta\sigma^2$ is the deviation from the mean value, the quiescent weights will get the same relative error.

---

[9] Steyskal, H., (1991), Array error effects in adaptive beamforming, *Microwave Journal*, Sept., pp. 101-112.

[10] Bull, J.F., Arnao, M.A., and Burgess, L.R., (1990), Hypersensitivity effects in adaptive antenna arrays, *IEEE AP-S Symposium*, 1990, pp. 396-399.

For rectangular distributed noise, with noise figures $F_0 \pm \Delta F_{max}$, the expected mean sidelobe level contribution with no jammers will be, from Eq. (A.6):

$$\text{Sidelobe level} \approx \frac{1}{3}\frac{(\Delta\sigma^2/\sigma^2)}{N\eta_A} = \frac{1}{3}\frac{(\Delta F_{max}/F_0)^2}{N\eta_A} \tag{3.2}$$

(provided all channels see 290K external noise).

Figure 3 shows simulated patterns, for configuration B using Applebaum's algorithm, with relative noise figure deviations ΔF_{max} = 0, ±0.1, ±0.2 and ±0.4 dB respectively. The expected mean sidelobe contribution level is, from Eq. (3.2), -∞, -48, -42 and -36 dB respectively.

If σ_i^2 is known this can be compensated for to give good quiescent patterns by adding a matrix $\sigma^2 I - \Phi_n$ or, as in Reference 4, use the modified steering vector $s_d^m = \Phi_n s_d$.

One method to improve the result, in which the noise figures do not have to be accurately known, is to make their relative variation smaller by artificially increasing the noise in the covariance matrix according to Eq. (2.40). This will make the relative variation, and thus the sidelobe contribution, a factor 1 + σ_{art}^2/σ^2 smaller.

Another method is to modify the noise eigenvalues of the covariance matrix. In the ideal, uniform noise figure case, these are all equal to σ^2 so that identifying them by their magnitude and setting them all equal to σ^2, Eq. (2.39), will improve the result. As discussed in Section 2 and Reference 6 the nonuniform noise figures will also modify the signal eigenvectors slightly but this effect is of minor importance.

Figure 4 shows patterns when these two methods have been used for the ΔF_{max} = ±0.4 dB case.

If the steering vector is parallel to the desired signal vector, $\hat{s}_d = \hat{x}_d$, the Frost and Applebaum algorithms give identical results as discussed in Section 2. Their eigenvalue spectra, however, are not equal. The eigenvalue decomposition in Section 2 assumed identical noise figures. When these are not identical the signal eigenvectors are still almost the same but there will be a small noise subspace component in the steering vector, Δs_d in Eq. (2.38), which will give most of the sidelobe level increase. Thus, identifying the signal subspace by the magnitude of the eigenvalues and projecting the steering vector on this subspace to obtain a

projected steering vector, according to Eq. (2.41), will improve the result for Frost's algorithm.

Figure 5 illustrates this for configuration A by showing a pattern using this method together with the original pattern, both with $\Delta F_{max} = \pm 1.5$ dB, and the pattern with no nonuniformity.

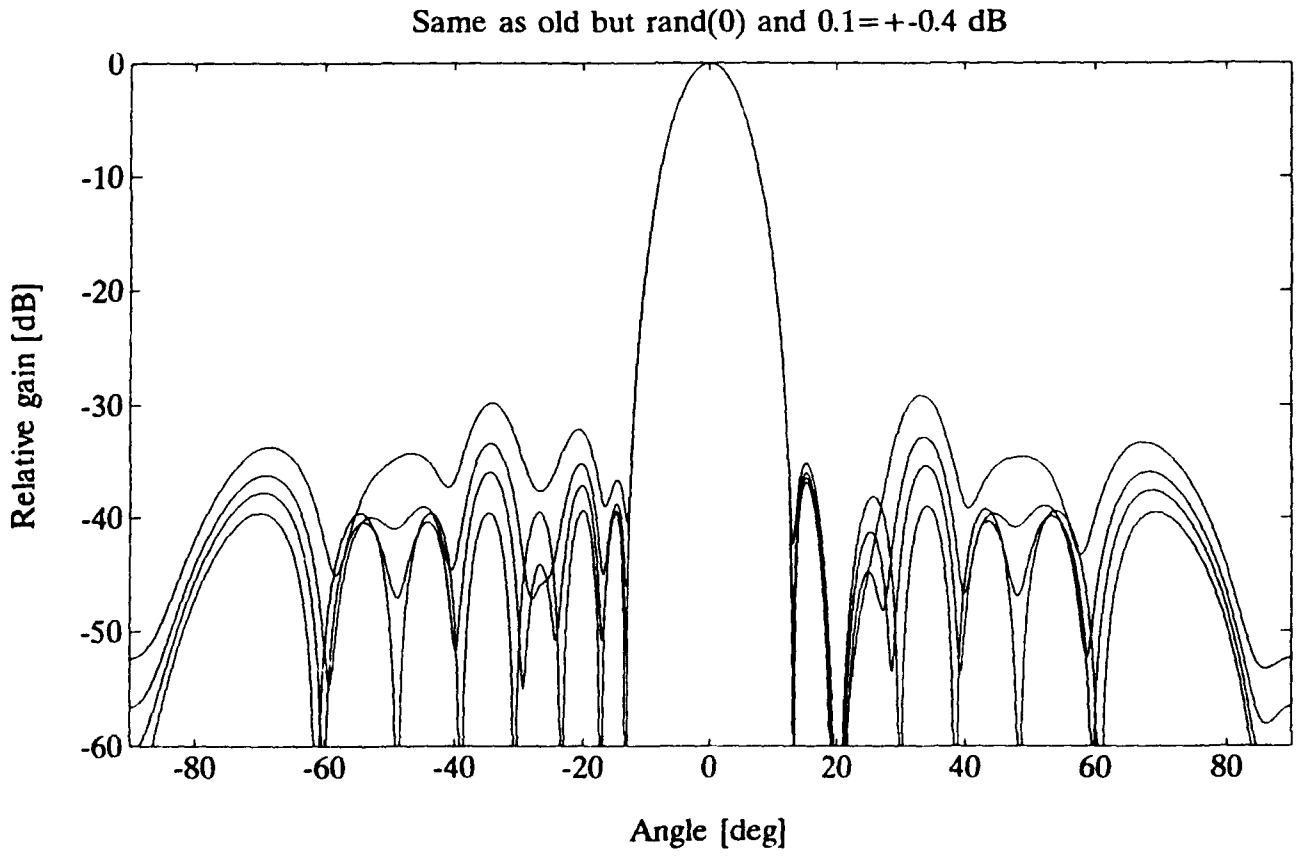

Figure 3. Simulated Patterns for Configuration B Using Applebaum's Algorithm. Noise figure span: 0, ±0.1, ±0.2 and ±0.4 dB.

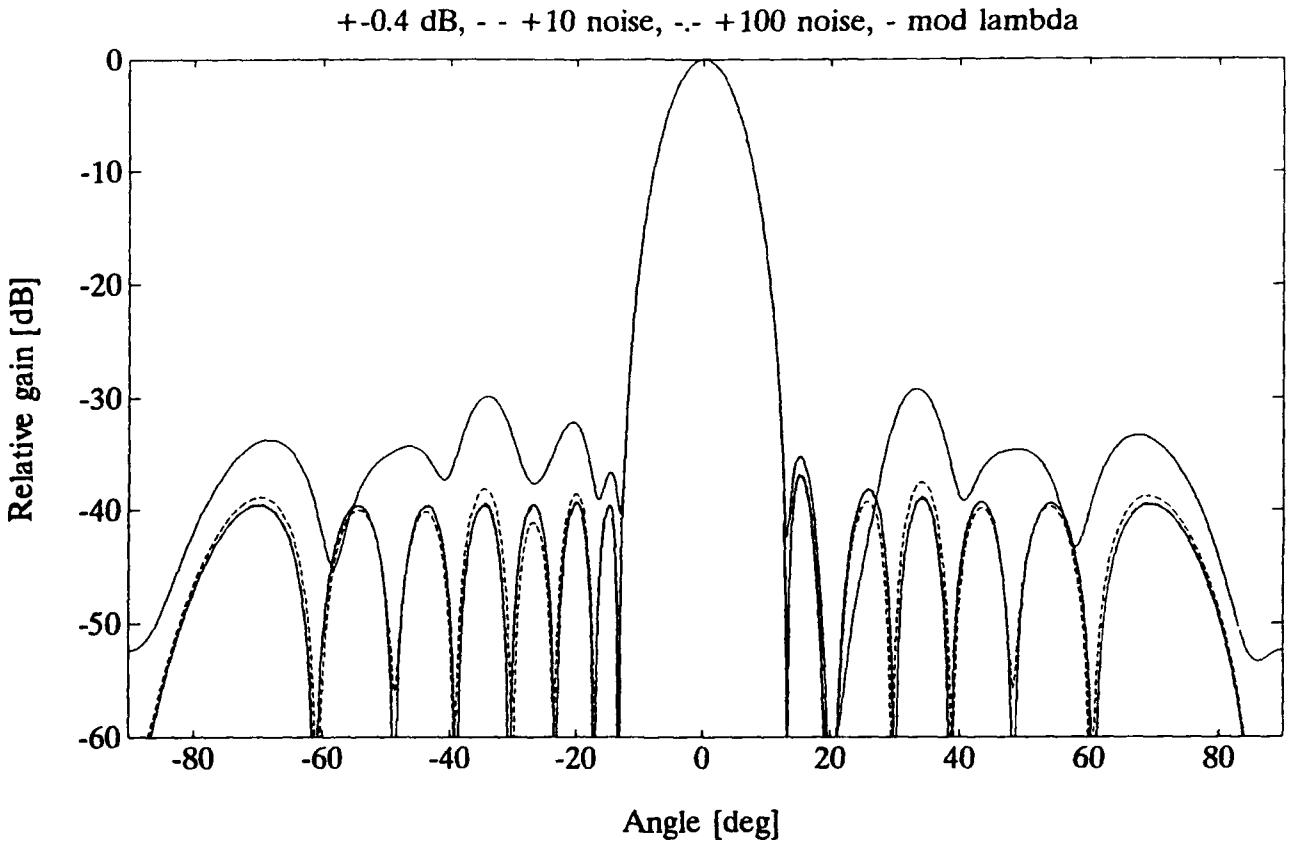

Figure 4. Simulated Patterns for Configuration B Improved by Adding Artificial Noise and by Setting the Noise Eigenvalues to σ^2. Noise figure span = ±0.4 dB.
——— Original pattern, - - - Artificial noise = $10\sigma^2$,
-·-·- Artificial noise = $100\sigma^2$, ——— Noise eigenvalues set to σ^2. (The two last patterns are almost identical).

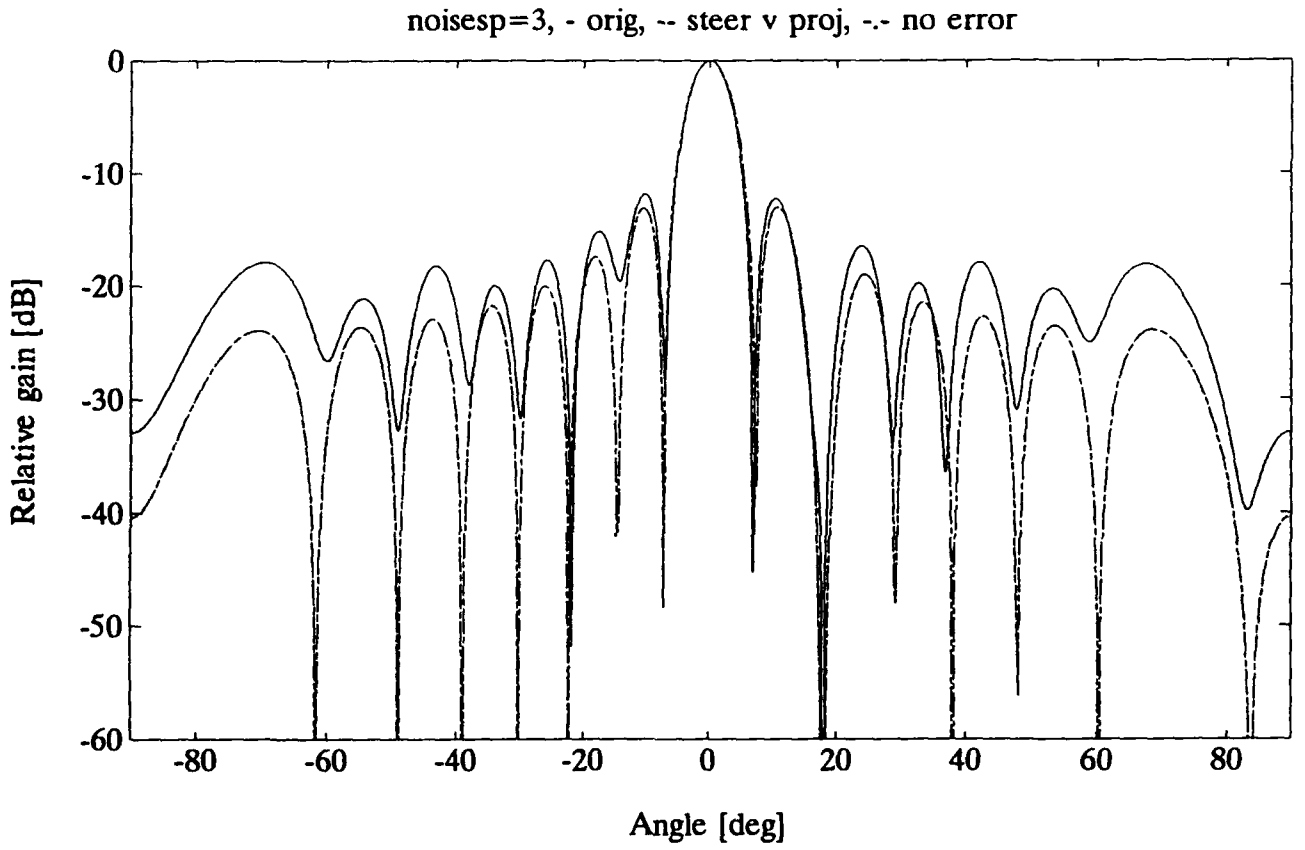

Figure 5. Simulated Pattern for Configuration A with Correction by Projecting the Steering Vector onto the Signal Subspace, and the Results for Uniform Noise Figures. Noise figure span = ±1.5 dB. ——— Original pattern, - - - Frost's algorithm with steering vector projection, -·-·-·- No errors. (The latter two are coincident in the plot.)

4. FROST'S ALGORITHM WITH TAPERED QUIESCENT WEIGHTS

To get a radiation pattern with low sidelobes for the Applebaum criterion we only have to use a steering vector, s_d, corresponding to the desired quiescent pattern. For Frost's criterion such a steering vector does not solve the problem. From Eq.(2.19) we get the quiescent weights:

$$\mathbf{w}_F^* \sim \left[\hat{\mathbf{s}}_d - \frac{P_d}{P_d+\sigma^2}(\hat{\mathbf{x}}_d^+ \cdot \hat{\mathbf{s}}_d)\hat{\mathbf{x}}_d\right] \tag{4.1}$$

where the projection $(\hat{\mathbf{x}}_d^+ \cdot \hat{\mathbf{s}}_d)$ is of the order of one. The weight vector is thus a linear combination of the steering vector and the signal direction vector $\hat{\mathbf{x}}_d$. If the signal is very weak, $P_d \ll \sigma^2$, then $\mathbf{w}_F^* \sim \hat{\mathbf{s}}_d$ and the Frost case has gone smoothly over into Applebaum's. Figure 6 shows the adapted patterns for configuration B when the signal to noise ratio per channel, SNR, is equal to 0 dB, -12 dB ($P_d/\sigma^2 = 1$), -20 dB, and -30 dB together with the Applebaum pattern, corresponding to SNR = $-\infty$ dB. The ratio $P_d/(P_d+\sigma^2)$ is equal to 0.94, 0.5, 0.14, 0.016, and 0 respectively. It is seen that very low SNR is required for a good pattern. When there is no jammer the broadside gain can be found from Eq. (2.26) to be 18.4, 2.3, 0.34, and 0.03 dB below the Applebaum gain. To get good patterns even for stronger signals the following modifications of the Frost algorithm may be used.

A) Increase the noise artificially by adding a matrix $\sigma_{art}^2 \mathbf{I}$, Eq. (2.40), to the covariance matrix so that $P_d \ll \sigma_{tot}^2 = \sigma^2+\sigma_{art}^2$. This will result in a slightly lower SNIR when a jammer is present although, of course, the added noise is not present in the real signal. From Eq. (4.1) it is seen that, with no jammer present, this is equivalent to a low power signal as in Figure 6.

B) The problem with Frost's criterion is that the desired signal, $\mathbf{x}_d$, destroys some nice properties of the covariance matrix. If this signal could be subtracted from the total signal the problem would be solved. However, as noted from Figure 6, for the Frost case to become an Applebaum case, it is necessary that the residual signal power $\Delta P_d \ll \sigma^2$, or that the residual signal-to-noise ratio per channel

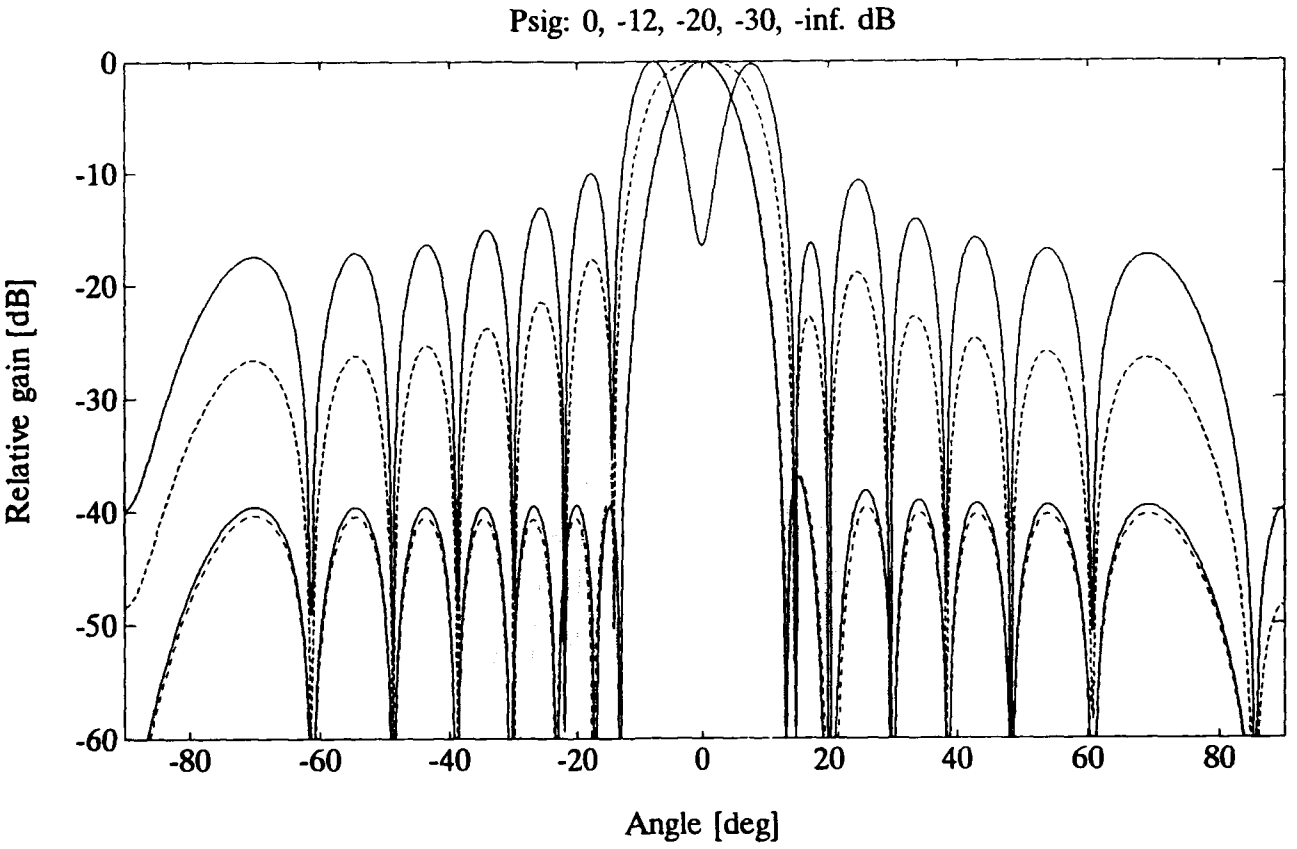

Figure 6. Adapted Patterns Using Frost's Algorithm, Configuration B. Signal to noise ratio per channel, SNR, = ——— 0 dB, - - - -12 dB,····· -20 dB, -·-·-· -30 dB and ——— -∞ dB.

$(SNR)_{res}$ « $1/N$, which is not easy to obtain. One possible method could be to use signals from subarrays with a null in the desired signal direction to obtain the adaptive weights but apply them to subarrays with a maximum in this direction to get the antenna signal, as in the Duvall beamformer.[11] This assumes in principle that all antenna element patterns are identical, and that the signal and jammers are uncorrelated plane waves so that the optimal pattern has deep directional nulls.

C) If the artificial noise increase is different for the channels, so that the total artificial covariance matrix is:

$$\Phi_{art} = \Phi + \sigma^2_{art}\mathbf{D} - \sigma^2\mathbf{I} \tag{4.2}$$

where $\mathbf{D}$ is a diagonal matrix, the total noise part of the covariance matrix becomes: $\Phi_{n,tot} = \sigma^2_{art}\mathbf{D}$. Using Eq. (2.25) with $\Phi_A = \sigma^2_{art}\mathbf{D}$ the quiescent weights can be written as:

$$\mathbf{w}^*_{Fq} \sim \mathbf{D}^{-1}\left[\hat{\mathbf{s}}_d - \frac{P_d\,\hat{\mathbf{x}}^+_d\mathbf{D}^{-1}\hat{\mathbf{s}}_d}{\sigma^2_{art} + P_d\hat{\mathbf{x}}^+_d\mathbf{D}^{-1}\Delta\hat{\mathbf{x}}_{d\perp}}\Delta\hat{\mathbf{x}}_{d\perp}\right]$$

$$= \mathbf{D}^{-1}\left[\hat{\mathbf{s}}_d - \alpha''\Delta\hat{\mathbf{x}}_{d\perp}\right] \tag{4.3}$$

where α'' is a scalar.

Thus, if $\hat{\mathbf{s}}_d$ is the usual plane wave steering vector, equal to $\hat{\mathbf{x}}_d$ and if $\mathbf{D}$ contains the inverse of the desired amplitude weights such as Dolph-Chebyshev, $\mathbf{D}_{ii} = 1/w_{Di}$, the desired quiescent weights are obtained. (If the artificial noise is allowed to be correlated between the channels, quiescent weights with irregular phase may also be obtained while keeping Φ Hermitian.)

$$\mathbf{w}^*_{Fq} \sim \mathbf{D}^{-1}\hat{\mathbf{s}}_d \tag{4.4}$$

---

[11] Widrow, B., Duvall, K.M., Gooch, R.P., and Newman, W.C., (1982), Signal cancellation phenomena in adaptive antennas: causes and cures, *IEEE Trans. Antennas and Propagat.*, May, pp. 469-478.

and in general:

$$\mathbf{w}_F^* \sim \Phi_{art}^{-1} \hat{\mathbf{s}}_d \tag{4.5}$$

This method corresponds physically to a situation where the antenna edge elements are, for tapered quiescent weights, more noisy than the central ones (compare Section 3). To get maximum SNIR the antenna will then put more weights on the central elements. It can also be used for Applebaum's algorithm. As $\hat{\mathbf{s}}_d$ is now parallel to $\hat{\mathbf{x}}_d$ the result will then, according to Eq. (2.25), be identical to that of the Frost algorithm.

The relative jammer gain, or null depth, can be found in the same way as when $\mathbf{D} = \mathbf{I}$, Eq. (2.28) with the result:

$$\text{Relative jammer gain} = \frac{|\hat{\mathbf{x}}_j^+ \cdot \mathbf{w}^*|^2}{|\hat{\mathbf{x}}_d^+ \cdot \mathbf{w}^*|^2}$$

$$= \frac{\eta_q(\theta_j)}{\eta_q(\theta_d)} \cdot \frac{\left| 1 + \frac{P_d}{\sigma_{art}^2} \frac{\hat{\mathbf{x}}_j^+ \mathbf{D}^{-1} (\hat{\mathbf{s}}_d \hat{\mathbf{s}}_d^+ - \hat{\mathbf{x}}_d \hat{\mathbf{x}}_d^+) \mathbf{D}^{-1} \hat{\mathbf{s}}_d}{\hat{\mathbf{x}}_j^+ \mathbf{D}^{-1} \hat{\mathbf{s}}_d} \right|^2}{\left| 1 + \frac{P_j}{\sigma_{art}^2} \frac{\hat{\mathbf{x}}_d^+ \mathbf{D}^{-1} (\hat{\mathbf{s}}_d \hat{\mathbf{s}}_d^+ - \hat{\mathbf{x}}_j \hat{\mathbf{x}}_j^+) \mathbf{D}^{-1} \hat{\mathbf{s}}_d}{\hat{\mathbf{x}}_d^+ \mathbf{D}^{-1} \hat{\mathbf{s}}_d} \right|^2} \tag{4.6}$$

where $\eta_q(\theta_j) = |\hat{\mathbf{x}}_j^+ \mathbf{D}^{-1} \hat{\mathbf{s}}_d|^2 / \langle w_D^2 \rangle$ and $\eta_q(\theta_d) = |\hat{\mathbf{x}}_d^+ \mathbf{D}^{-1} \hat{\mathbf{s}}_d|^2 / \langle w_D^2 \rangle$ are the quiescent aperture efficiencies in the jammer and desired signal directions and $\langle w_D^2 \rangle$ is the mean square of the elements in $\mathbf{D}^{-1}$.

When $\hat{\mathbf{x}}_d = \hat{\mathbf{s}}_d$ the equation simplifies to:

$$\text{Relative jammer gain } (\hat{\mathbf{x}}_d = \hat{\mathbf{s}}_d)$$

$$= \frac{\eta_q(\theta_j)}{\eta_q(\theta_d)} \cdot \frac{1}{\left[1 + \frac{P_j}{\sigma_{art}^2} \langle w_D \rangle \left(1 - \frac{\eta_q(\theta_j)}{\eta_q(\theta_d)} \right) \right]^2} \tag{4.7}$$

where $\langle w_D \rangle$ is the mean value of the elements in $\mathbf{D}^{-1}$ and where now $\eta_q(\theta_d) = \langle w_D \rangle^2 / \langle w_D^2 \rangle$.

Figure 7 shows radiation patterns for basic configuration B using both the Applebaum algorithm with a Chebyshev type steering vector and the above method using the diagonal elements $\mathbf{D}_{ii} = 1/w_{Di}$, where w_{Di} are the Chebyshev weights with $w_{Di,max} = 1$, and with $\sigma_{art} = \sigma$. The resulting null depths are -139 dB using this method, which is also obtained from Eq. (4.7), and -144 dB for the Applebaum pattern using the Chebyshev steering vector.

When there are errors in the array that are corrected for by some method such as a steering vector projection, Eq. 41), or by noise eigenvalue modification, Eq. (2.39), the covariance matrix mod. ication in Eq. (4.2) should be made as the last step.

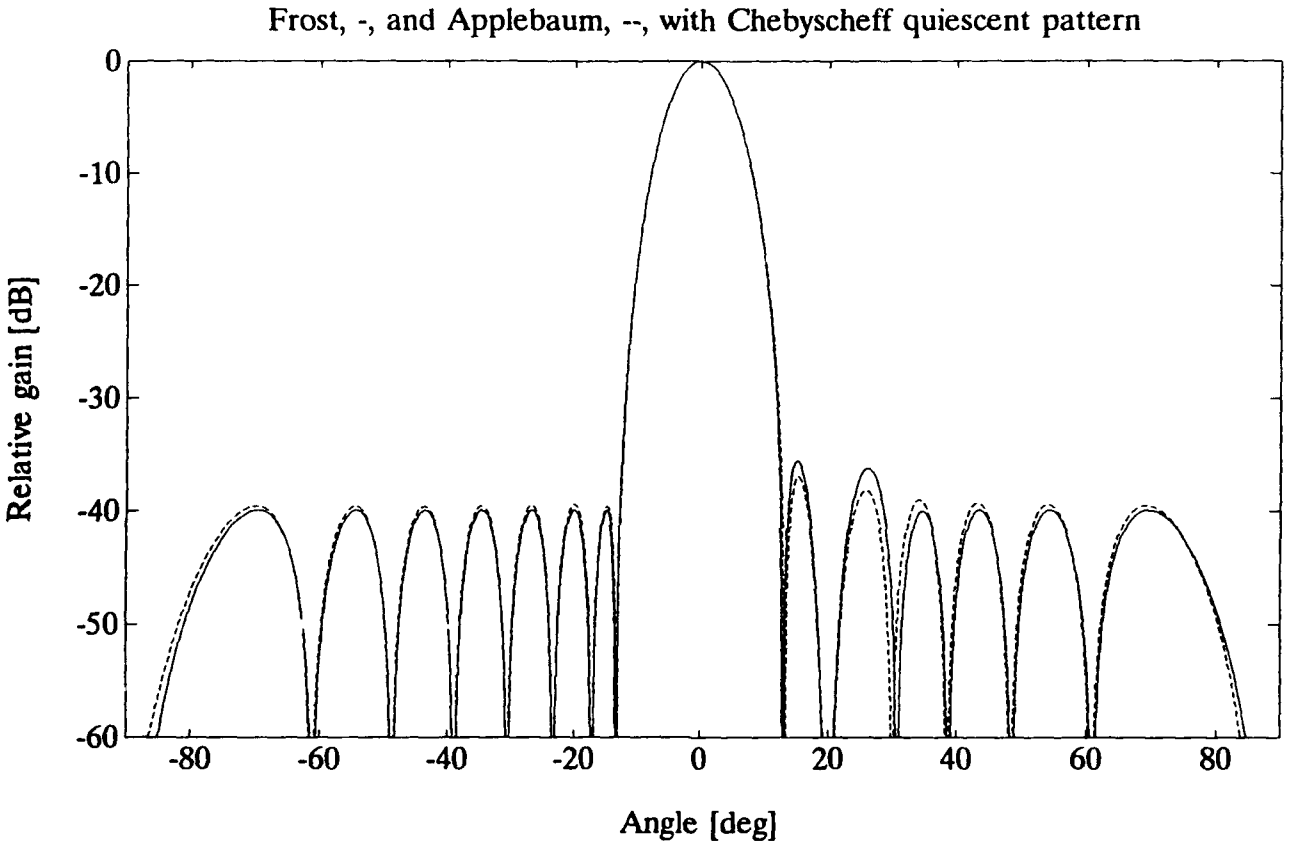

Figure 7. Radiation Patterns for Configuration B. ——— Modified noise covariance matrix, - - - - Applebaum's Algorithm with Chebyshev Steering Vector.

5. GAIN AND PHASE SHIFT ERRORS

These errors can in principle be measured by a calibration routine and corrected for, but in this Section the case when this correction has not been made is considered. They were also discussed in Steyskal.[9,12]

When the channels have errors in gain and phase shift the signal vector into the beamformer will be deformed. Since the adaptive algorithm does not assume anything about the amplitude and phase relations for the jammers, for example a plane wave assumption, the jammers will still be eliminated with essentially the same factor as without these errors. Due to the gain and phase shift errors however, the steering vector s_d is no longer optimum and an optimal pattern will not result.

5.1 Random Error Effects in the Applebaum Algorithm

If the gain and phase shift errors are in front of the thermal noise sources, which we will assume are all equal, the noise covariance matrix will still be $\sigma^2\mathbf{I}$ and the quiescent Applebaum weights will be identical to the error free weights, $w_{q0} \sim s_d$. For random errors this will give an increase in the average sidelobe levels and, as seen from Eqs. (2.12) and (2.35), this increase is, for the adapted pattern, essentially the same as for the quiescent pattern, described by an added sidelobe level contribution, Eq. (A.6):

$$\text{Sidelobe level} = \frac{\varepsilon^2+\delta^2}{N\,\eta_A} \tag{5.1}$$

where ε and δ are the gain and phase shift RMS errors relative to their mean values respectively.

If the errors are after the thermal noise sources there will also be variations in the output noise power in the channels, as discussed in Section 3, which is correlated with the gain errors. The covariance matrix is now given by $\Phi = C\Phi_0 C^+$ where C is a diagonal matrix containing the gain and phase shift errors,

---

[12] Steyskal, H., (1990), Array error effects in adaptive beamforming, JINA 90, *Conf. Proc.*, pp. 475-478.

$C_{ii} = \exp(\varepsilon_i + j\delta_i)$, and where Φ_0 is the error free covariance matrix. By correcting only the steering vector, by setting $s_d^c = Cs_d$ (so that $\hat{s}_d^c = \hat{x}_d$ for non-tapered steering vectors), the weight vector becomes $w = C^{-1}w_0$, which is the error free weights w_0 corrected for the gain and phase shift errors and giving the ideal pattern. When this steering vector correction is not made there will be weight errors:

$$\Delta w^* = \Phi^{-1}(\hat{s}_d - \hat{s}_d^c) \tag{5.2}$$

If the errors are small, the relative errors in the complex quiescent weights, $\Delta = \Delta w_{qi}/w_{qi}$, when the gain errors are in front of or after the noise sources are related by: $\Delta_f = -\Delta_a^*$, so that the added sidelobe level contribution is still given by Eq.(5.1). Normally there will of course be a combination of the two situations discussed.

Figures 8 and 9 illustrate results using Applebaum's algorithm, Eq. (2.2), with normally distributed errors with standard deviations 0.3 dB and 2°, for configurations A and B respectively, together with the quiescent patterns and the adaptive patterns without any errors. The sidelobe contributions from Eq. (5.1) are -38 and -37 dB respectively. The null depths were -122 dB in the simulation shown in Figure 8, and -141 and -147 dB in Figure 9 when the errors were in front of and after the noise sources respectively. The calculated results, using Eq. (2.13) and the error free values of $\eta_q(\theta_j)$ and $\eta_q(\theta_d)$, were -121 dB and -144 dB respectively. For configuration B in Figure 9, where the induced sidelobe level is higher than the regular sidelobes, the true $\eta_q(\theta_j)$ may vary significantly between different simulations.

Note also that when there are gain errors, the true antenna aperture efficiency is not given by $\eta = |\hat{x}_d \cdot \hat{s}_d|^2/|w|^2$, which is the efficiency referred to the channel outputs, but $\eta = |\hat{x}_d \cdot \hat{s}_d|^2/|w^+CC^+w|^2$. This will give some errors when using Eq. (2.15) for the signal gain.

5.2 Random Error Effects in the Frost Algorithm

In the Frost algorithm the deformed signal x_d is also included in the covariance matrix. If $\hat{x}_d = \hat{s}_d$, as when correcting the steering vector as described above, the

last term in Eq. (2.25) will vanish, as will the last terms in Eqs. (2.37) and (2.38) and the Frost weights will be identical to the Applebaum weights. When there are uncorrected gain and phase shift errors, s_d will have components in the noise

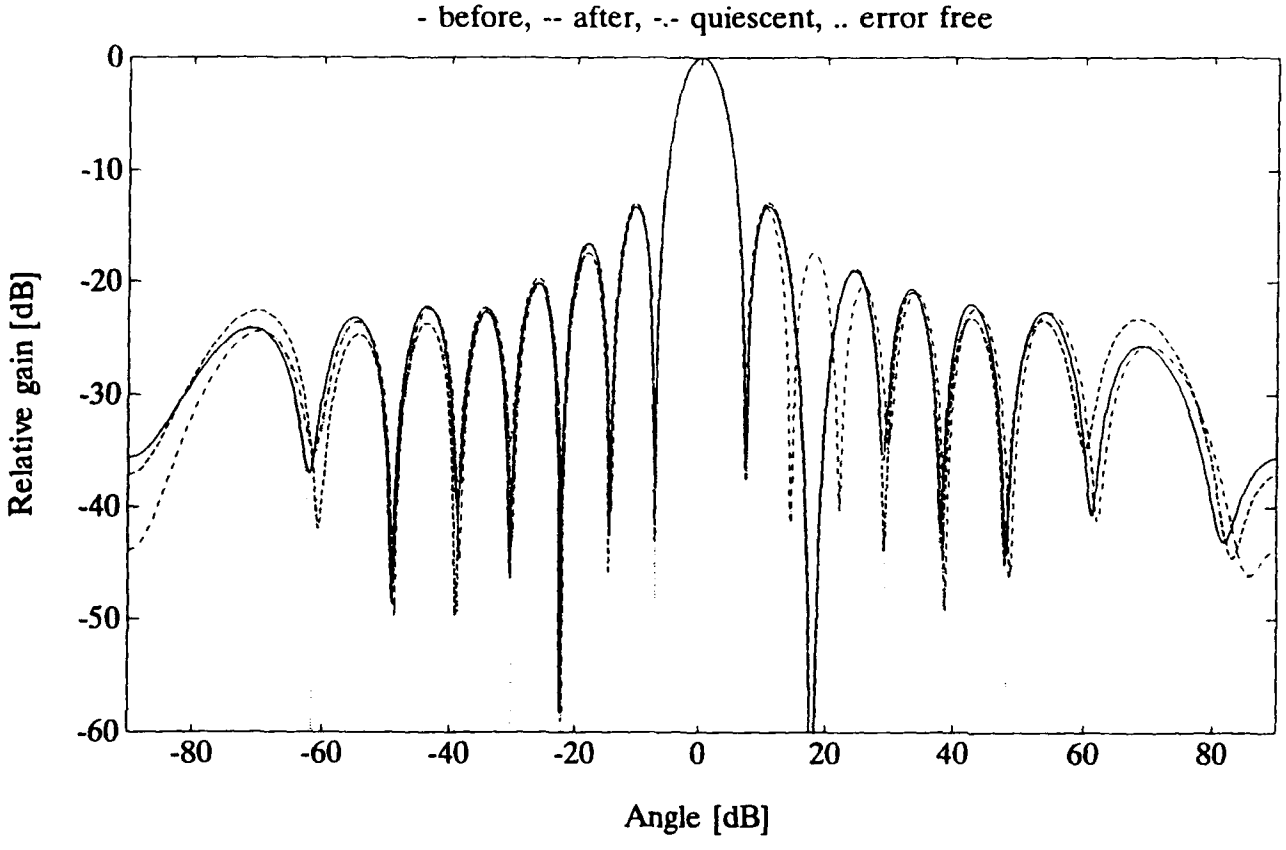

Figure 8. Configuration A, Applebaum's Algorithm with 0.3 dB and 2° RMS Errors. ———— errors in front of the noise sources, - - - - errors after the noise sources, -·-·-· quiescent pattern, ····· error free pattern

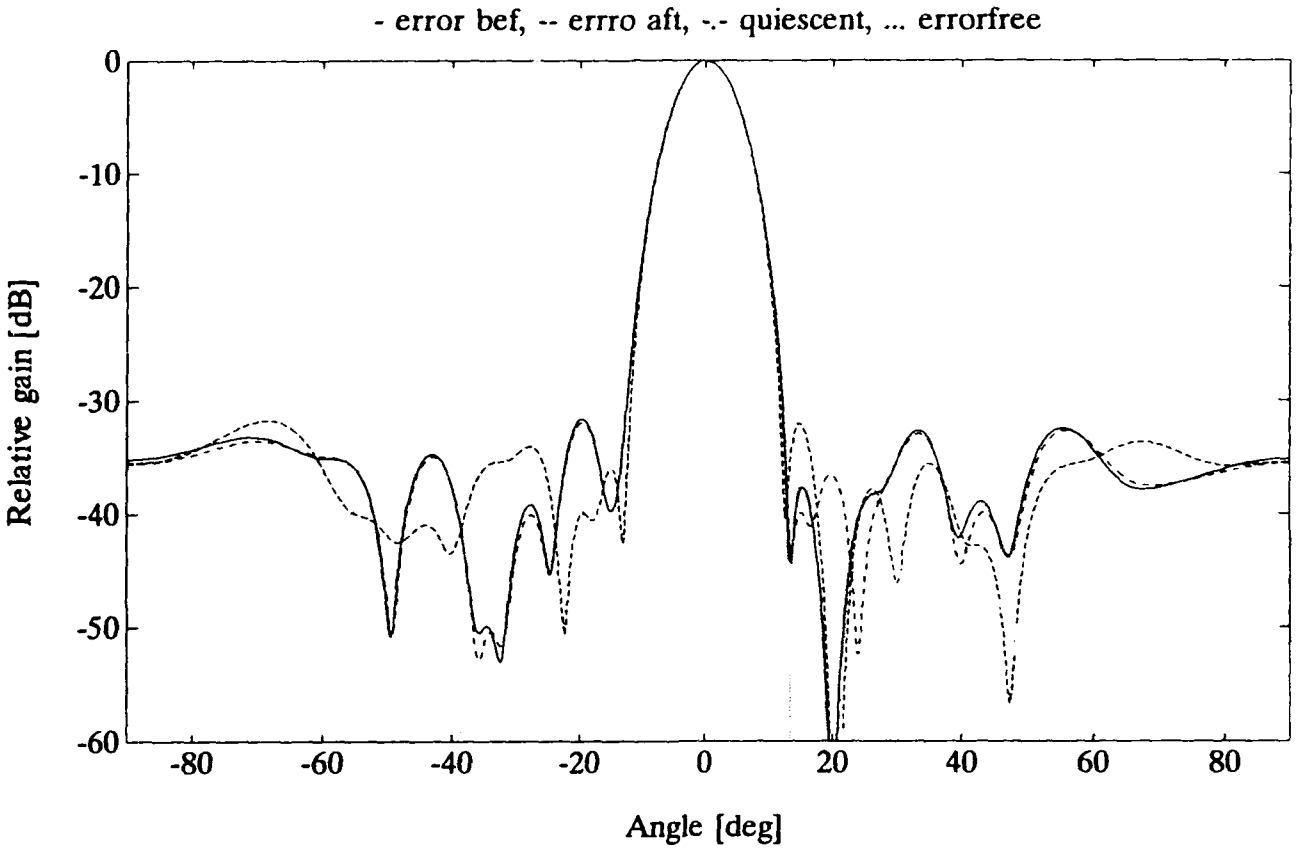

Figure 9. Configuration B. Same parameters as in Figure 8.

subspace which, as λ_M/σ^2 may be large, can have a substantial effect. Comparing Eq. (2.38) with Eq. (2.35) we see that the total error will be approximately λ_M/σ^2 larger than for the Applebaum algorithm. Since λ_M is approximately equal to $P_d + \sigma^2 = Np_d + \sigma^2$ this factor can be very large for strong signals and/or many elements. Alternatively, as α' in Eq. (2.24) is, for not too strong signal power, approximately equal to P_d/σ^2, we get from Eq. (2.25):

$$\mathbf{w}_F^* \sim \mathbf{w}_A^* - \frac{P_d}{\sigma^2}\Phi_A^{-1}\Delta\hat{\mathbf{x}}_{d\perp} \tag{5.3}$$

$$\Delta\mathbf{w}_F = \Delta\mathbf{w}_A + \frac{P_d}{\sigma^2}\Delta\mathbf{w}_d \tag{5.4}$$

where $\Delta\mathbf{w}_A$ is the same error as in the Applebaum algorithm and where $\Delta\mathbf{w}_d$ is equal to $\Delta\mathbf{w}_A$ when the gain errors are after the noise sources, remaining essentially independent of the position of these errors and being equal to zero when the corrected steering vector, $\mathbf{s}_d^c = C\mathbf{s}_d$, is used. Adding the two terms quadratically the sidelobe level contribution is from Eq. (A.6), assuming small errors:

$$\text{Sidelobe level} = \frac{\varepsilon^2+\delta^2}{N}\left[1 + \frac{P_d^2}{\sigma^4}\right] \tag{5.5}$$

Physically this large effect on the Frost algorithm can be thought of as an attempt to cancel the orthogonal signal, $\mathbf{x}_d - \hat{\mathbf{s}}_d(\hat{\mathbf{s}}_d^+\mathbf{x}_d)$, which is considered as a coherent jammer by the algorithm.

Figure 10 shows the same type of patterns as Figure 8 when using Frost's algorithm, Eq. (2.6), giving a much worse result (in this example, $P_d/\sigma^2 + 1 = 161$ and $\lambda_2/\sigma^2 = 158$). Since the second error term in Eq. (5.4) will now dominate, the patterns with errors in front of and after the noise sources are almost identical.

The resulting signal gain in this simulation was only -4.2 dB. With 0.3 dB and 2° RMS errors, the expected quiescent Applebaum efficiency is, using Eq. (A.2), $\eta_q(\theta_d) \approx 0.998$ and the Frost gain, using Eq. (2.26) is -5.8 dB.

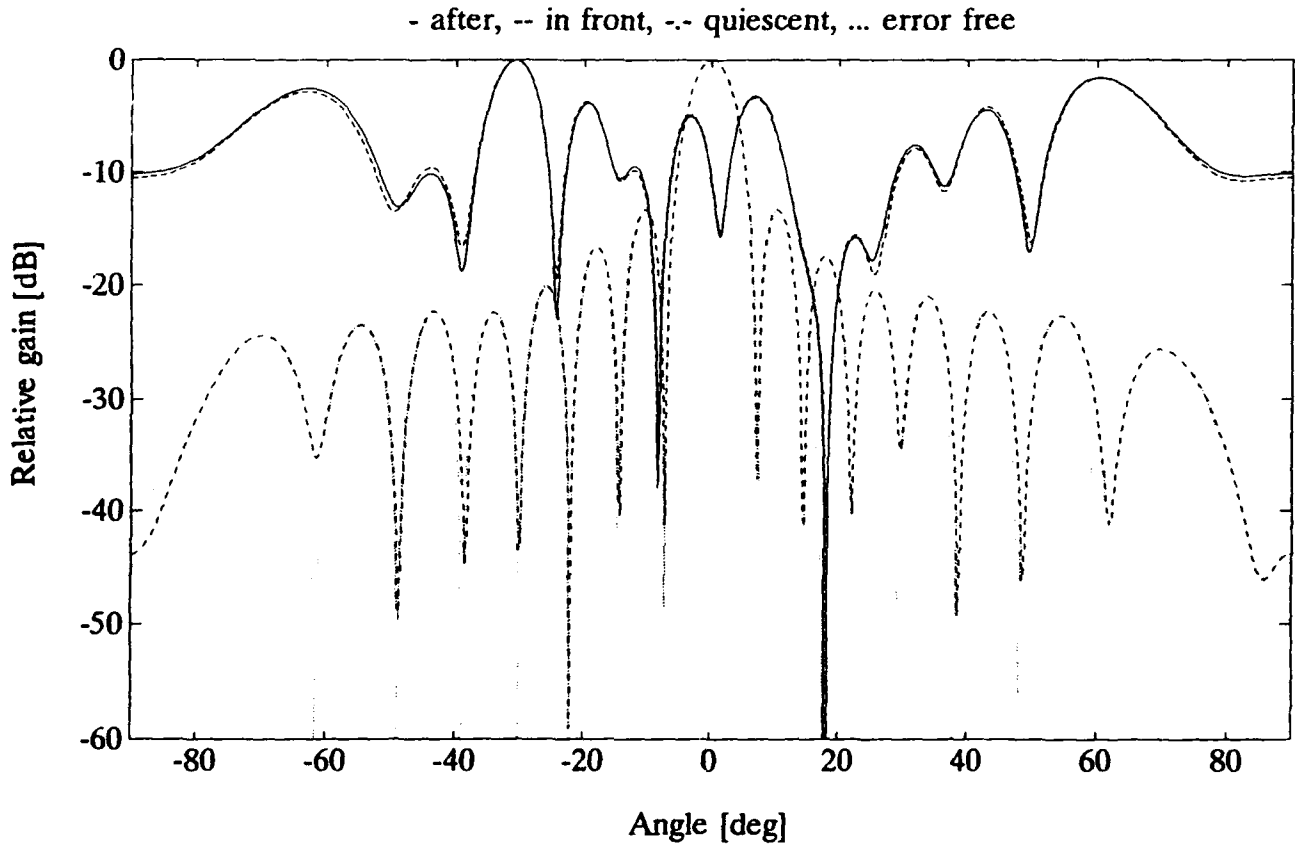

Figure 10. Configuration A, Frost's Algorithm. Same parameters as in Figure 8.

5.3 Improvement of the Frost Algorithm

The poor result for Frost's algorithm in the previous section can be improved however. As discussed above, the major cause of the problem is that the signal vector is not parallel to the steering vector, that is, $\hat{\mathbf{x}}_d \neq \hat{\mathbf{s}}_d$. We know however that the signal vector, $\mathbf{x}_d$, is contained in the signal subspace but has no component in the noise subspace when the channels have identical noise. One method to partly

cure the problem is then to identify the signal subspace by the magnitude of the eigenvalues and project the steering vector on this subspace to obtain a projected steering vector, Eq. (2.41), as was also done in Section 3. This will make the last term in Eqs. (2.37) and (2.38) equal to zero.

In the quiescent case (desired signal but no jammer present), with identical channel noise after the gain errors, the projected steering vector and the resulting weight vector will be exactly parallel to the signal vector: $\mathbf{w}_{Fq}^{*} \sim \mathbf{s}_d^p \sim \mathbf{x}_d = \mathbf{C}\mathbf{x}_{d0}$, where $\mathbf{x}_{d0}$ is the error free signal vector. Since the ideal weight vector is, from Section 5.1, $\mathbf{w}_{ideal} \sim \mathbf{C}^{-1}\mathbf{x}_{d0}^{*}$, we get:

$$\mathbf{w}_{Fq} \sim \mathbf{C}^{+}\mathbf{C}\mathbf{w}_{ideal} \tag{5.6}$$

and the weights will get a normalized mean square error of $\langle\Delta^2\rangle = 4\varepsilon^2$ independent of the phase error δ. This will give a sidelobe contribution of:

$$\text{Sidelobe level} = \frac{4\varepsilon^2}{N} \tag{5.7}$$

which in our example with 0.3 dB and 2° errors will give a sidelobe contribution 3 dB higher than for the Applebaum case, Eq. (5.1).

When the gain errors are after the noise sources the projected steering vector is almost identical to that above, giving the same sidelobe level. In Section 5.1 we found that using a corrected steering vector $\mathbf{s}_d^c = \mathbf{C}\mathbf{s}_d$ will result in the ideal pattern. Here we have indeed $\mathbf{s}_d^p = \mathbf{s}_d^c$. However since they are not exactly equal and since the noise eigenvalues are much smaller than the signal eigenvalues (provided the signal is not very weak) the last term in Eq. (2.38) is still significant when $\mathbf{s}_d = \mathbf{s}_d^c$.

This steering vector projection method assumes of course that the signal and noise subspaces can be correctly identified. When this may be in doubt, in practice when $P_d/\sigma^2 < 1$, the elimination of the noise eigenvectors is not so important.

Another method to improve the pattern is to make the factors P_d/σ^2 and λ_M/σ^2 smaller by artificially increasing the noise in the covariance matrix to give a new artificial covariance matrix as in Eq. (2.40). The sidelobe contribution is still given by Eq. (5.5) with σ^2 replaced by $\sigma_{tot}^2 = \sigma^2 + \sigma_{art}^2$. To get a good pattern the

artificial noise required is dependent on the total power, P_d, received by the antenna.

Figure 11 shows patterns when all noise subspace components of the steering vector have been eliminated, giving sidelobe contributions of -35 dB from Eq. (5.7), and patterns with added noise $\sigma^2_{art} = 10\ \sigma^2$ and $100\ \sigma^2$, giving sidelobe contributions of -14 and -31 dB from Eq. (5.5). The signal gain was 12, 10, and 12 dB respectively in agreement with the gain obtained from Eq. (A.2) with $\langle\Delta^2\rangle = 4\varepsilon^2$, and from Eq. (2.26) replacing σ^2 with σ^2_{tot} using $\eta_q(\theta_d) = 0.998$ as in Section 5.2.

When a low sidelobe pattern is desired, the method described in Section 4, Eq. (4.2), can be used if the steering vector projection, Eq. (2.41), is first used to correct for the errors or if Eq. (4.2) is used with a large σ^2_{art}. For the steering vector projection method Eq. (5.6) is still valid, giving a sidelobe contribution of:

$$\text{Sidelobe level} = \frac{4\varepsilon^2}{\eta_A N} \tag{5.8}$$

If Eq. (4.2) is used directly we can use Eq. (2.25) with $\Phi_A = \sigma^2_{art}\mathbf{D}$. Performing the same type of analysis as for the Applebaum case we obtain the sidelobe level contribution, equivalent to Eq. (5.5):

$$\text{Sidelobe level} = \frac{\varepsilon^2+\delta^2}{\eta_A N}\left[1 + \frac{P_d^2}{\sigma^4_{art}}\langle w_D\rangle^2\right] \tag{5.9}$$

where $\langle w_D\rangle^2$ is the mean value of the weight coefficients in $\mathbf{D}^{-1}$.

Figure 12 shows similar patterns as Figure 11 but for configuration B. The expected sidelobe level contributions from Eqs. (5.8) and (5.9) are -34, -18, and -34 dB respectively.

5.4 Null Depth for the Frost Algorithm

The null depth for the Frost algorithm may be found using Eqs.(2.28) or (4.6). The unit signal vector $\hat{\mathbf{x}}_d$ can, to second order in ε and δ, be written as, [compare Eq. (8.26)]:

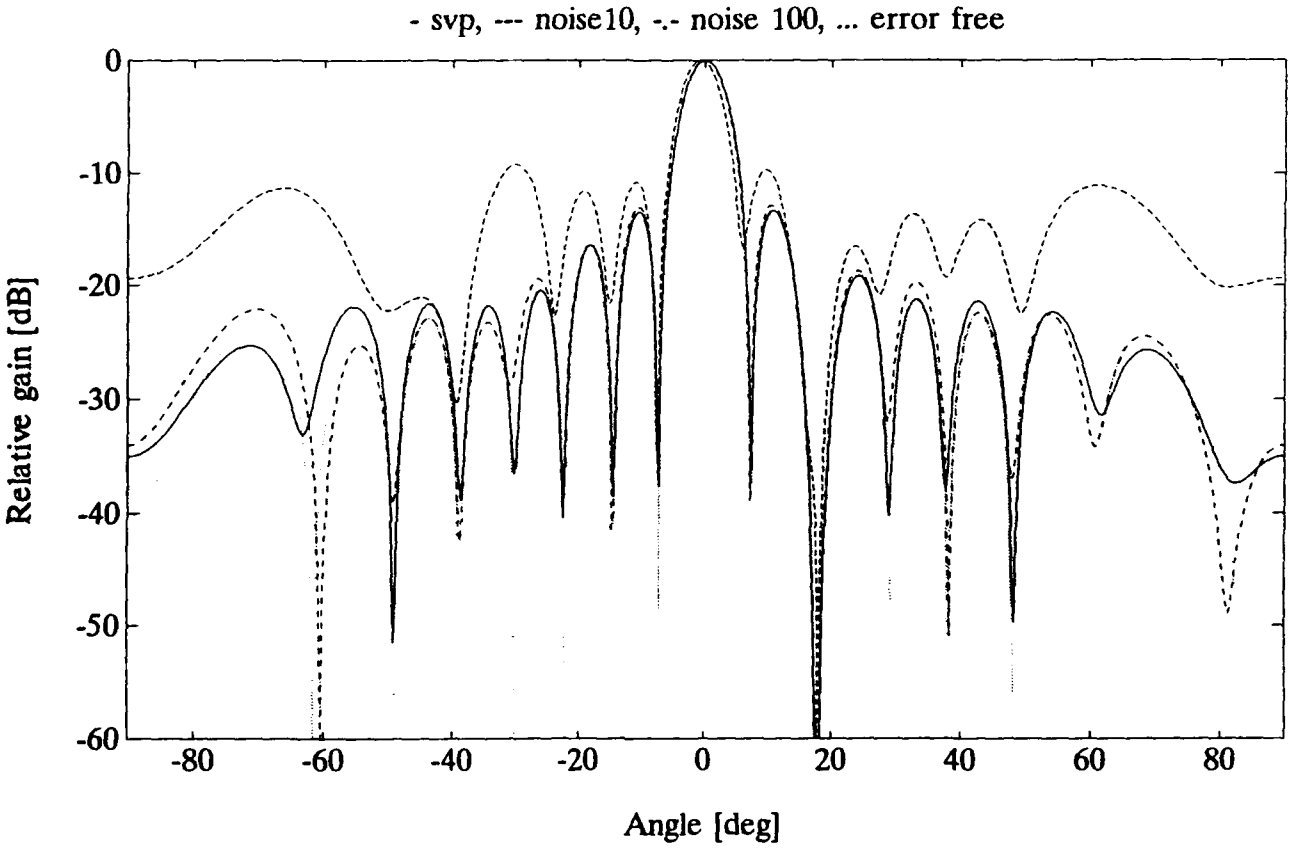

Figure 11. Configuration A, Frost's Algorithm with 0.3 dB and 2° RMS Errors. - - - $\sigma^2_{art} = 10\sigma^2$, -·-·-· $\sigma^2_{art} = 100\sigma^2$, ——— signal subspace steering vector, ····· no errors.

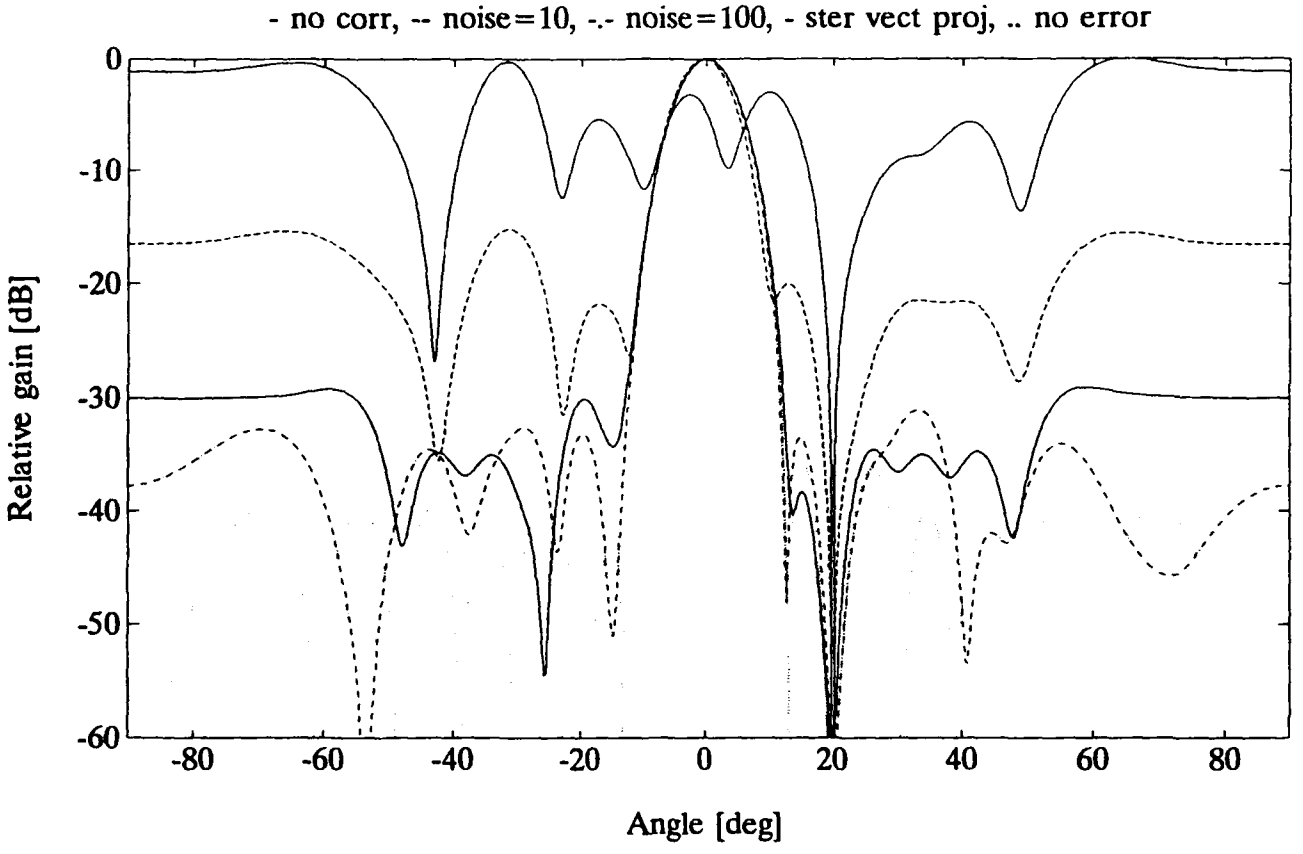

Figure 12. Patterns for Configuration B, Using Frost's Algorithm. RMS errors 0.3 dB and 2°. —— no correction, - - - - $\sigma^2_{art}=10\sigma^2$, ·····- $\sigma^2_{art}=100\sigma^2$, —— signal subspace steering vector, ····· no errors.

$$\hat{\mathbf{x}}_d = \hat{\mathbf{x}}_{d0}\left(1-\left(\quad \varepsilon^2+\delta^2\right)/2\right) + \mathbf{r}\,\frac{\varepsilon+j\delta}{\sqrt{N-1}} \tag{5.10}$$

where $\hat{\mathbf{x}}_{d0}$ is the error free unit signal vector and $\mathbf{r}$ is a random vector where each element, except along $\hat{\mathbf{x}}_{d0}$, has expectation value = 0 and standard deviation = 1. Using this in Eq.(4.6) with $\hat{\mathbf{x}}_{d0} = \hat{\mathbf{s}}_d$ and assuming that the jammer is in the sidelobe region we obtain:

$$\text{Null depth} = \frac{\eta_q(\theta_j) + \dfrac{P_d^2}{\sigma_{art}^4}|r_j|^2\,\dfrac{\varepsilon^2+\delta^2}{N}}{\eta_q(\theta_d)\left[1 + \dfrac{P_j}{\sigma_{art}^2}\langle w_D\rangle\right]^2} \tag{5.11}$$

where $\eta_q(\theta_d)$ and $\eta_q(\theta_j)$ are the quiescent (no jammer nor desired signal) aperture efficiencies and where r_j is the projection $r_j = \mathbf{r}^+\mathbf{D}^{-1}\hat{\mathbf{x}}_j$. When no steering vector projection is used, $|r_j|^2$ has the expectation value:

$$|r_j|^2 = \langle w_D^2\rangle\ . \tag{5.12}$$

When the steering vector method is used the null depth is essentially the same as above because the projection of the steering vector on the jammer vector $\hat{\mathbf{x}}_j$ is not changed apart from a scaling constant close to one (unless the errors are very large). When using the modification of the covariance matrix in Eq. (4.6) we get, since $\mathbf{r}$ is now essentially parallel to $\mathbf{x}_j$, with expected length = 1:

$$|r_j|^2 = \langle w_D\rangle^2 \tag{5.13}$$

For configuration A, where $\langle w_D^2\rangle = \langle w_D\rangle = 1$, Eq. (5.11) gives -98 dB for the direct inversion, -98 dB for the steering vector projection, -97 dB for $\sigma_{art}^2 = 10\ \sigma^2$ and -81 dB for $\sigma_{art}^2 = 100\ \sigma^2$, while the results for configuration B are -97, -98, -97, and -93 dB respectively. These results are also close to the average results from several simulations. Since the null depths depend on one single projection of a random vector on the jammer vector, the results vary significantly between different simulations.

5.5 Effects of Pointing Error

A special type of phase error occurs when there is an antenna pointing error giving a linear phase error in s_d.[10] This will have no effect on the Applebaum pattern shape but will of course give a lower gain in the desired signal direction. For Frost's algorithm there will, as for the random errors, be a stronger effect, which can be partly corrected for in the same way as the random errors.

Figure 13 shows patterns, for configuration A and Frost's algorithm, when there is a 1.6° pointing error (approximately 1/4 of the 3 dB beam width) using no corrections, with $\sigma^2_{ant} = 100\ \sigma^2$, and when using the signal subspace steering vector. The resulting signal direction gains were -24.6, 8.6, and 12.0 dB respectively. The gain values for the direct inversion and for $\sigma^2_{ant} = 100\ \sigma^2$ are also obtained using Eq. (2.26). As seen, the pattern for the projected steering vector will try to follow the true signal. For the Applebaum case, where the beam will point in the steering vector direction, the gain was 11.2 dB.

6. ERRORS IN QUADRATURE SIGNAL GENERATION

In analog quadrature signal (IQ) generation the IF-signal, $a_0\cos((\omega+\omega_{LO})t+\psi)$, is mixed with the LO-signals $\cos(\omega_{LO}t)$ and $\sin(\omega_{LO}t)$ to generate the I and Q video signals $a_I = a_0\cos(\omega t+\psi)$ and $a_Q = a_0\sin(\omega t+\psi)$, which together represent the complex video signal $a = a_0\exp(j(\omega t+\psi))$. There may however be an unbalance in amplitude (α) and phase (β)[13] which, like the gain and phase errors in Section 5, may be corrected for if they are known.[14] Without such correction the signals become:

---

[13] Barton, P., (1980), Digital beam forming for radar, *IEEE Proc.*, Pt. F, Aug., pp. 266-277.

[14] Churchill, F.E., Ogar, G.W., and Thompson, B.J., (1981), The correction of I and Q errors in a coherent processor, *IEEE Trans. on Aerospace and Electronic Systems*, Jan., pp. 131-137.

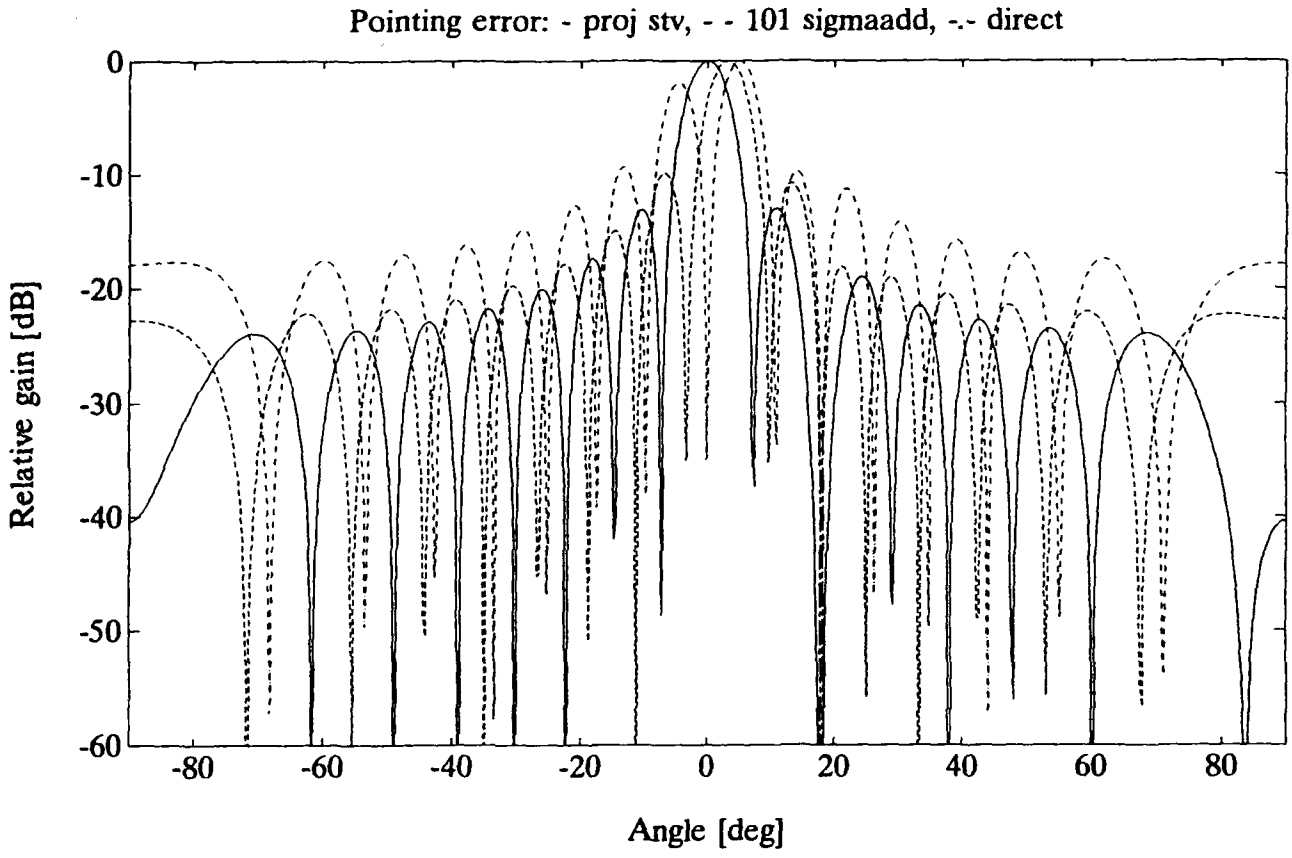

Figure 13. Patterns for Configuration A_2 Using Frost's Algorithm. 1.6° pointing error. -·-·- no correction, - - - $\sigma^2_{art}=100\sigma^2$, ——— signal subspace steering vector

$$a_I = a_0[\cos\Psi + \frac{\alpha}{2}\cos\Psi - \frac{\beta}{2}\sin\Psi]$$
$$a_Q = a_0[\sin\Psi - \frac{\alpha}{2}\sin\Psi - \frac{\beta}{2}\cos\Psi] \quad (6.1)$$

where $\Psi = \omega t + \psi$. The complex signal a_C can now be written as:

$$a_C = a_I + ja_Q = a + \frac{\alpha - j\beta}{2}a^* = a + \frac{\Delta}{2}a^* \quad (6.2)$$

where a is the correct signal and where Δ is the total complex unbalance.

If the video frequency $\omega \neq 0$ the signal consists of the correct signal at ω with phase ψ, $a_0\exp[j(\omega t+\psi)]$, plus an error signal at $-\omega$ with phase $-\psi$, $\frac{\Delta}{2}a_0\exp[-j(\omega t+\psi)]$, that is, corresponding to the image frequency of the I and Q mixers.

Often the errors of the IQ converters are uncorrelated between the channels. Furthermore, if the antenna element modules have large gain and phase shift errors, which are compensated for by using a calibration routine (separating out the ω-component), these corrections will tend to decorrelate otherwise correlated IQ error signals.

For digital IQ generation, using a Hilbert filter to get the Q signal, the result will be the same as in Eq. (6.1) with the difference that the phase error $\beta=0$ and that the amplitude error is given by the length of the filter, and is not a random variable.

6.1 Error Effects on the Quiescent Patterns

For a non-adaptive antenna, an uncorrelated error signal at the image frequency will correspond to an average sidelobe level contribution in the total power pattern of:

$$\text{Sidelobe level} = \frac{1}{4}\frac{<\Delta^2>}{N\ \eta_A} \quad (6.3)$$

while, if the errors are really identical in all channels, the error signals will add to form a sidelobe peak of:

$$\text{Sidelobe peak level} = \frac{1}{4}\,|\Delta|^2 \tag{6.4}$$

Figure 14 shows quiescent patterns for configuration B with Gaussian unbalances having standard deviations of α=0.07 and β=0.07, being equivalent to the 0.3 dB and 2° amplitude and phase errors in Section 5, and giving a sidelobe contribution of -37 dB from Eq. (6.3). The figure shows the separate patterns for the true and the image frequencies and the total pattern valid for ω=0. From this figure we can see that the quiescent pattern for the true frequency is not affected by the IQ errors.

6.2 Pattern Effects for Nonzero Video Frequency

In the adaptive process both frequency components, ω and $-\omega$, are included in the covariance matrix and the antenna will try to cancel both signals so that there will still be a good null in the jammer direction.

The image frequency component of the jammer will give a random signal in each channel with total expected power $P_j<\Delta^2>/4 = N \cdot p_j<\Delta^2>/4$. Using this in Eq. (2.17) we get the average sidelobe level contribution in the true frequency pattern:

$$\text{Sidelobe level} = \frac{1}{\left[N + \dfrac{4\sigma^2}{<\Delta^2>p_j}\right]^2 \eta_A} \tag{6.5}$$

Figure 15 shows the adapted patterns for Applebaum's algorithm, configuration B, when $\omega \neq 0$ and with the same unbalances as in Figure 14, giving -23 dB sidelobes from Eq. (6.5). This average sidelobe contribution has a standard deviation equal to the average itself so that the average sidelobe level can vary considerably between different simulations. The image frequency pattern also has a good null while its average level relative to the true frequency peak is the same as the quiescent pattern sidelobe level, -37 dB from Eq. (6.3).

Since the signals at the true and image frequencies are uncorrelated with totally different phase relations between the channels, two degrees of freedom of the array are needed to get a null at 20° for both frequencies.

Figure 16 shows the same type of patterns for configuration A for both the Applebaum and Frost algorithms, which, as seen, give very similar results. The

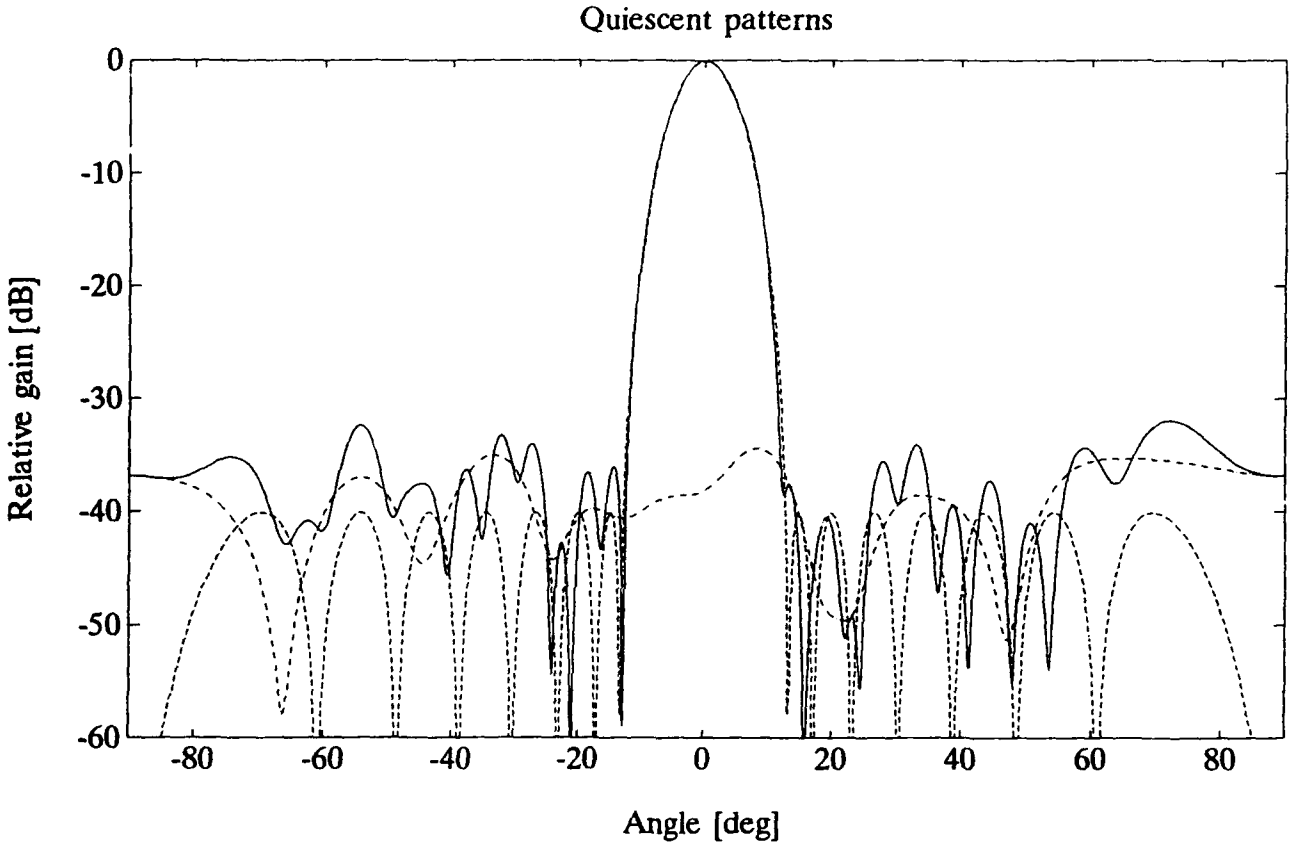

Figure 14. Quiescent Patterns for Configuration B. Uncorrelated errors $\alpha = \beta = 0.07$ (RMS). ——— Total pattern (ω=0), - - - - true frequency, -·-·-·- image frequency.

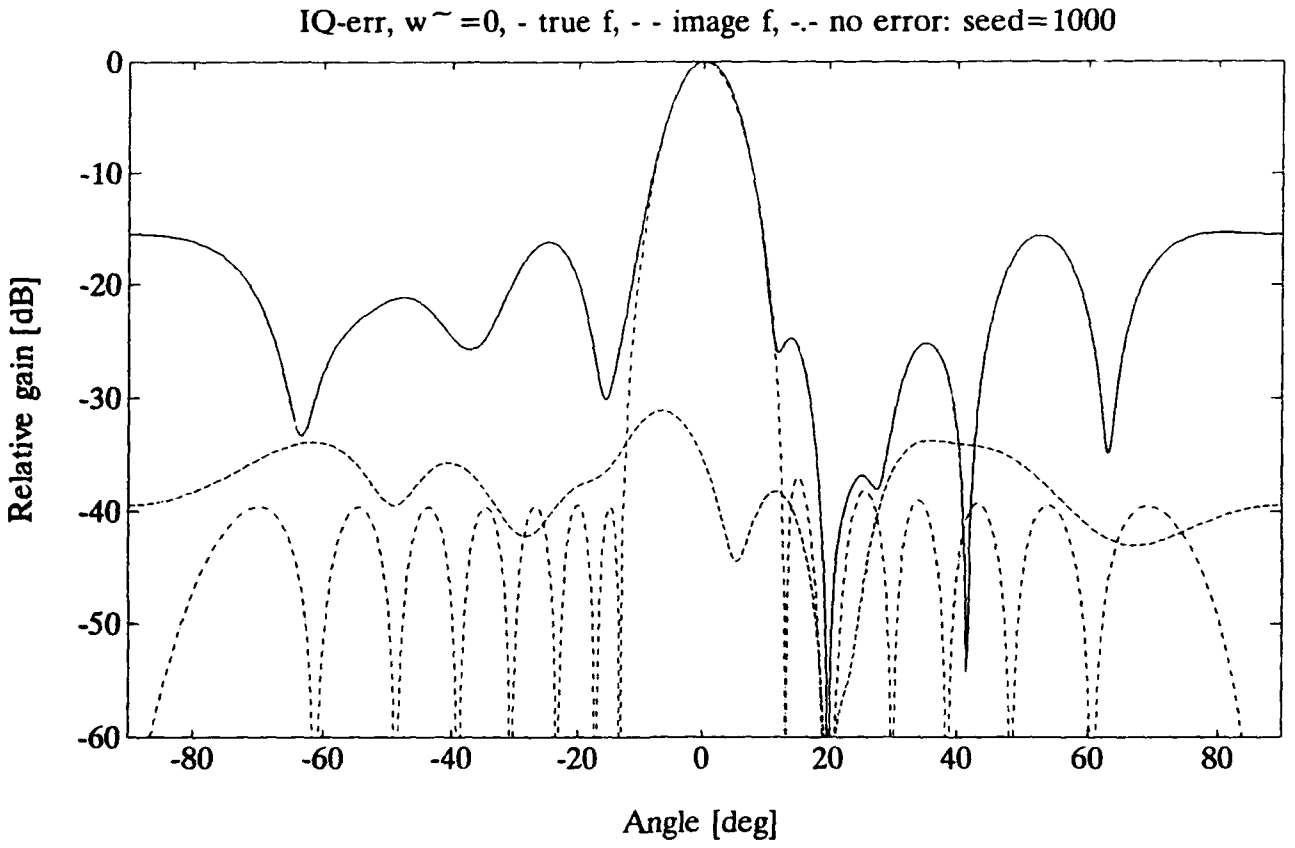

Figure 15. Adapted Patterns for Configuration B, Using Applebaum's Algorithm. Uncorrelated errors $\alpha = \beta = 0.07$ (RMS). ——— true frequency, - - - - image frequency, ····· no IQ errors.

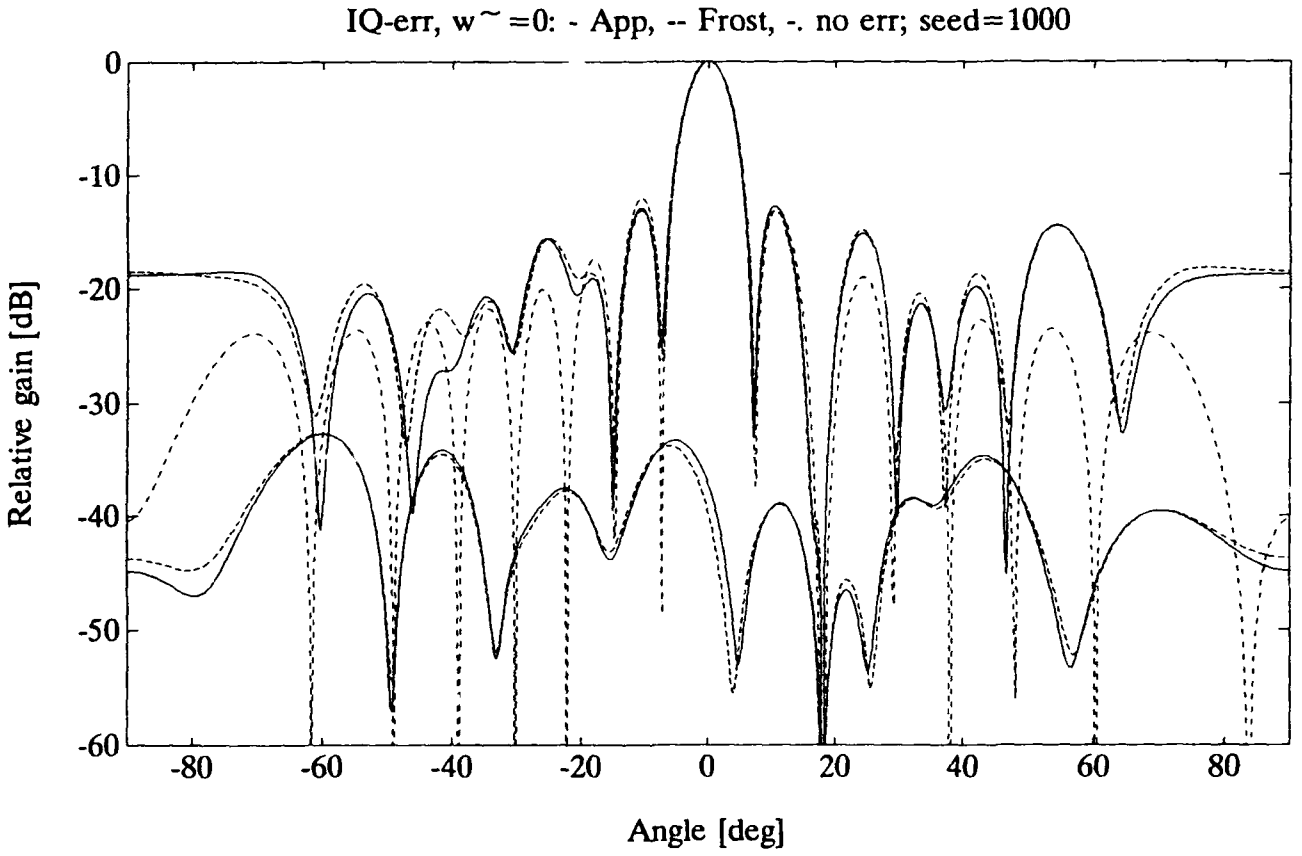

Figure 16. Adapted Patterns for Configuration A, $\omega \neq 0$, True and Image Frequencies. Uncorrelated errors $\alpha = \beta = 0.07$ (RMS). ——— Applebaum's algorithm, - - - - Frost's algorithm, ····· no IQ errors.

reason is that when $\omega \neq 0$, the true and image frequency signals are uncorrelated so that the error of the desired signal, $\Delta/2 \cdot a_d^*$, is simply considered as one more uncorrelated jammer by the Frost algorithm. The sidelobe level contribution due to this signal is also given by Eq. (6.5) with p_j replaced by p_d, giving -34 dB in this configuration. One more degree of freedom will however be required.

6.3 Pattern Effects with Zero Video Frequency

When the video frequency for one of the signals is zero the corresponding error signal $\Delta/2 \cdot a^*$ is completely correlated with the true signal and there will not be any new image signal frequency generated but the signal vector will be deformed as in Section 5.

For the Applebaum case with jammer video frequency $\omega_j = 0$, but desired signal video frequency $\omega_d \neq 0$, the total jammer vector is essentially a plane wave and the effect on the desired signal pattern is very small. The expected sidelobe level contribution is, as seen using Eq. (2.12), approximately given by Eq. (6.3) multiplied by the total quiescent pattern gain in the jammer direction, which is also given by Eq. (6.3) and by the regular sidelobe pattern. Close to the jammer direction however, the true and image frequency patterns will have equal, but nonzero, magnitude with expectation value given by Eq. (6.3). When, in addition, $\omega_d = 0$ the signal pattern will simply be the complex sum of the true and image frequency patterns, as in Figure 14 for the quiescent case, with a null in the jammer direction.

Figure 17 shows simulated patterns for configuration B when using Applebaum's algorithm when $\omega_j = 0$ and $\omega_d \neq 0$.

For the Frost case with $\omega_j = 0$ but $\omega_d \neq 0$ the image frequency signal $-\omega_d$ will still act as a new jammer giving an increased sidelobe level contribution given by Eq. (6.5) with p_j replaced by p_d, giving -34 dB for configuration B. When $\omega_j \neq 0$ but $\omega_d = 0$ the desired signal will be deformed as in Section 5, resulting in a very deformed pattern. The situation $\omega_j = \omega_d = 0$ corresponds to a complete correlation between the desired signal and jammer, a situation which will always give very bad patterns.

Figure 18 shows simulated patterns for configuration B when using Frost's algorithm when $\omega_j = 0$, $\omega_d \neq 0$ and when $\omega_j \neq 0$, $\omega_d = 0$.

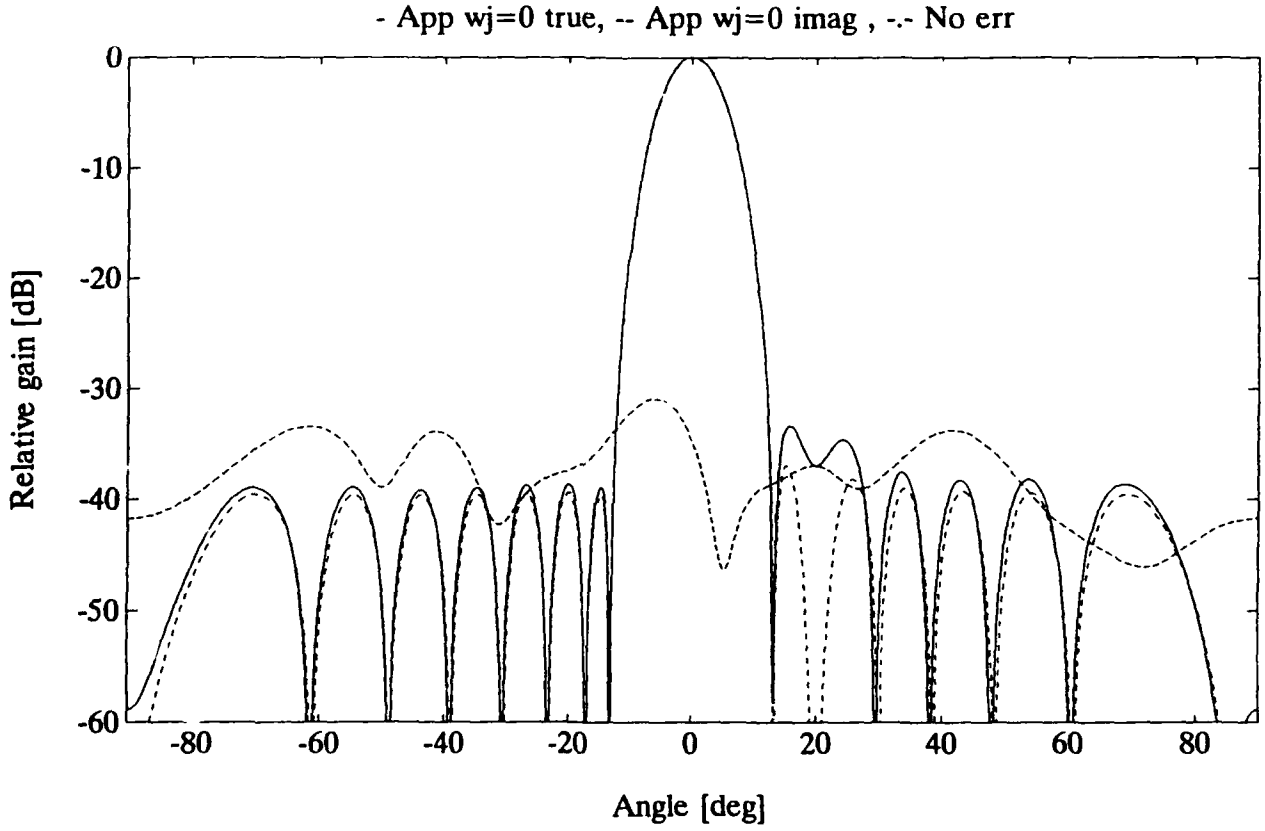

Figure 17. Adapted Patterns for Configuration B, Applebaum's Algorithm. Uncorrelated errors $\alpha = \beta = 0.07$ (RMS). $\omega_j=0$, $\omega_d\neq0$. ——— true frequency, - - - - image frequency, ····· no IQ errors.

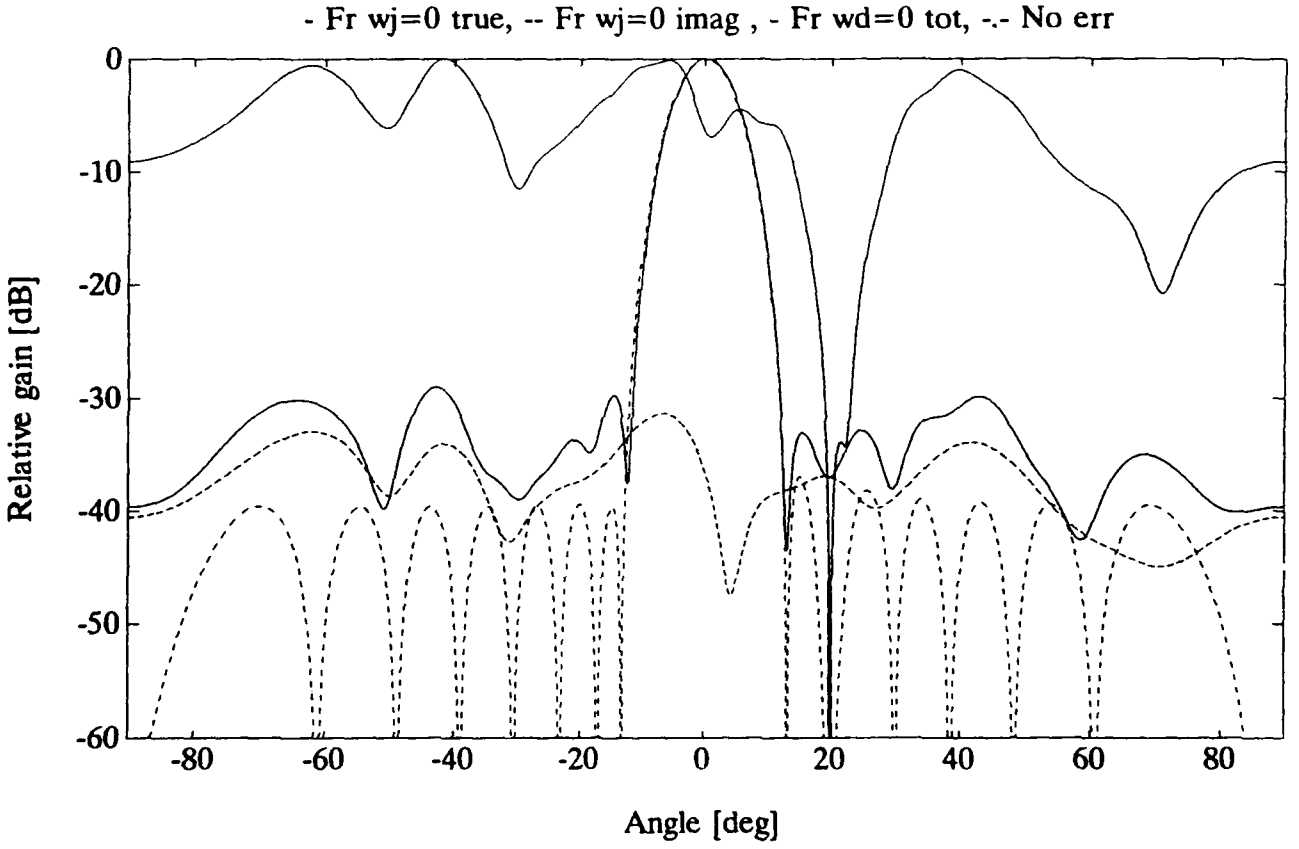

Figure 18. Adapted Patterns for Configuration B, Frost's Algorithm. Uncorrelated errors $\alpha = \beta = 0.07$ (RMS). ——— (lower) true frequency $\omega_J=0$, $\omega_d\neq0$, - - - - image frequency, ——— (upper) total pattern $\omega_J\neq0$, $\omega_d=0$, ····· no IQ errors.

6.4 Pattern Effects for Identical Channels

In Figure 19, the same kind of patterns as in Figures 15 and 17 for Applebaum's algorithm are shown when the errors are identical in all channels, $\alpha = \beta = 0.07$, giving a sidelobe peak of -26 dB from Eq. (6.4). Due to the change in the sign of the phase of the error signal, a signal from direction θ will generate error signals that will look like a plane wave from direction $-\theta$. To illustrate this, the main lobe has been moved to 10° and the jammer to 31°. The image frequency peak at $\theta = -\theta_d = -10^\circ$ is given by Eq. (6.4). There is also an extra null at -31°. This happens because the patterns for the two frequencies are mirror images of each other. Therefore, generating a null at 31° for the image frequency will cause a null for the true frequency at -31°, and vice versa. Two degrees of freedom are still required.

7. DC OFFSET ERRORS

The DC offset errors in the video circuits and A/D converters will, as opposed to the other error types considered, give error signals that are independent of the input signal. Like the gain, phase shift, and IQ errors in Sections 5 and 6, it may be corrected for by a calibration routine. For non-adaptive antennas, random DC-offset errors will give an RMS output signal level, at video frequency $\omega = 0$, relative to the maximum, or saturated, power of:

$$\frac{P_{DCoff}}{P_{max}} = 8 \frac{<\Delta_q^2>}{N \eta_A} 2^{-2b} \tag{7.1}$$

where Δ_q is the ratio of the DC offsets (Δ) and the quantization step (q) in the A/D converters, $<\Delta_q^2>$ is the mean square and b is the number of bits in the A/D converter. Alternatively we can write the DC offset signal to quantization noise ratio as:

$$\frac{P_{DCoff}}{P_{quant}} = 12<\Delta_q^2> \tag{7.2}$$

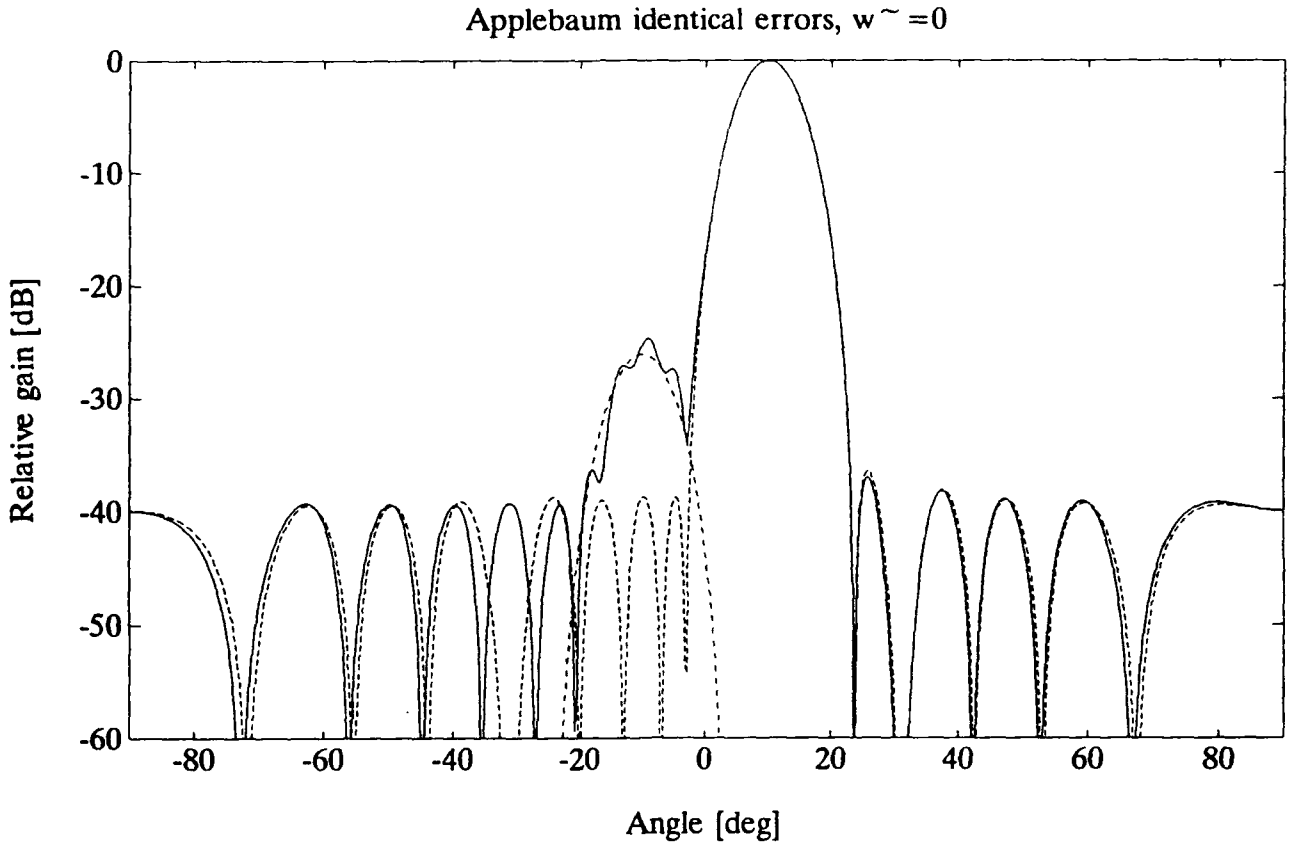

Figure 19. Adapted Patterns for Configuration A, Applebaum's Algorithm. Identical errors $\alpha = \beta = 0.07$. ——— total pattern (ω_d=0), - - - - true frequency, ·-·-·-· image frequency.

If the errors are correlated between the channels, or even identical, the DC offset will look like an incident plane wave, at broadside for identical errors, with a video signal frequency of zero (center of RF band). However, when there are large gain, phase shift, and/or IQ errors that are compensated for, this compensation will tend to decorrelate the DC offset signals.

In adaptive beamforming the DC-offset signal will be considered as a jammer signal by the process and will thus be partly eliminated. This will require one degree of freedom.

Figure 20 shows adapted patterns for configuration B, using Applebaum's criterion, when the RMS value of the offset is equal to the RMS noise voltage at the input of the A/D converters, giving an equivalent total jammer power of $P_j = N\sigma^2$. It is here assumed that the video frequency $\omega \neq 0$ so that the DC offset is uncorrelated with all signals. Patterns for both uncorrelated and identical errors are shown as well as the patterns without any error. Here, the desired signal is at 20° and the jammer at 43° to better show the null at 0° for the pattern with identical errors. This null may give a severe effect when the desired signal is close to broadside. It is seen from Eq. (2.13) with $P_j/\sigma^2 = N\cdot\Delta^2/\sigma_v^2$ that, for large N, Δ must be very small for the corresponding null depth to be small.

For uncorrelated errors there is no null but an increase in sidelobe level. Using Eq.(2.17) with $P_j/\sigma^2 = N\langle\Delta^2\rangle/\sigma_v^2$, where $\langle\Delta^2\rangle$ is the mean square of the DC offset errors, we get the average sidelobe level contribution:

$$\text{Sidelobe level} = \frac{1}{\left[N + \dfrac{\sigma_v^2}{\langle\Delta^2\rangle}\right]^2 \eta} \tag{7.3}$$

giving -23.4 dB in the simulated case. This has a standard deviation equal to the average itself and the sidelobes can thus vary considerably between different simulations. In this -40 dB sidelobe configuration we would thus need at least $\Delta_{RMS} < 0.1\sigma_v$ when the errors are uncorrelated.

Since no additional error signals are introduced by the desired signal the result for the Frost algorithm is the same.

For digital IQ-generation there is no DC-offset error for the Q signal if this is created in a Hilbert filter, stopping any DC component. There may be an offset

error for the I signal (possibly converted to the frequency $-f_S/4$) but as there should never be any DC component in the signals this may be filtered out if necessary.

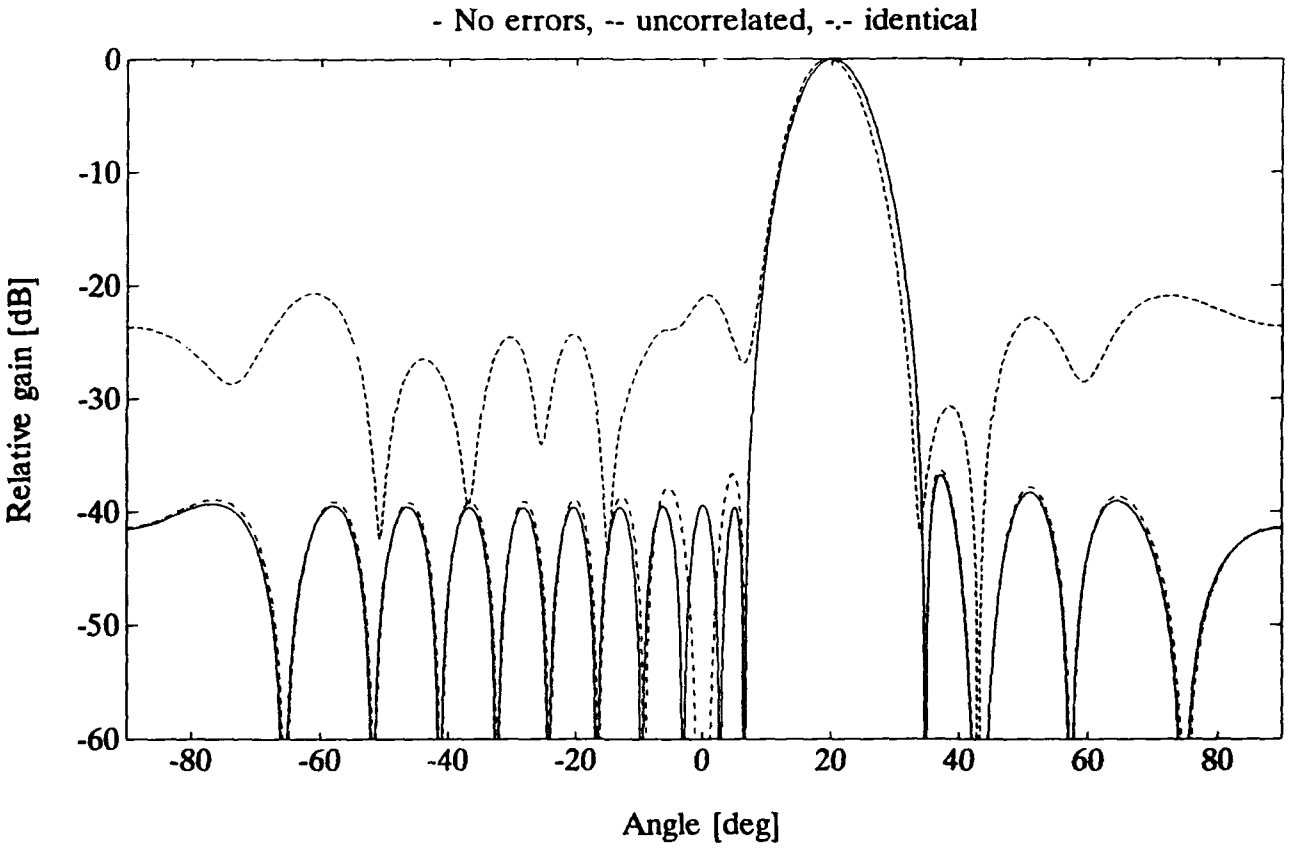

Figure 20. Configuration B with DC-offset Errors, Using Applebaum's Algorithm. ——— $\Delta=0$, - - - - - uncorrelated with $\Delta_{RMS}=\sigma_v$, ·-·-·- identical with $\Delta=\sigma_v$.

8. SAMPLED COVARIANCE MATRIX

In the previous sections it was assumed that the covariance matrix used was the correct one. In practice we don't know the expectation values of the matrix elements, $E\{x_i x_j^*\}$, but only their estimation in the form of mean values over a finite number of time samples, Eq. (2.8). The finite number of samples also means that some nice properties of the covariance matrix used in Section 2, such as no correlation between jammer signals and noise and between noise in different channels, are only approximately true.

8.1 SNIR as a Function of the Number of Samples

In Reed[15] it is shown (see also Reference 3, Chapter 6) that, for Applebaum's criterion, $K \geq 2N\text{-}3$ samples are necessary for the expected SNIR to be within 3 dB of its asymptotic value. For Frost's criterion, more samples, or $K \geq 2N[1 + P_d/(2\sigma^2)]$, are required (Reference 3, Chapter 6).

We can define three different types of SNIR's when using sampled covariance matrices, Φ. For Applebaum's algorithm the "maximized" SNIR is the value of the maximized function, Eq. (2.1). When $\hat{\mathbf{x}}_d = \hat{\mathbf{s}}_d$:

$$\mathrm{SNIR}_{\max} = \frac{\mathbf{w}^T \mathbf{x}_d \mathbf{x}_d^+ \mathbf{w}^*}{\mathbf{w}^T \Phi_A \mathbf{w}^*} = \frac{P_d}{\sigma^2} \hat{\mathbf{s}}_d^+ \Phi_A^{-1} \hat{\mathbf{s}}_d \tag{8.1}$$

which is equal to Applebaum's [4, Eq. (2.43)] in the asymptotic case. This is approximately related to the asymptotic value $\mathrm{SNIR}_{\mathrm{asym}}$, obtained with an infinite number of samples (using the correct asymptotic covariance matrix) by:

$$\mathrm{SNIR}_{\max} \approx \mathrm{SNIR}_{\mathrm{asym}} \frac{1}{1 - \frac{N-1}{K}} \tag{8.2}$$

where K is the number of time samples used in the estimation of Φ_A.

---

[15] Reed, I.S., Mallett, J.D., and Brennan, L.E., (1974), Rapid convergence in adaptive arrays, *IEEE Trans. Aerospace and Electronic Systems*, Nov., pp. 853-863.

The reason that $SNIR_{max} > SNIR_{asym}$ is that the sampled noise, together with the jammers, can be considered as K jammers (one strong and K-1 weak when there is one real jammer). Of these jammers N-1 can be canceled leaving K-(N-1) weak noise-jammers. [Eq. (8.2) can be shown approximately by an series expansion, Eq. (8.8), of Φ^{-1} and it has the correct behavior when $K = N$-1 and when $N = 1$.]

More important is the expected value of the SNIR, obtained when using the calculated weights and random uncorrelated noise. This is, when $\hat{x}_d = \hat{s}_d$, given by, (Reference 15, Eqs. (15) and (18)):

$$SNIR_{exp} = \frac{\mathbf{w}^T \mathbf{x}_d \mathbf{x}_d^+ \mathbf{w}^*}{\mathbf{w}^T \Phi_A \mathbf{w}^*} = SNIR_{asym}\left[1 - \frac{N-1}{K+1}\right] \tag{8.3}$$

8.2 No Signal Incident on the Array

This is the situation for the Applebaum algorithm with no jammer and for the Frost algorithm with no jammer and a very weak desired signal. The effects of sampling will enter as errors in the estimation of the noise covariance matrix. This estimation error is the essential factor determining the resulting sidelobe level and gain loss in the Applebaum case and the absolute sidelobe level in the Frost case. This is also true when there are jammers present except, of course, close to the jammer directions.

That K is large enough to give a good expected SNIR as discussed above does not necessarily mean that the pattern looks good in terms of average sidelobe levels, etc.

If we estimate the elements of the noise covariance matrix using K samples:

$$\Phi_{nij} = \langle x_i x_j^* \rangle = \frac{1}{K} \sum_{k=1}^{K} x_{i,k} x_{j,k}^* \tag{8.4}$$

the following statistical relations can be shown, assuming that $x_{i,k1}$ and $x_{j,k2}$ are uncorrelated when $i \neq j$ or $k1 \neq k2$:

Expectation value: $$E\{\Phi_{nij}\} = \sigma^2 \delta_{ij} \tag{8.5}$$

$$\text{Standard deviation: } \sqrt{\text{Var}\{|\Phi_{nij}|\}} = \frac{\sigma^2}{\sqrt{K}} \tag{8.6}$$

so that:

$$\Phi_n = \sigma^2\left[\mathbf{I} + \frac{1}{\sqrt{K}}\mathbf{R}\right] \tag{8.7}$$

where σ^2 is the noise power in each channel, $\mathbf{I}$ is the identity matrix and $\mathbf{R}$ is a Hermitian matrix where each element is a random variable with expectation value = 0 and standard deviation = 1, (equally distributed in the real and imaginary parts for the off-diagonal elements). As an example, Figure 21 shows results from a simulation with two complex, normally distributed, random variables with $\sigma^2 = 1$. The upper left figure shows the magnitude of the mean values as function of the number of samples, whereas the upper right shows the magnitude of the variances or the mean square sum, Φ_{n11} and Φ_{n22}, and the lower left shows the magnitude of their covariance, $|\Phi_{n21}|$. Lines for the expected values and the standard deviations are also shown.

As seen, the elements in the covariance matrix approach their asymptotic values rather slowly. If $\sqrt{K}$ is large enough so that the eigenvalues of $\mathbf{R}/\sqrt{K}$, which are of the order $\sqrt{N}/K$, are less than 1, the inverse can be found using the series expansion (Reference 2, Appendix 1):

$$[\mathbf{I} + \mathbf{A}]^{-1} = \mathbf{I} - \mathbf{A} + \mathbf{A}^2 - \mathbf{A}^3 + \mathbf{A}^4 - \ldots. \tag{8.8}$$

This gives the inverse of the covariance matrix to the first order:

$$\Phi_n^{-1} \cong \frac{1}{\sigma^2}\left[\mathbf{I} - \frac{1}{\sqrt{K}}\mathbf{R}\right] \tag{8.9}$$

and the resulting complex conjugate of the quiescent Applebaum weight vector:

$$\mathbf{w}_q^* = \mathbf{w}_{qa}^* - \frac{1}{\sqrt{K}}\mathbf{R}\cdot\mathbf{w}_{qa}^* \sim \mathbf{s}_d - \frac{1}{\sqrt{K}}\mathbf{R}\cdot\mathbf{s}_d \tag{8.10}$$

where $\mathbf{w}_{qa}$ is the asymptotic quiescent weight vector. Thus the weight vector $\mathbf{w}_q$

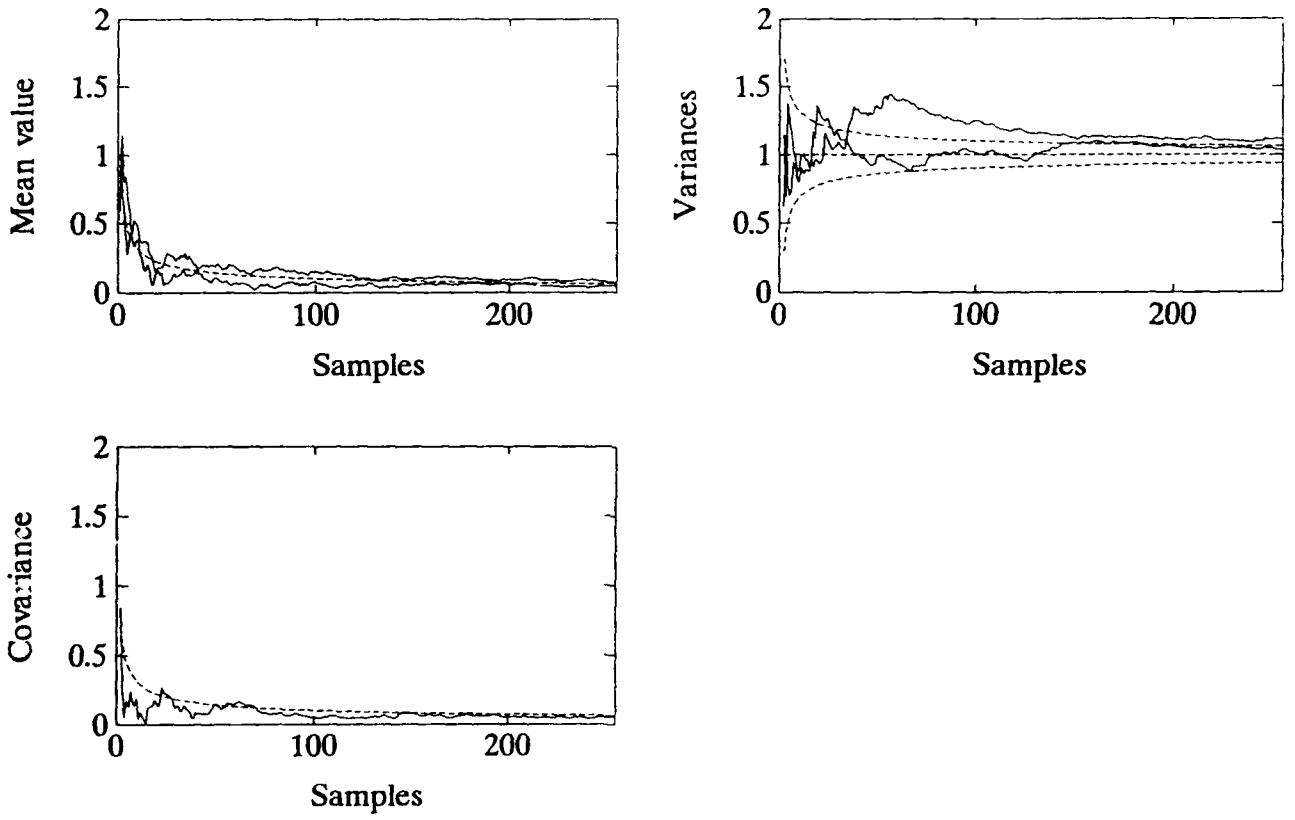

Figure 21. Two, Normally Distributed, Simulated Sequences. a) Mean values, b) Variances, c) Covariance. - - - - Expectation value and standard deviations.

will, to the first order, have a normalized mean square error, Eq. (A.3) of:

$$\langle \Delta_1^2 \rangle = N/K \tag{8.11}$$

which will result in a mean sidelobe level, Eq. (A.6), of:

$$\text{Sidelobe level} = \frac{\langle \Delta_1^2 \rangle}{N\eta_A} = \frac{1}{K\eta_A} . \tag{8.12}$$

The effects of the random matrix elements can be decreased by adding an artificial noise covariance matrix $\sigma_{art}^2 \mathbf{I}$, Eq. (2.40), increasing the magnitude of the diagonal elements. This will make the relative standard deviation of the matrix elements a factor $(1 + \sigma_{art}^2/\sigma^2)$ smaller. The results for the normalized errors and sidelobe levels will still apply if we simply replace K by:

$$K_{art} = K(1 + \sigma_{art}^2/\sigma^2)^2 \tag{8.13}$$

Since the SNIR when there are no jammers is equal to the signal power per channel times the antenna gain we can combine the rigorous result in Eq. (8.3) with the gain loss in Eq. (A.2) to get a higher order, "rigorous", weight error. (The result in Eq. (8.3) was derived in Reference 15 for $\hat{s}_d = \hat{x}_d$ or $\eta_A(\theta_d) = 1$.) The result of this is:

$$\langle \Delta_R^2 \rangle = \frac{N}{K + 1 - N} \approx \frac{\langle \Delta_1^2 \rangle}{1 - \langle \Delta_1^2 \rangle} . \tag{8.14}$$

The antenna aperture efficiencies obtained from several simulations are shown in Figure 30 together with the efficiency obtained from Eqs. (A.2) and (8.14):

$$G(\theta_d) = N\,\eta(\theta_d) = N\eta_0(\theta_d)\left[1 - \frac{N - 1/\eta_0(\theta_d)}{K + 1}\right] \tag{8.15}$$

where $G(\theta_d)$ is the antenna gain, $\eta(\theta_d)$ is the resulting aperture efficiency and $\eta_0(\theta_d)$ is the asymptotic efficiency.

The absolute, sampling induced, sidelobe gain is, from Eq. (A.2), (see also Reference 8):

$$\text{Sidelobe gain} = \frac{N}{K+1} \tag{8.16}$$

and the relative sidelobe level is, from Eq. (A.5):

$$\text{Sidelobe level} = \frac{1}{\eta(\theta_d)(K+1)} = \frac{1}{\eta_0(\theta_d)(K+1-N)+1} \tag{8.17}$$

This and the results from several simulations are shown in Figure 31.

Figure 22 shows adapted patterns for basic configuration B using Applebaum's algorithm and K = 32 (=2N), 128, 512 and 2048 samples together with the asymptotic ($K = \infty$) result. As seen, the mean sidelobe level is high for the lower K. Equation (8.17) gives sidelobe contributions of -11, -19, -26, and -32 dB respectively.

Figure 23 shows the results with K=32 when using σ^2_{art} = 0, 10 σ^2 and 100 σ^2 respectively together with the asymptotic pattern. The sidelobe contributions from Eq. (8.17) with the modification of Eq. (8.13) are -11, -35, and -54 dB respectively.

The Frost case with a very weak signal is, as was shown in Section 4, very similar to the Applebaum case with the difference that the tapered quiescent weights can be obtained from a modification of the covariance matrix, Eq. (4.2), rather than from a tapered steering vector.

Applying Eq. (4.2) to Eq. (8.7) we get to the first order:

$$\Phi_{nF}^{-1} = \frac{\mathbf{D}^{-1}}{\sigma^2_{art}}\left[\mathbf{I} - \frac{\sigma^2}{\sigma^2_{art}}\frac{\mathbf{D}^{-1}\mathbf{R}}{\sqrt{K}}\right] \tag{8.18}$$

to be compared with Eq. (8.9) for the Applebaum case. The gain and sidelobe level results for the Applebaum case above can then still be used if K is replaced by:

$$K_D = K\,\frac{\sigma^4_{art}}{\langle w_D^2\rangle \sigma^4} \tag{8.19}$$

where $\langle w_D^2\rangle$ is the mean square of the elements in $\mathbf{D}^{-1}$.

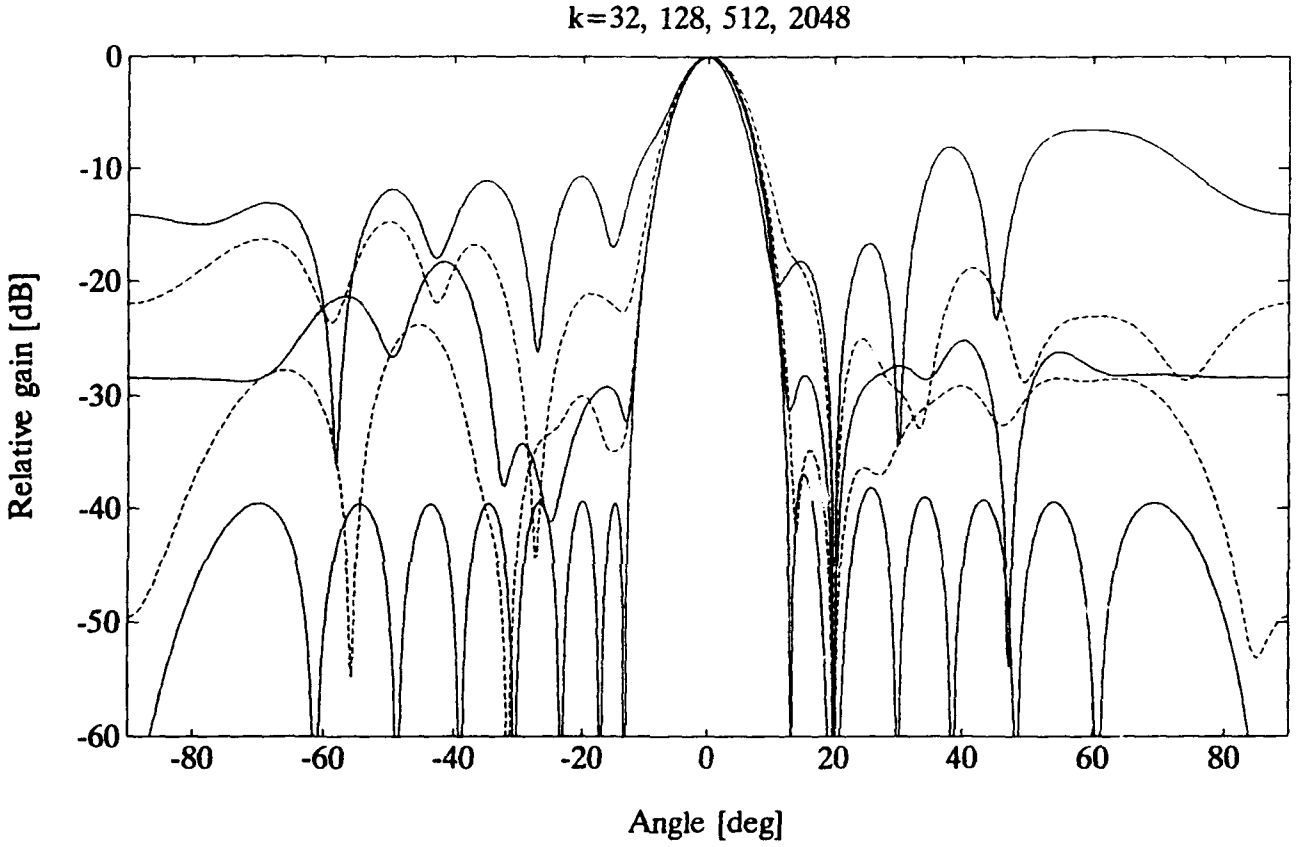

Figure 22. Adapted Patterns for Configuration B, Using Applebaum's Algorithm. K = 32, 128, 512, 2048 and ∞.

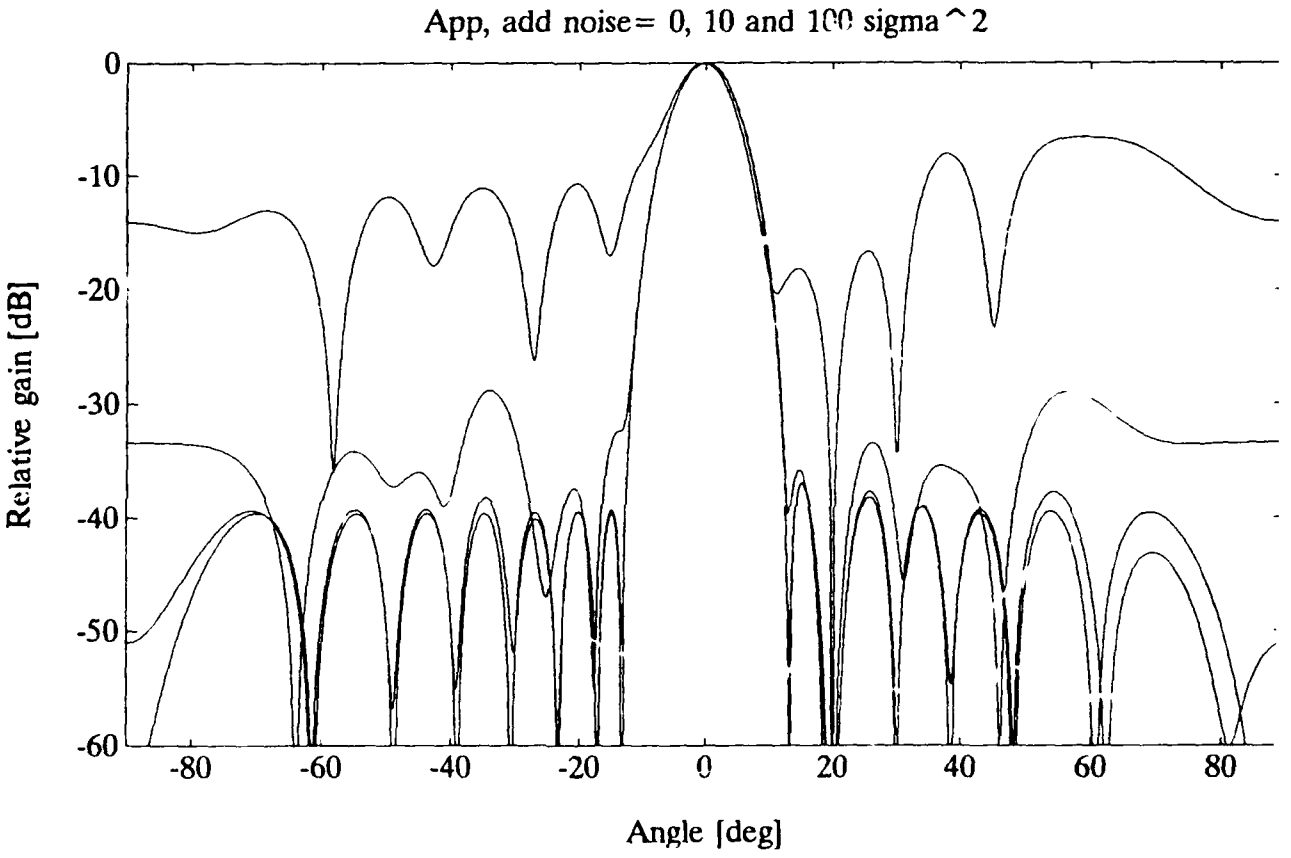

Figure 23. Configuration B_2 Applebaum's Algorithm. Asymptotic ($K=\infty$) and K = 32 with added artificial noise σ^2_{an} = 0, 10 σ^2 and 100 σ^2.

The reason for the pattern degradation in the basic algorithm is the random matrix **R**, which makes the noise eigenvalues nonequal. One method to partially solve the problem is to calculate the eigenvalues and eigenvectors and try to identify the noise eigenvalues, which are of the order of σ^2 with standard deviation $\sigma^2\sqrt{N/K}$, and set them to their "correct" value σ^2, or to some other constant value, Eq. (2.39). As the noise eigenvectors only have to span the noise space they can still be used as they are.

Since the signal eigenvalues are often significantly larger than the noise eigenvalues the identification of the eigenvalues is often not very difficult. When the jammers are so weak that this is not the case they are probably not so important to cancel out. With this method, the error induced sidelobes will be very small and the gain is essentially equal to the error free gain.

Figure 24 shows adapted patterns using K=32 samples, when setting all eigenvalues less than $3\sigma^2$ equal to σ^2, (the largest noise eigenvalue in this example was $2.1\sigma^2$). As seen there is a big improvement in the sidelobe region. This method is also discussed in Reference 7.

8.3 The Applebaum Case with One Jammer

Now the sampled covariance can be written:

$$\Phi_A = \mathbf{x}_{Kj}\mathbf{x}_{Kj}^{+} + \Phi_{n\perp} = (\mathbf{x}_j + \mathbf{n}_{\|})(\mathbf{x}_j + \mathbf{n}_{\|})^{+} + \mathbf{n}_{\perp}\mathbf{n}_{\perp}^{+} \tag{8.20}$$

where $\mathbf{x}_{Kj}$ is a "total" jammer vector, being the sum of the true jammer vector, $\mathbf{x}_j$, and a noise vector, $\mathbf{n}_{\|}$, containing the time correlation between the K noise samples in each channel and the jammer. The noise vector, $\mathbf{n}_{\perp}$, is the rest of the true noise vector, $\mathbf{x}_n = \mathbf{n}_{\|} + \mathbf{n}_{\perp}$, and is uncorrelated with $\mathbf{x}_j$. The matrix $\Phi_{n\perp} = \mathbf{n}_{\perp}\mathbf{n}_{\perp}^{+}$ is equal to the sampled noise covariance matrix, Φ_n, to the order $\sigma^2/\sqrt{K}$. (The elements are slightly smaller however, giving a slightly smaller gain decrease so that, including the jammer signal, the expected SNIR is still given by Eq. (8.3).) The elements of $\mathbf{n}_{\|}$ will have expectation value zero and standard deviation $\sigma/\sqrt{K}$. Using Eq. (2.10) with $\mathbf{A} = \Phi_n$, or Eq. (2.27), the weights for one jammer are:

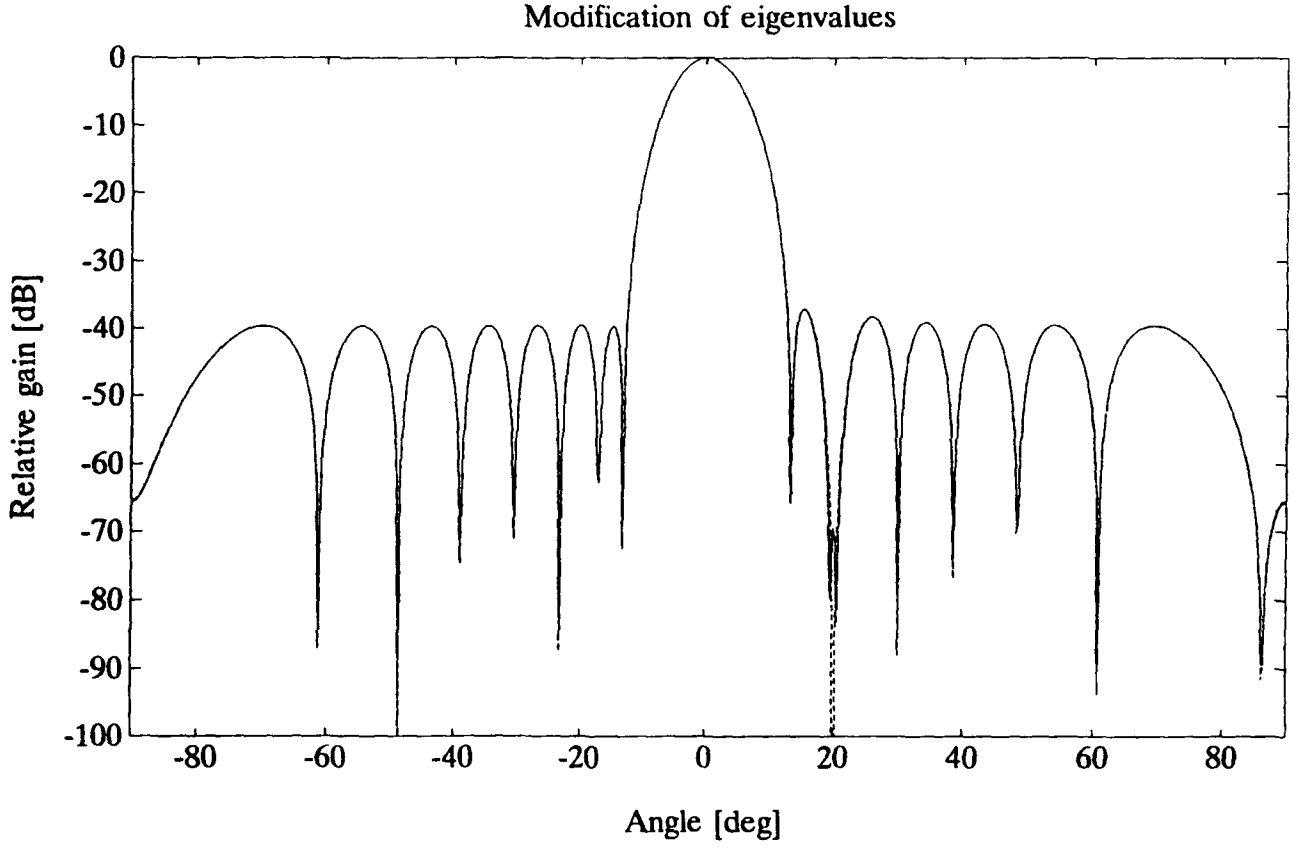

Figure 24. Patterns for Configuration B, Using Applebaum's Algorithm. K = 32. —— All eigenvalues less than $3\sigma^2$ set to σ^2. - - - Asymptotic pattern.

$$\mathbf{w}^* = \left[I - \frac{P_K \Phi_n^{-1} \hat{\mathbf{x}}_{Kj} \hat{\mathbf{x}}_{Kj}^+}{1 + P_K \hat{\mathbf{x}}_{Kj}^+ \Phi_n^{-1} \hat{\mathbf{x}}_{Kj}} \right] \cdot \mathbf{w}_q^* \tag{8.21}$$

where $P_K = P_j + N\sigma^2/K$ is the total power in the total jammer vector $\mathbf{x}_{Kj}$. This gives a quiescent pattern, with sampling induced sidelobes and a "jammer plus correlated noise" cancellation beam.

If we assume that there is a perfect null in the $\mathbf{x}_{Kj} = \mathbf{x}_j + \mathbf{n}_{||}$ "direction", the null depth in the true jammer direction, $\hat{\mathbf{x}}_j$, is obtained by projecting the $\mathbf{n}_{||}$ vector onto the w vector. Assuming $\mathbf{n}_{||}$ is a random vector in element space, the expected result is:

$$\text{Jammer gain} \quad = G(\theta_j) = \frac{N}{KP_j}\frac{\sigma^2}{} = \frac{\sigma^2}{Kp_j} \tag{8.22}$$

where p_j is the jammer power per channel. This jammer gain has a standard deviation approximately equal to the expectation value itself. The null depth is obtained from Eqs. (8.22) and (8.15).

$$\text{Null depth} = \frac{G(\theta_j)}{G(\theta_d)} = \frac{\sigma^2}{KP_j\,\eta(\theta_d)} \tag{8.23}$$

This is illustrated in Figure 32.

For more than one jammer the result is essentially the same because nulling any linear transformation of the jammers (to get uncorrelated jammers) will also null each separate jammer.

In the simulations shown in Figure 22 the null depth for $K = 32 = 2N$ was -67 dB while Eq. (8.23) gives -63 dB.

When artificial noise is added Eqs. (8.22) and (8.23) are still valid, using the true σ^2 and K, but the aperture efficiency, $\eta(\theta_d)$, is now obtained from Eq. (8.15) using K_{art} from Eq. (8.13). In the simulations in Figure 23 the null depths are -73, -71, and -70 dB respectively while Eq. (8.23) gives -66 to -63 dB. This is also illustrated in Figure 22.

In the patterns in Figure 24 where the noise eigenvalue modification has been

used, the absolute jammer gain is essentially the same as in Figure 22. However, since the array gain has increased, the null depth, Eq. (8.23) has improved. This is further illustrated in Figure 32.

When using this eigenvalue modification method, even fewer than $K = 2N$ samples may be used because the random matrix $\mathbf{R}$ is, to a large extent, eliminated and the sampling only enters through the projected noise vector $\mathbf{n}_{\perp\!\!\!\perp}$. Figure 25 shows patterns for configuration B using Applebaum's algorithm, with K = 32, 16, and 8 samples together with the asymptotic, $K = \infty$, pattern. As seen, all patterns have good sidelobes. The null depths have, however, decreased to -71, -62, and -55 dB in these simulations as compared to the asymptotic -144 dB and -66, -63, and -60 dB from Eq. (8.23) with $\eta(\theta_d)$ being the error free efficiency.

In the basic algorithm the reason for the loss of expected SNIR is mainly loss of antenna gain, while the null depths are usually good. When using the noise eigenvalue modification, and when adding artificial noise with sufficient magnitude, the antenna gain is very close to the error free gain and the reason for the loss of SNIR is the decreased null depth, increasing the received jammer signal. Using Eq. (8.22) for the expected jammer gain, the expected SNIR becomes for these methods, when there is one jammer present, approximately:

$$\mathrm{SNIR}_{\mathrm{exp}}(G=G_{\mathrm{asym}}) \approx \mathrm{SNIR}_{\mathrm{asym}} \frac{K}{1+K} \tag{8.24}$$

In the simulations in Figure 25 the expected SNIR decreases to 20.8, 20.5, and 19.4 dB compared to the asymptotic 20.9 dB and 20.7, 20.6, and 20.3 dB from Eq. (8.24). Like the null depth, the SNIR has a large standard deviation so that for few samples these numbers may vary significantly from simulation to simulation. Simulated SNIR results are illustrated in Figure 33.

8.4 The Frost Case with Desired Signal But No Jammer

Here the situation is similar to the Applebaum case with one jammer. The total sampled signal vector $\mathbf{x}_{Kd} = \mathbf{x}_d + \mathbf{n}_{\perp\!\!\!\perp}$ is now nearly, but not exactly, parallel to the true signal vector $\hat{\mathbf{x}}_d$ (which is here assumed equal to the steering vector $\hat{\mathbf{s}}_d$) so that a null will not result but the array gain may be decreased significantly for small K.

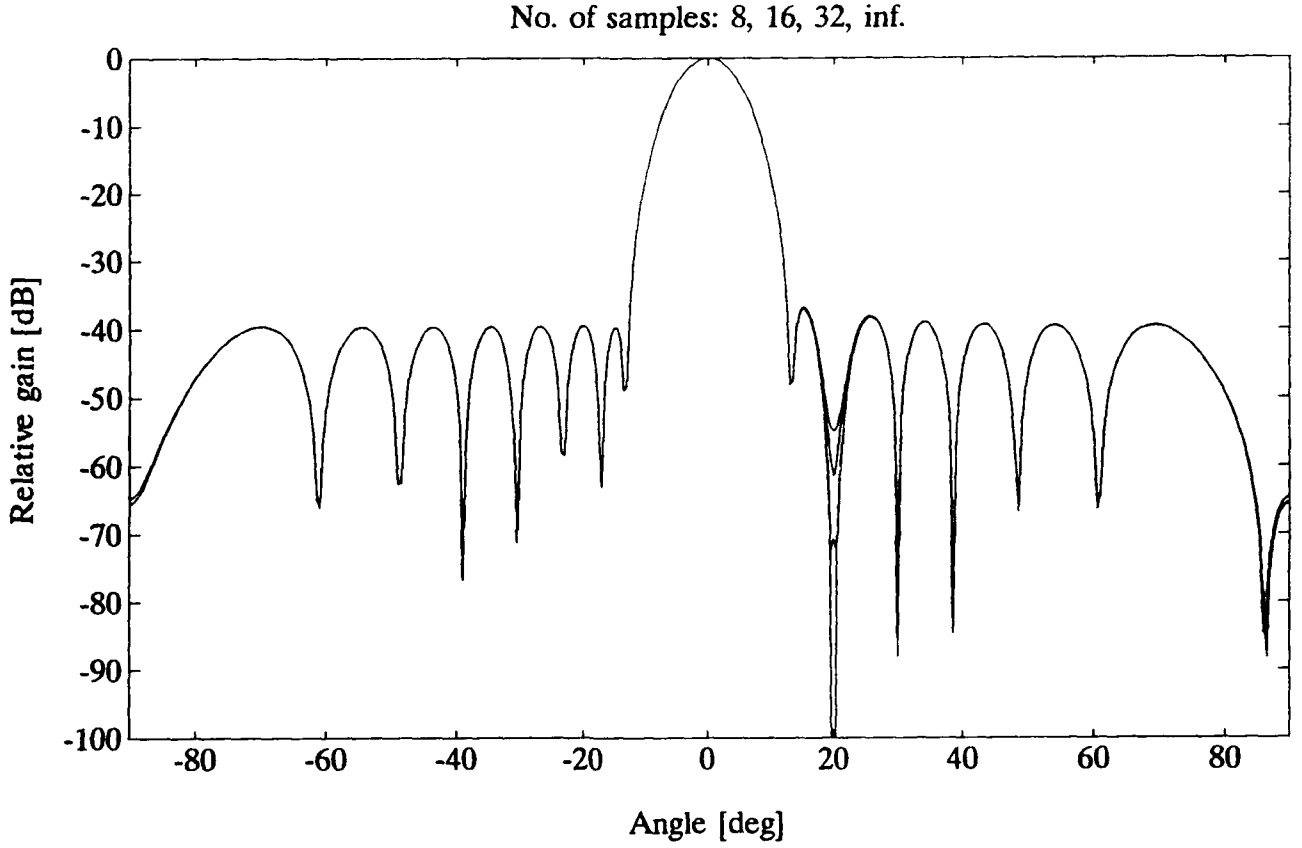

Figure 25. Patterns for Configuration B, Using Applebaum's Algorithm. K = 32, 16, 8 and ∞. All eigenvalues less than $3\sigma^2$ set to σ^2.

The random part of the remaining covariance matrix $\Phi_{n\perp} = \mathbf{n}_\perp \mathbf{n}_\perp^\dagger$ will also give a gain decrease as discussed in Section 8.2 and, as seen from Eq. (8.21), the total aperture efficiency is essentially the product of the quiescent efficiency, affected by the errors in $\Phi_{n\perp}$ and obtained from Eq. (8.15), and an efficiency affected by the error, $\mathbf{n}_\parallel$, in $\mathbf{x}_{Kd}$:

$$G_F = N\eta_q\eta_{||} \tag{8.25}$$

Using the fact that $\mathbf{n}_{||}$ is a random vector with standard deviation $\sigma/\sqrt{K}$ in all elements we can write the unit total signal vector $\hat{\mathbf{x}}_{Kd} = \mathbf{x}_{Kd}/|\mathbf{x}_{Kd}|$ to second order in $\sigma/\sqrt{KP_d}$:

$$\hat{\mathbf{x}}_{Kd} = \hat{\mathbf{x}}_d\left[1 - \frac{N-1}{2}\frac{\sigma^2}{KP_d}\right] + \mathbf{r}\frac{\sigma}{\sqrt{KP_d}} \tag{8.26}$$

where $\mathbf{r}$ is a random vector where each element, except along $\hat{\mathbf{x}}_d$, has expectation value = 0 and standard deviation = 1. Since the errors are included in the adaptive process the resulting weight errors will be correlated and Eq. (A.2) cannot be used in the main beam region. Instead we can, if we consider the total signal $\mathbf{x}_{Kd}$ as a jammer, get the array gain in the true signal direction, $\hat{\mathbf{x}}_d$, by using Eq. (2.15). The quiescent aperture efficiency, $\eta_q(\theta_j)$, in the "jammer" direction, $\hat{\mathbf{x}}_{Kd}$, is now for uncorrelated channels obtained using Eq. (8.26). When $\hat{\mathbf{x}}_d = \hat{\mathbf{s}}_d$:

$$\eta_{qKd} = |\hat{\mathbf{s}}_d^+\cdot\hat{\mathbf{x}}_{Kd}|^2 = 1 - \frac{\sigma^2}{KP_d}(N-1) \tag{8.27}$$

so that from Eq. (2.15):

$$G_F(\theta_d) = N\eta(\theta_d) = N\eta_q(\theta_d)\frac{\left(1 + \frac{N-1}{K}\right)^2}{1 + \frac{N-1}{K}(P_d/\sigma^2+2)} \tag{8.28}$$

where $\eta_q(\theta_d)$ is the quiescent efficiency in the true signal direction, dependent on the errors in $\Phi_{n\perp}$ and is obtained from Eq. (8.15). Since we have neglected the effects of the errors in $\Phi_{n\perp}$ on $\eta_{||}$, Eq. (8.25), this should be considered as a first order approximation for $G_F(\theta_d)$, valid for not too small K. Also, since we have approximated the expectation value of a ratio by the ratio of the expectation values, we can expect some errors, especially for small K.

When the covariance matrix modification for the Frost algorithm, Eq. (4.2), is used, we get, using Eqs. (4.3) and (8.26) and the same method as when deriving

Eqs. (2.15) and (8.28):

$$G_F(\theta_d) = N\eta(\theta_d) = N\eta_q(\theta_d) \frac{\left[1 + \langle w_D \rangle \frac{N-1}{K}\right]^2}{1 + \langle w_D \rangle \frac{N-1}{K}(\langle w_D \rangle P_d/\sigma^2 + 2)} \tag{8.29}$$

where $\langle w_D \rangle$ is the mean value of the elements in $\mathbf{D}^{-1}$ and where $\eta_q(\theta_d)$ is obtained from Eqs. (8.15) and (8.19). When $\sigma_{art}^2 \neq \sigma^2$, $\langle w_D \rangle$ should be replaced by $\langle w_D \rangle \cdot \sigma^2/\sigma_{art}^2$. Simulated and calculated curves for the aperture efficiency $\eta(\theta_d)$ are shown in Figure 30.

The error in the unit signal vector will also give an increased sidelobe level. In the sidelobe region the errors will add incoherently and Eq. (A.2) can be used. As above, we can separate the weight errors into those due to an incorrectly sampled noise covariance matrix and those due to an incorrect steering vector being nonparallel to the total signal vector $\hat{\mathbf{x}}_{Kd}$. From Eqs. (2.24) and (2.25) the total weight error can be written as:

$$\langle \Delta^2 \rangle = \langle \Delta_n^2 \rangle + \langle \Delta_s^2 \rangle + \langle \Delta_n^2 \rangle \langle \Delta_s^2 \rangle \tag{8.30}$$

where $\langle \Delta_n^2 \rangle$ is due to the error in $\Phi_{n\perp}$ and is given by Eq. (8.14) together with Eq. (8.19), and where $\langle \Delta_s^2 \rangle$ is due to the steering vector error. Using Eq. (8.26) in Eq. (2.25) we get:

$$\langle \Delta_s^2 \rangle = \frac{P_d}{\sigma^2} \frac{N-1}{K} \tag{8.31}$$

where K should be replaced by K_D from Eq. (8.19) if the covariance matrix modification, Eq. (4.2) is used.

The relative sidelobe level is obtained by using Eq. (A.7) together with Eqs. (8.28) or (8.29). This is illustrated in Figure 31.

Figure 26 shows patterns for configuration B with $\sigma_{art}^2 = \sigma^2$, $10\sigma^2$ and $100\sigma^2$. The diagonal elements are given by $\mathbf{D}_{ii}$=1/(Chebyshev weights) with w_{Dmax}=1. The sidelobe level contributions, calculated as described above, are -17 dB for $\sigma_{art}^2 = 10\sigma^2$ and -37 dB for $\sigma_{art}^2 = 100\sigma^2$.

8.5 The Frost Case with Desired Signal and Jammer

Due to the sampling, both the thermal noises and the desired signal will be partly correlated with the jammer, and the covariance matrix can be written as:

$$\Phi = \mathbf{x}_{kj}\mathbf{x}_{kj}^{+} + \mathbf{x}_{kd}\mathbf{x}_{kd}^{+} + \Phi_{n\perp}$$

$$= (\mathbf{x}_j + \mathbf{x}_{d\parallel} + \mathbf{n}_{\parallel j})\,(\mathbf{x}_j + \mathbf{x}_{d\parallel} + \mathbf{n}_{\parallel j})^{+} + (\mathbf{x}_{d\perp} + \mathbf{n}_{\parallel d})(\mathbf{x}_{d\perp} + \mathbf{n}_{\parallel d})^{+} + \mathbf{n}_{\perp}\mathbf{n}_{\perp}^{+}. \qquad (8.32)$$

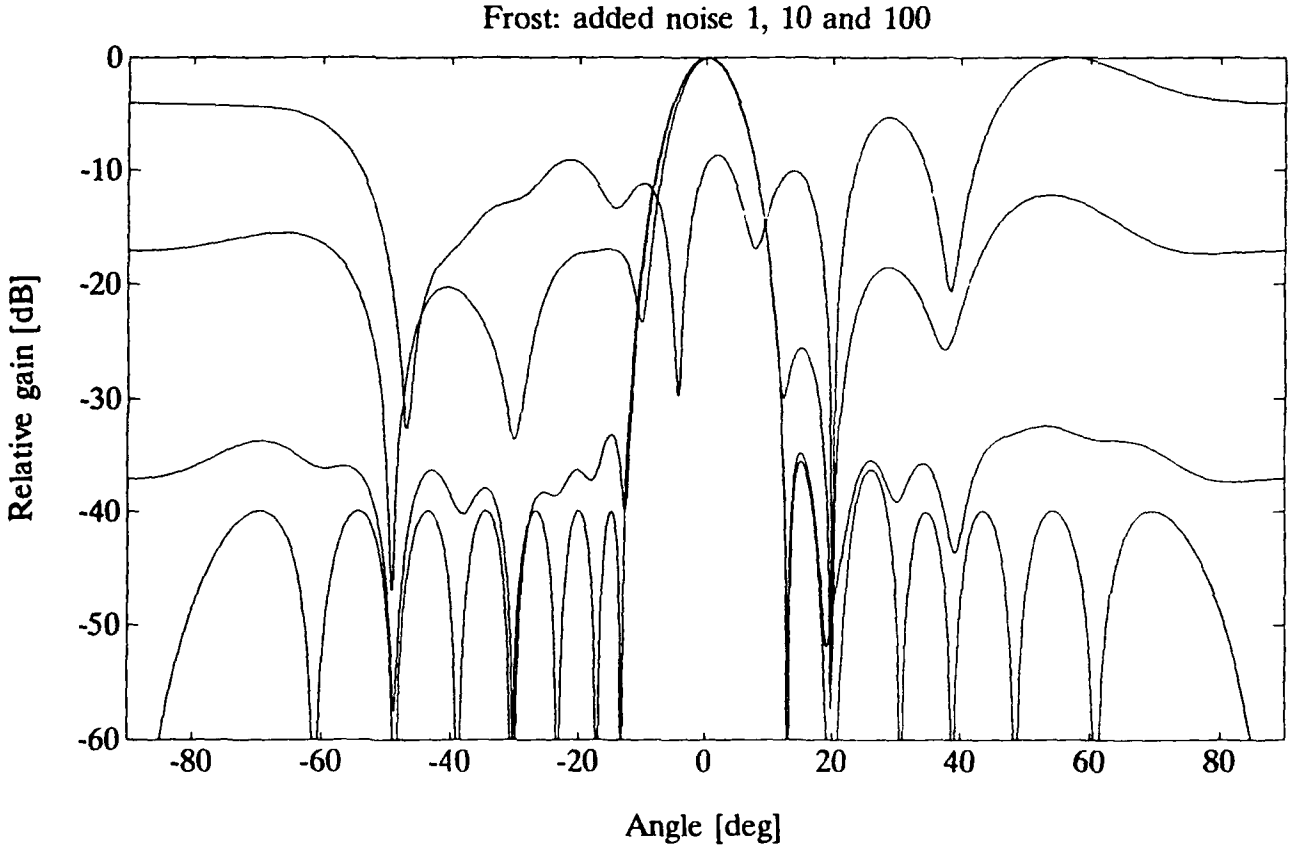

Figure 26. Patterns for Configuration B, Using Frost's Algorithm. Asymptotic (K=∞) and K = 32 with added artificial noise $\sigma_{an}^2 = \sigma^2$, $10\sigma^2$, and $100^2\sigma$.

In Eq. (8.32), $\mathbf{x}_{d\|}$ and $\mathbf{n}_{\|j}$ are the parts of $\mathbf{x}_d$ and $\mathbf{x}_n$ being correlated with $\mathbf{x}_j$. They have expected magnitudes $|\mathbf{x}_{d\|}|=\sqrt{P_d/K}$ and $|\mathbf{n}_{\|j}|=\sigma\sqrt{N/K}$, where $\mathbf{x}_{d\perp}$ is the rest of $\mathbf{x}_d$, being approximately equal to $\mathbf{x}_d$, and where $\mathbf{n}_{\|d}$ is the thermal noise which is correlated with $\mathbf{x}_d$ but not with $\mathbf{x}_j$, being approximately equal to $\mathbf{n}_{\|}$ in Eq. (8.20). The total jammer vector $\mathbf{x}_{Kj}$ is now uncorrelated with the total signal vector, $\mathbf{x}_{Kd}$, and with the noise vector $\mathbf{n}_{\perp}$. The total signal vector $\mathbf{x}_{Kd}$ is also parallel to the true signal vector $\mathbf{x}_d$ with essentially the same magnitude. Assuming that the total jammer vector $\mathbf{x}_{Kj}$ has been completely nullified, the null depth in the true jammer direction $\hat{\mathbf{x}}_j$ relative to the gain in the desired signal direction is obtained by projecting the vector $(\mathbf{x}_{d\|}+\mathbf{n}_{\|j})/|\mathbf{x}_{Kj}|$ onto the w vector. Assuming that $\mathbf{n}_{\|j}$ is a random vector in element space and that $P_j \gg P_d$, the expected result is:

$$\text{Null depth} = \frac{G(\theta_j)}{G(\theta_d)} = \frac{1}{KP_j}\left[\frac{^2\sigma}{\eta(\theta_d)} + P_d\right] \tag{8.33}$$

where $\eta(\theta_d)$ is the aperture efficiency, obtained from Eq. (8.28) or (8.29). The null depth will have a standard deviation approximately equal to the expected value itself. The null depth obtained from Eq. (8.33) and from several simulations is illustrated in Figure 32.

In the simulations in Figure 26 the null depths were -55, -49 and -49 dB respectively while Eq. (8.33) gives -45 dB.

When the error induced sidelobes have been reduced to a small value by using the artificial noise method or steering vector projection discussed below, the expected SNIR is, as for Applebaum's algorithm, decreased from its asymptotic value mainly by the decreased null depths. Using Eq. (8.33) for the null depth we get for one jammer:

$$\text{SNIR}_{\text{exp}} = \text{SNIR}_{\text{asym}} \frac{K}{(K+1)\eta_0/\eta + \text{SNIR}_{\text{asym}}} \tag{8.34}$$

where η_0 is the asymptotic aperture efficiency and η is the true aperture efficiency obtained from Eq. (8.29). This is illustrated in Figure 33 together with simulated results.

8.6 Effects of Steering Vector Projection

Since the problem with the high sidelobes in the Frost algorithm is that, due to the correlation between the signal and noise samples, the steering vector has noise eigenvector components, the steering vector projection, Eq. (2.41), as used for some other error types may be used here too. The sidelobes will then be similar to those of the Applebaum algorithm using a steering vector with small errors. The steering vector components in each of the noise eigenvectors is random with an expected RMS value of $\sigma/\sqrt{KP_d}$. The total mean square error in s_d after the projection will then be:

$$\langle \Delta^2 \rangle = \sigma^2 \frac{N-M}{KP_d} \approx \sigma^2 \frac{N}{KP_d} = \frac{\sigma^2}{KP_d} \tag{8.35}$$

where M is the number of signal eigenvectors. The resulting sidelobe level contribution for small errors is then:

$$\text{Sidelobe level} = \frac{\sigma^2}{K P_d \eta_A} \tag{8.36}$$

or σ^2/P_d times that of the basic Applebaum algorithm, Eq. (8.12). The gain and aperture efficiency is now given by Eq. (A.2):

$$G(\theta_d) = N\eta(\theta_d) = N\eta_0(\theta_d) \frac{1 + \dfrac{\sigma^2}{KP_d \eta_0(\theta_d)}}{1 + \dfrac{N\sigma^2}{KP_d}} \tag{8.37}$$

while the null depth is still given by Eq. (8.33) and the SNIR by Eq. (8.34).

Figure 27 shows adapted patterns for Frost's algorithm, configuration A, using K=32 samples. The weights have been calculated from a direct inverse of the sampled covariance matrix, Eq. (2.6), by using a projected steering vector, Eq. (2.41), and by using the asymptotic covariance matrix. As seen, the pattern for the direct covariance matrix inversion is very bad while the pattern obtained when using the

projected steering vector is much better. The sidelobe level using Eq. (8.36) is -37 dB. The null depth is only at -49 dB in this example while Eq. (8.33) gives -45 dB.

In Figure 28 this steering vector projection has been combined with the modification of the covariance matrix, Section 4, to get the Chebyshev quiescent pattern of configuration B. Thus first the noise space components have been eliminated from the steering vector, Eq. (2.41). Then the noise eigenvalues have been set to σ^2, Eq. (2.39), as in Figure 24 for the Applebaum case, and the corrected covariance matrix has been obtained using Eq. (2.31). A modified covariance matrix is then formed by modifying the diagonal elements as in Eq. (4.2) with $\sigma^2_{art} = \sigma^2$. Finally the weights are obtained from a direct inversion of this matrix, Eq. (2.2). The expected sidelobe level from Eq. (8.36) is -36 dB and the null depth, Eq. (8.33), is the same as in Figure 27, -45 dB. Also shown are the pattern for Applebaum's algorithm, as in Figure 24, the asymptotic Frost pattern and the Frost pattern obtained when only modifying the covariance matrix, Eq. (4.2).

This method may also be used when there are amplitude and phase errors. Figure 29 shows the same type of pattern as Figure 28 (except the direct inversion pattern) when there are 0.3 dB and 2° RMS errors present.

8.7 Pattern Parameters Versus the Number of Samples

Figures 30 to 33 show simulated and calculated results for the signal direction aperture efficiency $\eta(\theta_d)$, the average sidelobe level, the null depth, and the resulting SNIR respectively for basic configuration B. All simulated curves are averages over 100 simulations. The solid lines are the simulated results while the dashed are the calculated curves for Applebaum's algorithm and the dash-dotted the calculated for Frost's algorithm. The figures shows results when using direct inversion of the covariance matrix, when using artificial added noise, $\sigma^2_{art}=10\ \sigma^2$, and when using noise eigenvalue modification, including steering vector projection in the Frost case.

The curves are denoted with an *A* or a *F* for the Applebaum and Frost algorithms respectively. The direct inversion method is indicated by a *d*, *n* indicates the artificial noise method, *m* indicates the noise eigenvalue modification in the Applebaum algorithm and *pm* indicates the projected steering vector and noise

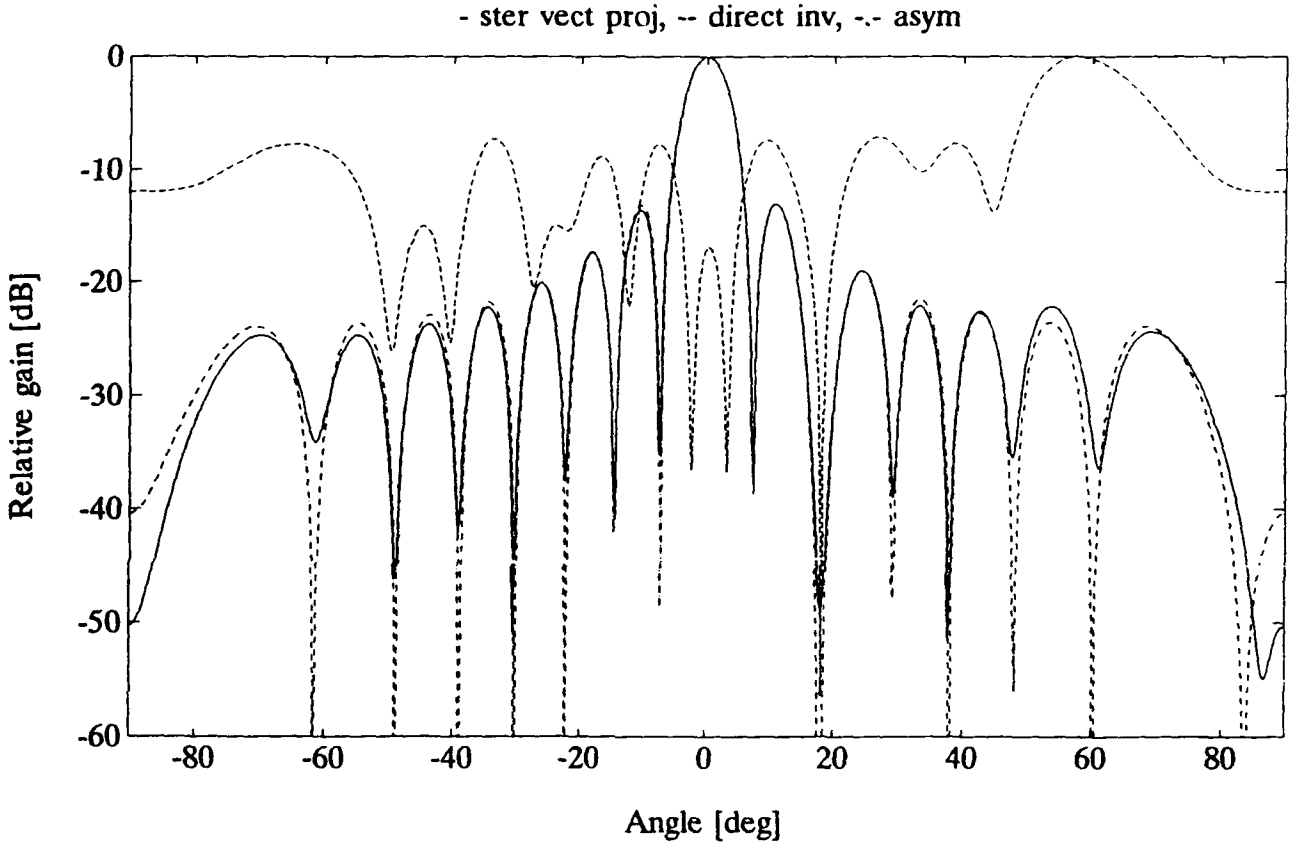

Figure 27. Patterns for Configuration A, Using Frost's Algorithm, K=32. - - - - direct inverse of the sampled covariance matrix, ——— projected steering vector, ------ asymptotic pattern.

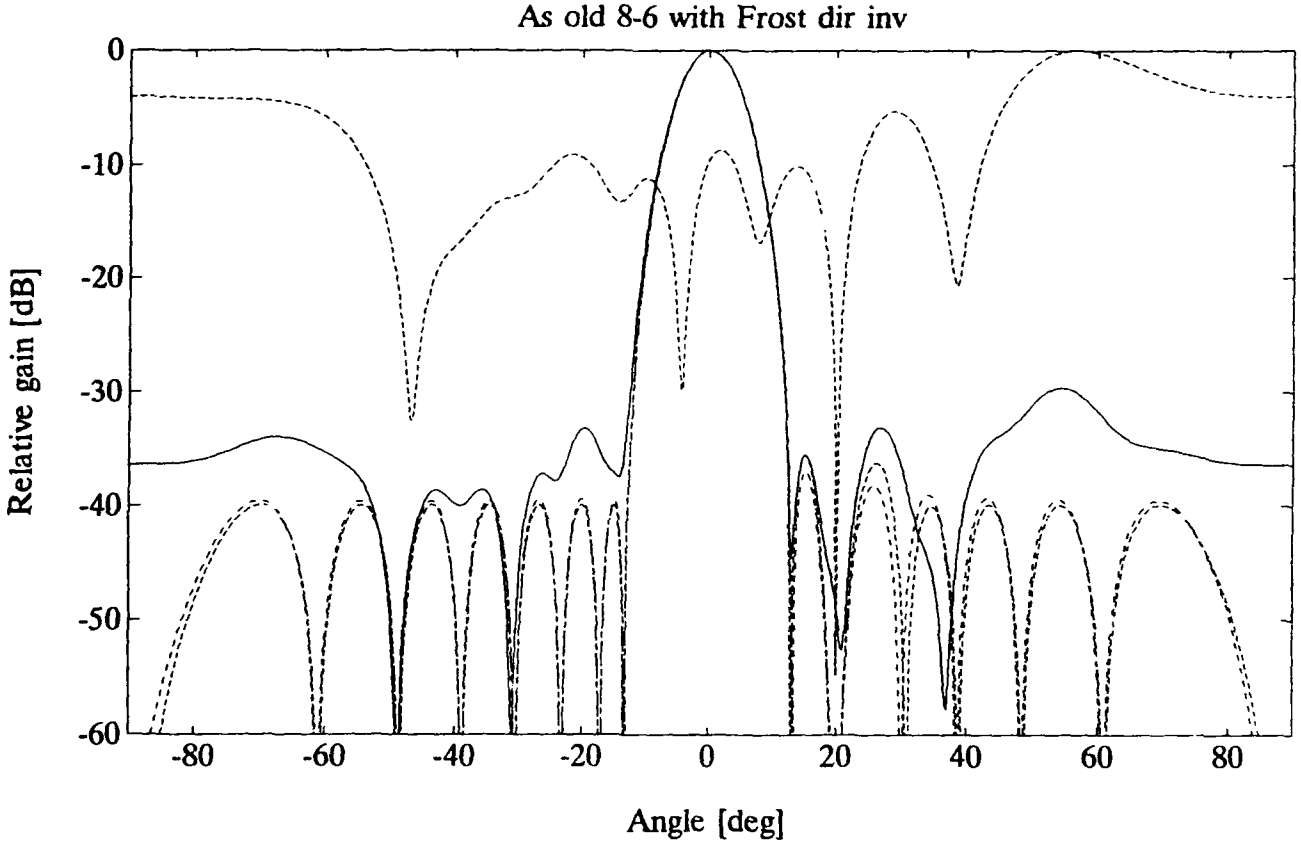

Figure 28. Configuration B, K=32. —— Frost, covariance matrix and steering vector modified, - - - (upper) Frost, direct inversion of modified covariance matrix, - - - (lower) Frost, K=∞, ····· Applebaum, as in Figure 24.

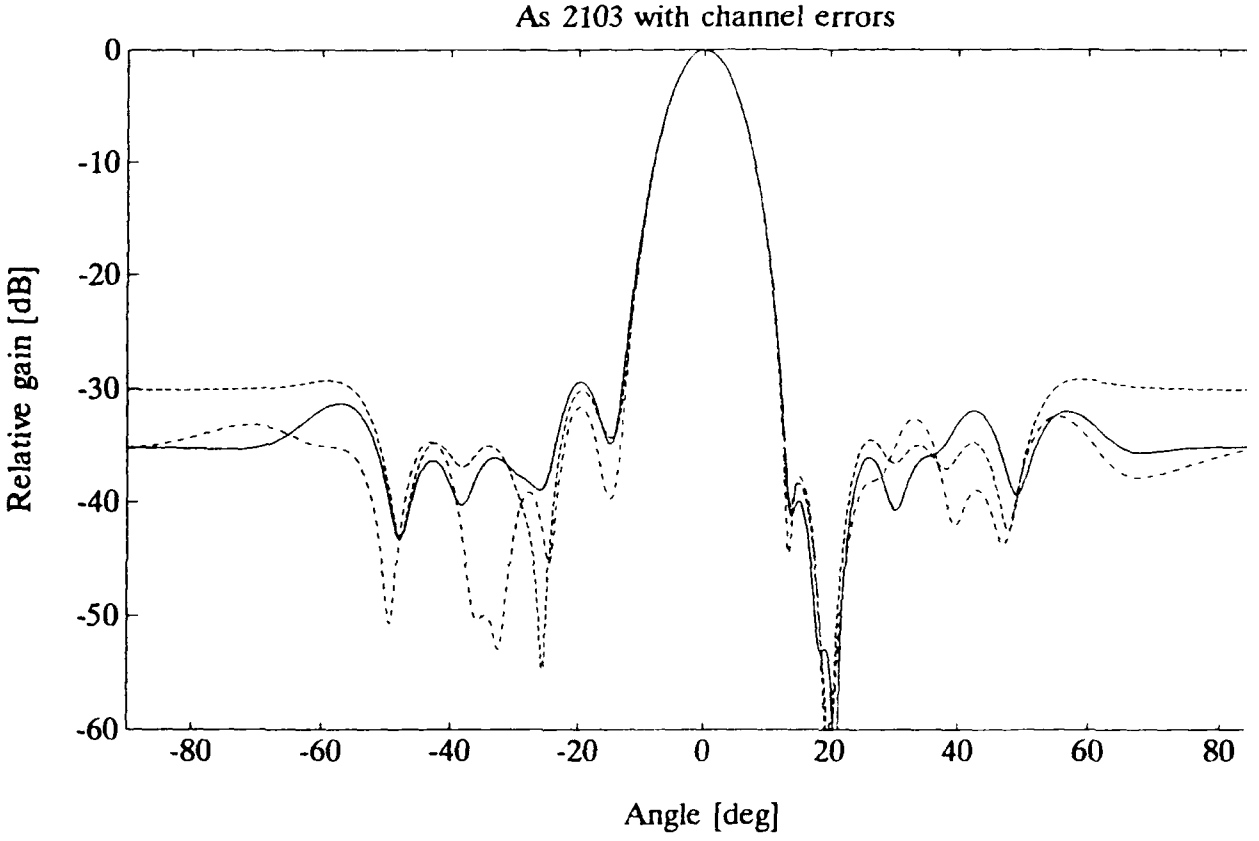

Figure 29. Configuration B. K=32. Same type of patterns as in Figure 28 (except the direct inversion pattern) with 0.3 dB and 2° RMS errors.

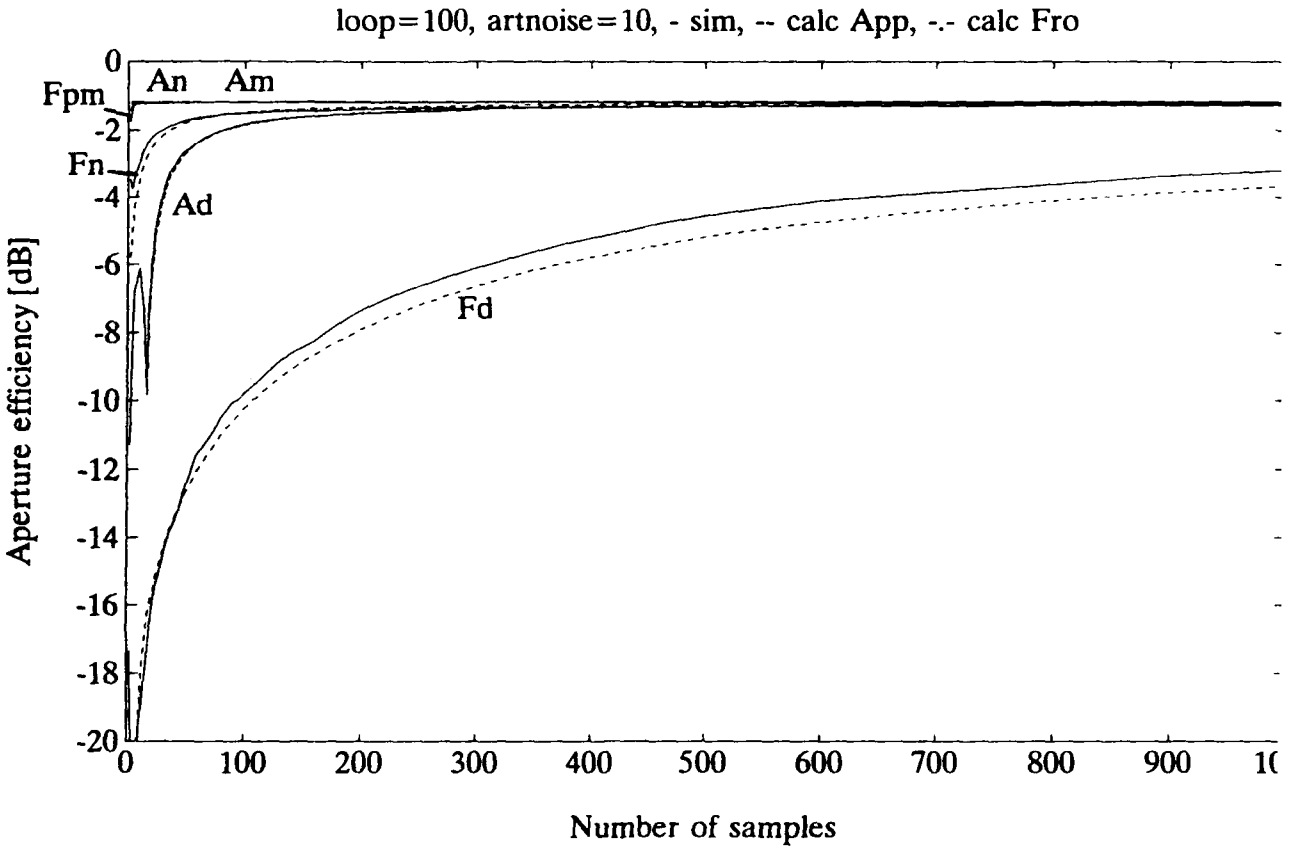

Figure 30. Simulated and Calculated Aperture Efficiency for Config ration B as Functions of the Number of Samples. See text. ——— simulations, - - - Applebaum, -·-·- Frost

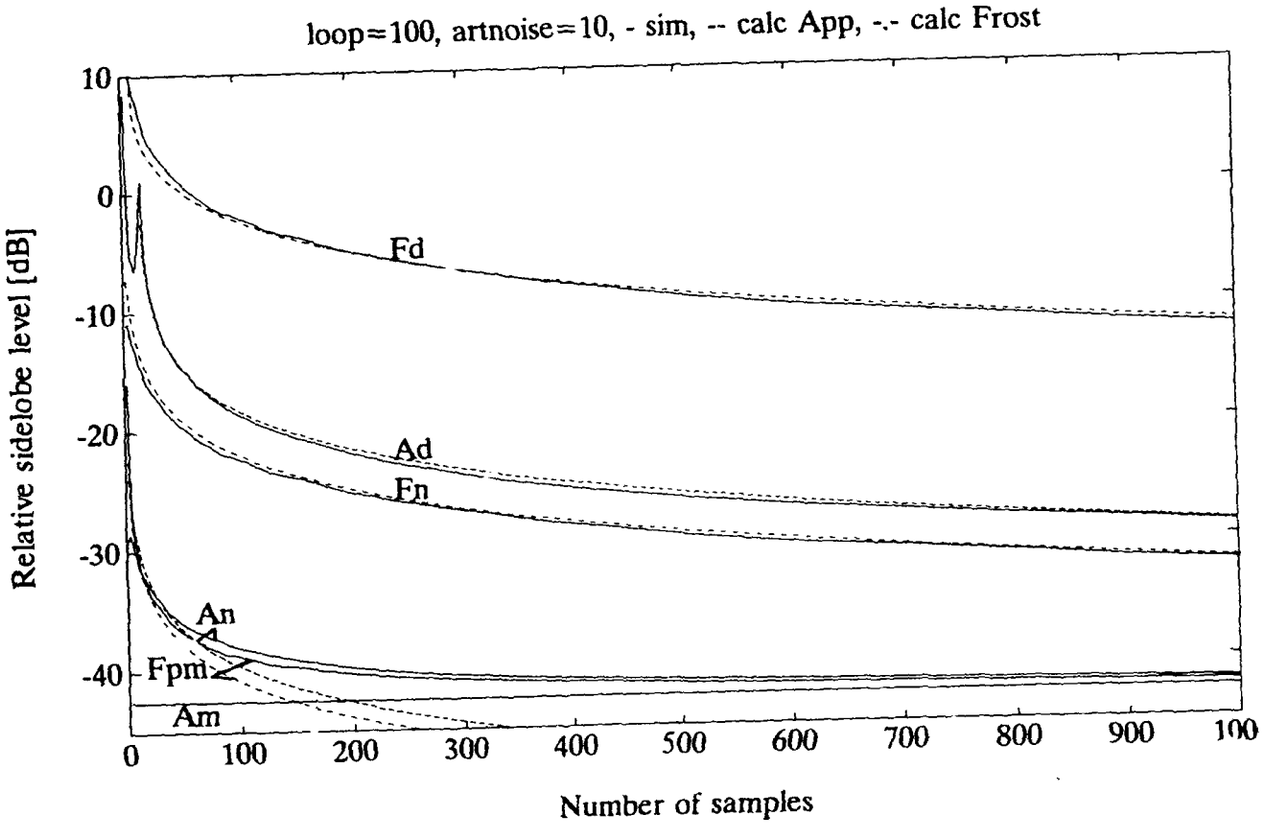

Figure 31. Simulated and Calculated Sidelobe Level for Configuration B as Functions of the Number of Samples. See text. ——— simulations, - - - Applebaum, ····· Frost

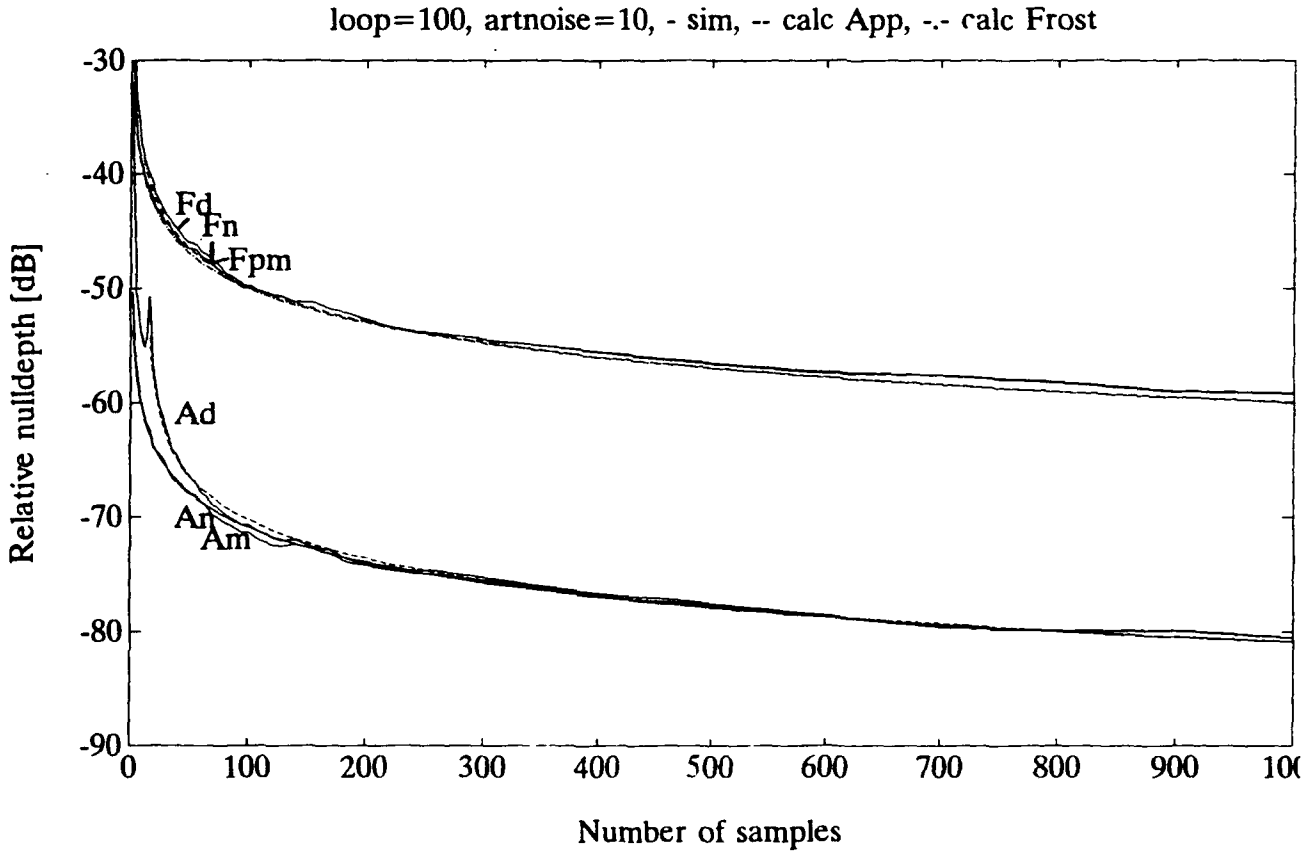

Figure 32. Simulated and Calculated Null Depth for Configuration B as Functions of the Number of Samples. See text. ——— simulations, - - - Applebaum, -·-·- Frost

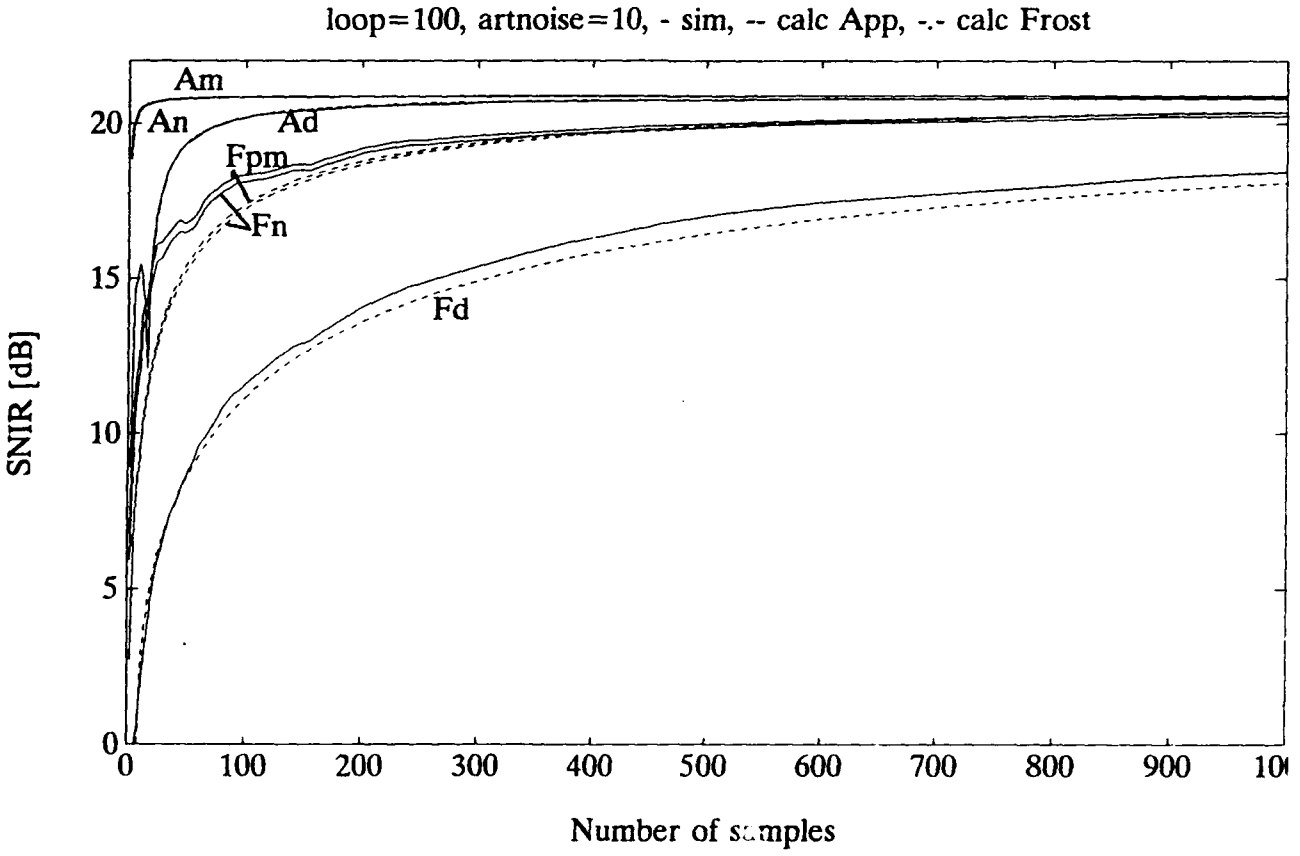

Figure 33. Simulated and Calculated SNIR for Configuration B as Functions of the Number of Samples. See text. ——— simulations, - - - Applebaum, -·-·- Frost

eigenvalue modification in the Frost algorithm. (In some cases it may be difficult to see the calculated curves since they are so close to the simulated curves.)

Since the sampled covariance matrix is singular for $K < N$ the basic Eq. (2.2) cannot be used in this case. If the modification of the Frost covariance matrix, Eq. (4.2), is used, this matrix will not be singular. In the Applebaum direct inversion curve a pseudoinverse has been used in this case. This is equivalent to using a partial steering vector projection method where the steering vector is projected on the "non-zero eigenvalue subspace". This is probably the the reason for the bump in the efficiency and SNIR curves below K=16 samples.

In the efficiency curves, Figure 30, the calculated curves are obtained using Eqs. (8.15) and (8.13) for the Applebaum case (except for the eigenvalue modification case where the gain is very close to the asymptotic value) and Eq. (8.29), and (8.37) for the Frost case. The agreement is very good except for the Frost, direct inversion curve where the calculated is slightly lower than the simulated. Here the relative variance of the denominator, Eq. (8.29) is rather large so that taking the ratio of the expectation values of the numerator and the denominator will give some errors. In fact, taking the inverse of the average of the inverse efficiency, $1/\langle 1/\eta \rangle$, gives a better agreement with the calculated result.

In the sidelobe curves, Figure 31, the calculated curves are obtained from Eqs. (8.13), (8.14) and (A.5) for the Applebaum case (except for the eigenvalue modification case where the sampling induced sidelobes are very small) and Eqs. (8.30), (8.14), (8.19), (8.31) and (A.7) for the Frost case together with the calculated efficiency above. The simulated curves show the total average sidelobe levels of the pattern outside $\theta = \pm 17.5^{\circ}$, including the regular sidelobes and nulls. The simulated results will thus go asymptotically to approximately -43 dB. The calculated results on the other hand only include the sampling induced effects.

In the null depth curves shown in Figure 32, the calculated curves are obtained from Eq. (8.23) for the Applebaum case and Eq. (8.33) for the Frost case together with the calculated efficiency above. The simulated and calculated curves are in general in very good agreement. It should be remembered that the standard deviation in each of the 100 simulations are equal to the expected value so that the standard deviation of the average is about 0.4 dB.

The SNIR results are shown in Figure 33. Here the calculated results are obtained from Eqs. (8.3), (8.24), (8.15) and (8.13) for Applebaum's case and Eqs. (8.34), (8.29) and (8.37) for the Frost case. Since the resulting aperture efficiency is the most important parameter for the direct inversion cases the agreement is also similar in these cases. For the artificial noise, projected steering vector, and modified noise eigenvector cases, the aperture efficiency is high and the SNIR is determined mainly by the null depths. The agreement between the simulated and the calculated curves for the Applebaum algorithm, using these methods, is very good while the simulated Frost results are slightly higher than the calculated result for few samples. This is again probably mainly an effect of the approximation of taking the ratio of the expectation values. As seen from Figures 30 and 32 both the gain and null depths are well approximated with these methods.

9. SIGNAL QUANTIZATION

If the ratio of the quantization step in the A/D converters (q) to noise RMS voltage (σ_v) is not too large the errors due to signal quantization will be random and uncorrelated between the channels (see Figures 8 and 9 in Reference 13). This will then simply increase the equivalent noise level of $q^2/12$ so that, with $q = \sigma_v$ which is often used, the results with $q = 0$ are applicable if we put $\sigma^2_{equiv} = \frac{13}{12}\sigma^2$ (0.35 dB noise increase).

Figure 34 shows two simulated patterns with $q = 0$ and $q = \sigma_v$ for configuration A, using $K = 1024$ samples, which are very similar. In these simulations the difference in the resulting SNIR was 0.3 dB and the null depths were -88 and -85 dB respectively while Eq. (8.23) gives -82 dB in both cases.

The small quantization steps (one q-step in one I or Q channel), which are present in the total signal at each time sample, has an amplitude of $\sqrt{6/N}$ times the quantization noise RMS value or $\sqrt{6/(13N)}$ the total noise RMS amplitude when $q = \sigma_v$. When many samples are averaged these small steps will disappear.

10. WEIGHT QUANTIZATION

We assume here that the weights are calculated correctly using a correct covariance matrix but that the beamformer can only use the first b bits of these weights. There is one sign bit and the least significant bit = $2^{-(b-1)}$. These rounded weights will not really be the optimal b-bit weights. For ordinary non-adaptive arrays the corresponding average sidelobe level contribution is:

$$\text{Sidelobe level} = \frac{2}{3}\,\frac{2^{-2b}}{N\langle w^2\rangle\eta} \tag{10.1}$$

where $\langle w^2\rangle$ is the mean square of the weights and η_A is the aperture efficiency. As the effects of the rounding were not considered in the weight calculation we can expect the effects in an adaptive array to be similar, including the null depths. Like the finite null depth due to sampling in Section 8, the null depth contribution in Eq. (10.1) will have a standard deviation equal to the expectation value itself.

Figure 35 shows radiation patterns for the Chebyshev standard configuration B, using 6, 8, 10 and 12 bits plus the pattern without quantization. It is seen that most patterns (except for 6 bits) are very similar except at the null at 20°. However in this example, the weights with 6 bits are identical with the 6-bit quiescent weights. The null depth for the 8, 10, and 12 bits are here equal to -67, -71, and -74 dB, to be compared with -144 dB for the pattern without quantization, and with the -57, -69, and -81 dB average level from Eq. (10.1).

If we have maximum bad luck however, all weights will have their maximum quantization error, one half quantization step, adding coherently in a jammer direction. The maximum sidelobe contribution due to this is equal to $6N$ times the average level given by Eq. (10.1), or approximately 20 dB above the average level in this example.

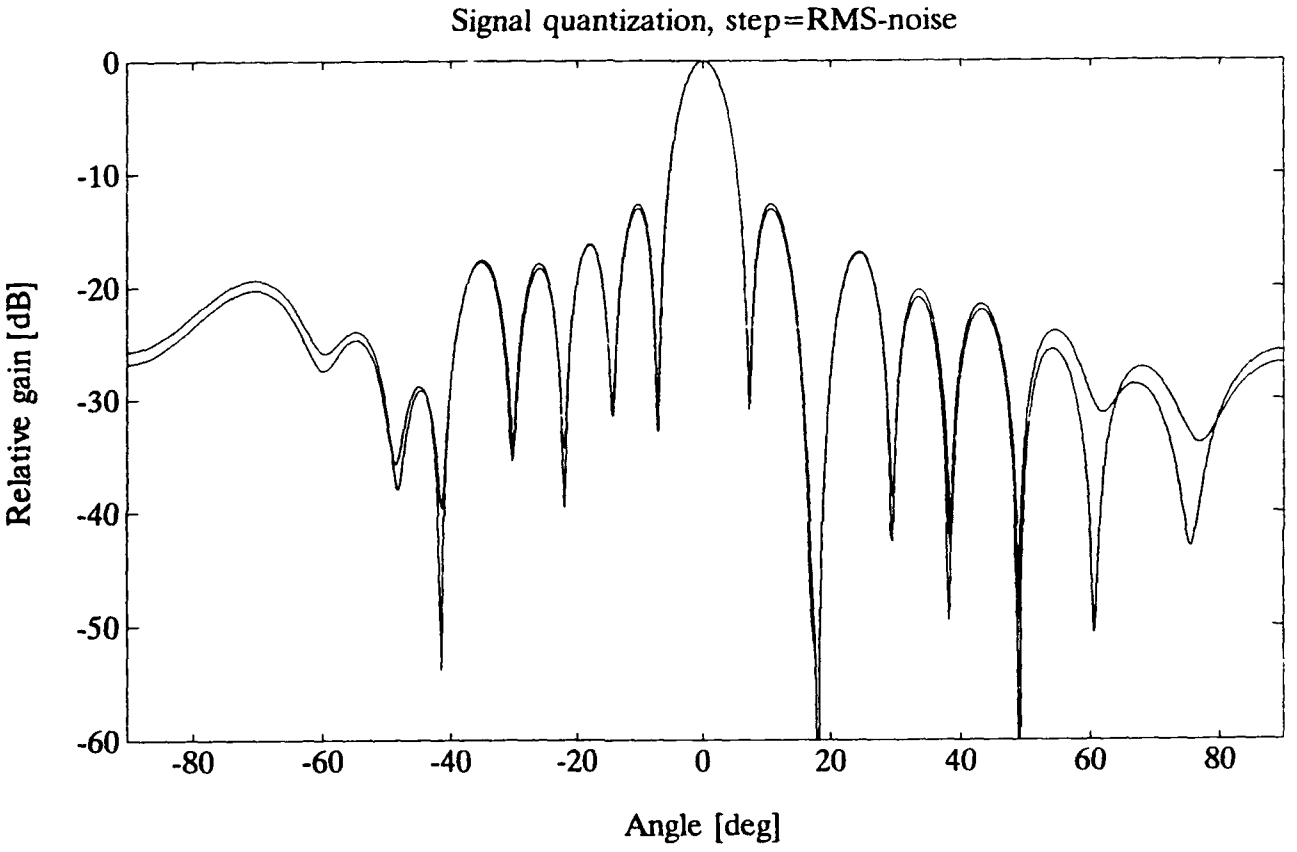

Figure 34. Simulated Patterns for Configuration A, K=1024. Effect of signal quantization, $q = 0$ and $q = \sigma_v$.

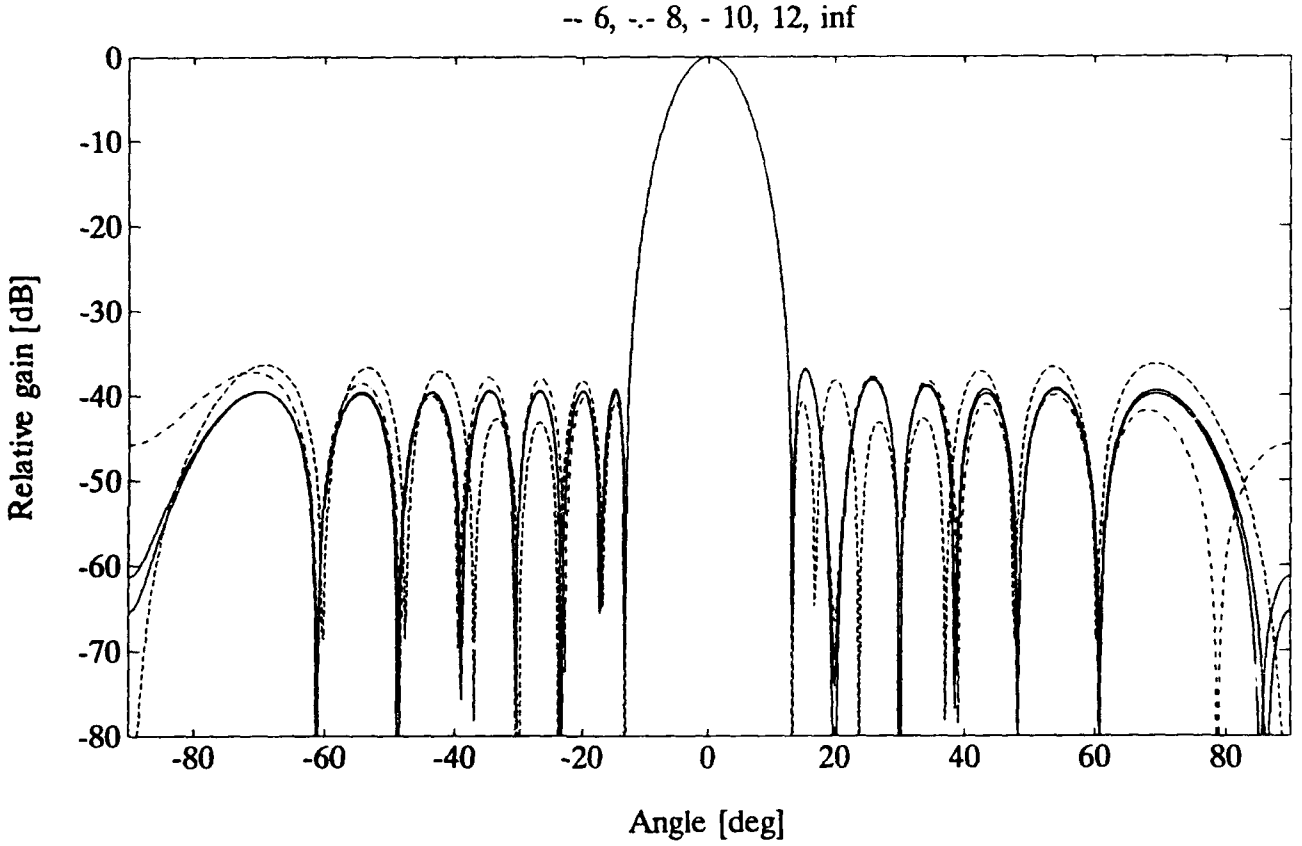

Figure 35. Effects of Weight Quantization on the Patterns. Configuration B; number of bits = 6, 8, 10, 12, and ∞. (The two last patterns are coincident in the plot except at the null.)

11. SATURATION

For strong input signals the receiving system becomes nonlinear. Here only the effects of this nonlinearity on the adaptive process will be considered. Generally, a nonlinearity will generate new frequency components (intermodulation products) of the type $f = nf_1 + mf_2$, where f_1 and f_2 are two input frequency components. Usually the components with $n = 1$, $m = 2$ and $n = 2$, $m = 1$ are the most important since they often are within the signal bandwidth. For the low frequency circuits, where the relative bandwidth is large, and for the A/D converters, after which there is no or little filtering but a possible folding into the signal frequency band, the components (harmonics) with n or $m = 0$ may also be important.

If the nonlinearity is before the splitting of the I and Q components the output signal, including harmonics, will be:

$$a_c = a_I + ja_Q = a_1\exp(j\omega t+\varphi) + a_3\exp(3(j\omega t+\varphi)) + a_5\exp(5(j\omega t+\varphi))+... \qquad (11.1)$$

where it has been assumed that the nonlinearities are symmetrical so that only the odd frequency components are generated. All a_i are nonlinear functions of input power. For not too high input power the power in the $n\omega$-component will be proportional to (input power)^n. When $m \neq 0$ the result will be similar. As the relative phases in the channels for the intermodulation products are different from those of the input frequencies, these signals will appear to come from different directions.

If the nonlinearity is after the splitting of the I and Q components, for example as a limited dynamic range of the I and Q A/D converters, all harmonics in the Q channel are delayed 1/4 period of the basic frequency component so that the extra 90° phase shift will also get multiplied with n. This is equivalent to a change in sign for the frequency components n = 3, 7, 11, 15 etc., giving the output signal:

$$a_c = a_I + ja_Q = a_1\exp(j\omega t+\varphi) + a_3\exp(-3(j\omega t+\varphi)) + a_5\exp(5(j\omega t+\varphi))+... \qquad (11.2)$$

If the I and Q channels are not identical, both the positive and negative frequency components must be used, as in Section 6 where the component $n = -1$ was generated. That is also true if the nonlinearity is nonsymmetric so that even frequency components are also generated. The IQ errors in Section 6 have much in common with the saturation effects, the main difference being the number of harmonics and signal power dependence.

If the nonlinearities are to have negligible influence on the adaptive process the total power in the new frequencies should not be higher than the noise power. For a Gaussian distributed noise jammer this means that the average jammer power per channel should not be larger than about 11 dB below the saturation level for 10 bit converters with a quantization step equal to the noise RMS voltage ($q = \sigma_v$), and about 15 dB below for 18 bit converters, provided that the the jammer is really Gaussian distributed far out in the tail of the distribution, which could be questioned. For CW jammers the power limit is more distinct; the power should be below the saturation level.

As an example, Figure 36 shows simulated radiation patterns for three different jammer input power levels for basic configuration A. The covariance matrix has been estimated from $K = 4096$ samples, corresponding to an RMS sidelobe level of -36 dB from Eq.(8.12).

It is assumed that all channels are identical. Radiation pattern means the pattern that the calculated weights will produce in a linear system. This is also equal to the radiation pattern of the basic signal component, when the dynamic ranges of the channels are identical. For identical channels the other induced frequency components will have similar patterns, shifted in angle. The nonlinearities are assumed to be lumped in the two 12 bit I and Q A/D converters. The quantization step is equal to noise RMS voltage ($q = \sigma_v$) so that, for a CW jammer, saturation begins at a jammer to noise ratio per channel of JNR = 63 dB. The saturation is assumed to be of a hard limit type, so that the output is linear up to the saturation level and constant above this limit. Patterns are shown for a Gaussian noise jammer with a jammer to noise ratio per channel of JNR = 53 dB, where there were no saturated samples at all, for JNR = 58 dB, where the nonlinearities has started to show up, and for JNR = 70 dB. When the jammer is at θ_j, 18° here,

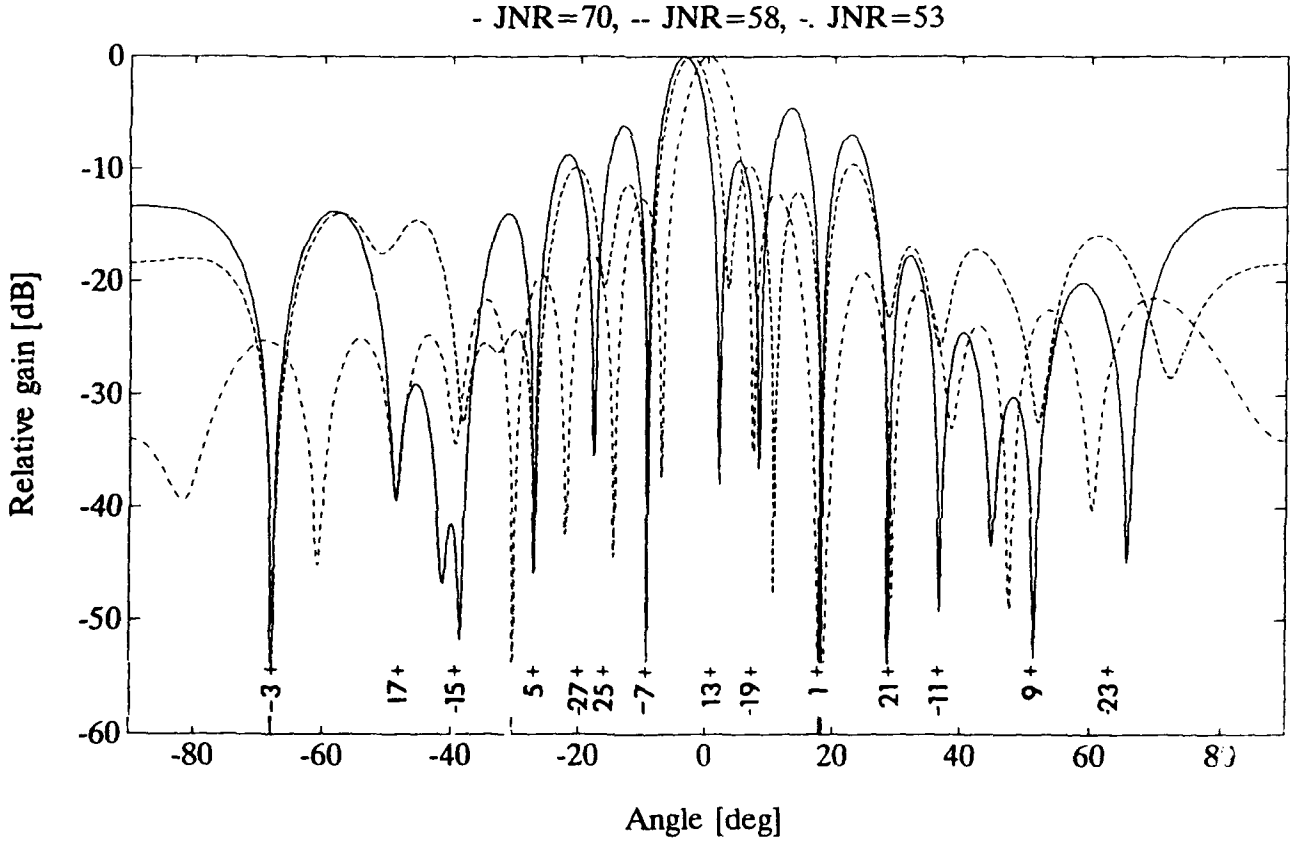

Figure 36. Saturated Patterns, Configuration A, Applebaum's Algorithm, K = 4096 samples: ——— JNR = 70 dB, - - - JNR = 58 dB, ····· JNR = 55 dB. The + marked numbers denote harmonic number from Eq.(11.3).

the equivalent directions, θ_n, of the nth harmonic can, for half wavelength element spacing, be found from (k is an integer to make θ_n real):

$$\sin \theta_n = n \sin \theta_j + 2k \tag{11.3}$$

If the channels have large errors that are corrected for, these corrections will leave the harmonics uncorrelated between the channels. These harmonics will then not give any deep nulls but an increased average sidelobe level, as in Eq. (2.17). The resulting SNIR will however be approximately equal to that for identical channels.

The directions obtained from Eq. (11.3) are indicated in the figure and it is seen that they correspond to nulls in the JNR = 70 dB pattern for quite high values of the harmonic number n. This shows how the adaptive process will try to eliminate all relevant signals to get a high total SNIR. This will of course cost some degrees of freedom, which may be important, especially for an antenna with few elements. In this example with N = 16 elements and one jammer the antenna would be able to null out harmonics up to n = 29. As the power for higher n may still be quite high compared to the noise (for very high power the saturated signal will become a square wave and the power in the harmonics will go as $1/n^2$) there will be some residual jammer power decreasing the SNIR. Of course, the algorithm does not eliminate the lowest order harmonics, leaving the other harmonics unaffected, but will affect all harmonics to give the lowest total SNIR. For the three different jammer powers in this example the deviations of the resulting SNIR from the asymptotic nonsaturated values were 0.3, 9.5, and 32.1 dB respectively. These numbers are for one particular statistical outcome of the simulations; the numbers vary somewhat between different simulations, in particular for the JNR = 58 dB case where there are relatively few saturated samples. The SNIRs here are the maximized SNIR obtained from Eq. (8.1) and not the asymptotic SNIR or the expected SNIR using the calculated weights. The difference for K = 4096 samples is very small, however.

For larger antennas more harmonics can be suppressed. The deviations from the asymptotic nonsaturated cases in simulations with N = 16, 32, 64, and 128 elements and JNR = 70 dB were equal to 32.1, 22.3, 6.7 and 0.8 dB respectively.

There is also a possibility that, as for n=13 in this example, a jammer outside the main beam will generate a frequency component with an equivalent direction within the main beam, which may have serious effect on the SNIR and main beam shape.

When the desired signal is present during the adaptation, as in Frost's algorithm, the corresponding intermodulation products will also be considered as new uncorrelated jammers by the adaptive process.

One possible method to improve the pattern and the SNIR would be to use only the nonsaturated signal vectors when forming the covariance matrix. This assumes of course that the same is also done for the total output signal from the antenna. Hence much of the information in the desired signal may be lost. Using only nonsaturated signal vectors in the JNR = 70 dB case would cause only about 20 percent of the samples to be used. Even fewer samples would be used for a saturated CW jammer.

For less hard saturations, without any knee in the transfer function, the magnitudes of the higher order harmonics will be smaller. These less hard saturations are more realistic for amplifiers and mixers. A non-linear transfer function of the type:

$$V_{out} = \frac{V_{in}}{\left[1 + (V_{in}/V_{max})^{p}\right]^{1/p}} \tag{11.4}$$

has also been used in the simulations ($p = \infty$ corresponds to the hard limit case). When p = 6 the compression at $V_{in} = V_{max}$ is 1 dB. For N = 16 and JNR = 70 dB the deviations of the resulting SNIR from the asymptotic nonsaturated value were for p = 6, 12, and 24 equal to 18.2, 25.7, and 29.7 dB respectively, to be compared with 32.1 dB for the hard limit case.

12. CONCLUSIONS

The effect of various imperfections on the pattern of adaptive arrays has been investigated. The algorithms considered were Applebaum's "Maximum signal to interference plus noise ratio" and Frost's "Constrained power minimization". In these algorithms there are no explicit constraints or requirements on the sidelobe

levels included and hence some types of array imperfections can cause severe degradation, in particular in Frost's algorithm where the desired signal is directly included in the adaptive process.

Three types of solutions to these problems have been discussed: to make the errors small enough or to compensate for them when they are known; to reduce their influence by adding artificial noise; and to use some a priori knowledge about the covariance matrix and its eigenvalue spectrum. In many cases, where the error is due to an incorrectly estimated covariance matrix or steering vector, the methods discussed will also improve the SNIR.

It may also be desirable to modify the correct covariance matrix slightly to obtain some desirable pattern properties at a very low cost in terms of resulting SNIR as discussed in Sections 3 and 4.

One type of error occurs when the steering vector used is not optimally chosen. This is the case for the amplitude and phase errors in Section 5 and for the IQ errors in Section 6, when the signal video frequency $\omega_d = 0$. The Frost algorithm is most affected by steering vector errors because some of the desired signal, which does not match the steering vector, is considered as a coherent jammer by the process. These errors can in principle be measured and corrected for. Alternatively, they can be partly corrected for by decreasing the importance of the desired signal by adding artificial noise or by using a priori knowledge about the noise eigenvalues and signal subspace eigenvectors.

Another type of imperfection is that some additional jammer signals may be created internally in the array. This is the case for the IQ errors in Section 6, when the video frequency $\omega \neq 0$, for the DC offset errors in Section 7, and for the saturation effects in Section 11. The first two could be compensated for if they are known, while the last one should be kept small by having sufficiently large dynamic range in the receiver modules and A/D converters, or by rejecting saturated samples.

A third error type is due to quantization of the signals, discussed in Section 9, and quantization of the calculated weights, discussed in Section 10. The first will give an additional equivalent noise contribution while the second will limit the obtainable null depth. The latter may be very serious and a sufficient number of bits is necessary.

If the noise covariance matrix is not an identity matrix, as is usually assumed, large effects on the pattern may result as discussed in Section 3. Forcing it to be equal, or close to, an identity matrix gives better sidelobes at the cost of a slightly lower SNIR.

As the covariance matrix can only be estimated by a time average it will have some errors. This problem is discussed in Section 8. In particular there will be apparent correlations between truly uncorrelated signals, including the noise. This type of error can also be partly corrected for by using a priori knowledge about the eigenvalue spectrum or by minimizing the relative errors by adding artificial noise.

References

1. Compton, R.T., (1988), *Adaptive Antennas*, Prentice Hall.
2. Hudson, J.E., (1981), *Adaptive Array Principles*, Peter Peregrinus.
3. Monzingo, R., and Miller, T., (1980), *Introduction to Adaptive Arrays*,John Wiley & Sons.
4. Applebaum, S.P., (1976), Adaptive arrays, *IEEE Trans. Antennas and Propagat.*, Sept., pp. 585-598.
5. Frost, O.L., (1972), An algorithm for linearly constrained adaptive processing, *Proc. IEEE*, Aug., pp. 926-935.
6. Schmidt, R., (1986), Multiple emitter location and signal parameter estimation, *IEEE Trans. Antennas and Propagat.*, March, pp. 276-280.
7. Gabriel, W.F., (1986), Using estimation techniques in adaptive processing antenna systems, *IEEE Trans. Antennas and Propagat.*, March, pp. 291-300.
8. Carlson, B.D., (1988), Covariance matrix estimation errors and diagonal loading in adaptive arrays, *IEEE Trans. Aerospace and Electronic Systems*, July pp. 397-401.
9. Steyskal, H., (1991), Array error effects in adaptive beamforming, *Microwave Journal*, Sept., pp. 101-112.
10. Bull, J.F., Arnao, M.A., and Burgess, L.R., (1990), Hypersensitivity effects in adaptive antenna arrays, *IEEE AP-S Symposium*, pp. 396-399.
11. Widrow, B., Duvall, K.M., Gooch, R.P., and Newman, W.C., (1982), Signal cancellation phenomena in adaptive antennas: causes and cures, *IEEE Trans. Antennas and Propagat.*, May, pp. 469-478.

12. Steyskal, H., (1990), Array error effects in adaptive beamforming, JINA 90, *Conf. Proc.*, pp. 475-478.

13. Barton, P., (1980), Digital beamforming for radar, *IEE Proc.* Pt. F, Aug., pp. 266-277.

14. Churchill, F.E., Ogar, G.W., and Thompson, B.J.,(1981), The correction of I and Q errors in a coherent processor, *IEEE Trans. Aerospace and Electronic Systems* Jan., pp. 131-137.

15. Reed, I.S., Mallett, J.D., and Brennan, L.E., (1974), Rapid convergence in adaptive arrays, *IEEE Trans. Aerospace and Electronic Systems*, Nov., pp. 853-863.

Appendix

Error Induced Gain Loss and Sidelobes

For an array antenna the gain is, for isotropic element patterns, given by:

$$G(\theta) = \frac{\left|\sum_{i=1}^{N} w_i \exp(j\mathbf{k}\cdot\mathbf{r}_i)\right|^2}{\sum_{i=1}^{N} |w_i|^2} = N\cdot\eta_A(\theta) \qquad \text{(A.1)}$$

where the w_i are the total element weights, including possible gain and phase shift errors, $\mathbf{k}$ is the propagation vector and $\mathbf{r}_i$ is the element position vector. When the weights have random errors, the total weight vector $\mathbf{w}$ can be written as a sum of a vector $\mathbf{w}_0$, parallel to the error free weight vector, and a vector $\Delta\mathbf{w}$, uncorrelated with the error free weight vector so that $\mathbf{w} = \mathbf{w}_0+\Delta\mathbf{w}$ and $E\{\mathbf{w}_0^+\cdot\Delta\mathbf{w}\} = 0$. If we also assume that the weight errors, $\Delta\mathbf{w}$, are mutually uncorrelated, the expected gain in direction θ can be written as:

$$G(\theta) = N\eta(\theta) = \mathrm{E}\left\{ \frac{\left| \sum_{i=1}^{N} (w_{0i} + \Delta w_i) \exp(j\mathbf{k}\cdot\mathbf{r}_i) \right|^2}{\sum_{i=1}^{N} |w_{0i}|^2 + \sum_{i=1}^{N} |\Delta w_i|^2} \right\}$$

$$= \frac{N\cdot\eta_0(\theta) + \langle\Delta^2\rangle}{1 + \langle\Delta^2\rangle} \qquad \text{(A.2)}$$

where $\langle\Delta^2\rangle$ is the normalized mean square error:

$$\langle\Delta^2\rangle = \frac{|\Delta\mathbf{w}|^2}{|\mathbf{w}_0|^2} = \sum_{i=1}^{N} |\Delta w_i|^2 \Big/ \sum_{i=1}^{N} |w_{0i}|^2 \qquad \text{(A.3)}$$

and $\eta_0(\theta)$ is the error free aperture efficiency as a function of the angle θ. In Eq. (A.2) we have also approximated the expectation value of the ratio with the ratio of the expectation values. This will often give a result that is slightly too low.

For very large errors we can see from Eq. (A.2) that $G(\theta) \to 1$.

The expected, error induced, sidelobe level relative to the error free gain in the desired signal direction is thus:

$$\text{Sidelobe level} = \frac{\langle\Delta^2\rangle}{N\eta_0(\theta_d)\left[1 + \langle\Delta^2\rangle\right]} \qquad \text{(A.4)}$$

and the sidelobe level relative to the actual signal gain:

$$\text{Sidelobe level} = \frac{\langle\Delta^2\rangle}{N\eta_0(\theta_d) + \langle\Delta^2\rangle} \qquad \text{(A.5)}$$

When the errors are small, or if we know that the error weights Δw_i do not give any contribution in the main beam direction, we can use:

$$\text{Sidelobe level} = \frac{\langle\Delta^2\rangle}{N\eta_0(\theta_d)} \qquad \text{(A.6)}$$

Sometimes, such as when the weights will tend to partly cancel the desired signal in the Frost algorithm, the components in Δw are mutually correlated and Eq. (A.2) is valid only in the sidelobe region. The relative sidelobe level can still be found from Eq. (A.4) if $N\eta_0(\theta_d)$ is replaced with the actual gain, $G(\theta_d)$.

$$\text{Sidelobe level} = \frac{<\Delta^2>}{G(\theta_d)\left[1 + <\Delta^2>\right]} \tag{A.7}$$

If the antenna elements have an element gain factor, $g(\theta)$, this is simply inserted in the numerator of Eqs. (A.1) and (A.2) and in both the numerator and denominator of Eqs. (A.4) to (A.7).

MISSION

OF

ROME LABORATORY

Rome Laboratory plans and executes an interdisciplinary program in research, development, test, and technology transition in support of Air Force Command, Control, Communications and Intelligence (C^3I) activities for all Air Force platforms. It also executes selected acquisition programs in several areas of expertise. Technical and engineering support within areas of competence is provided to ESD Program Offices (POs) and other ESD elements to perform effective acquisition of C^3I systems. In addition, Rome Laboratory's technology supports other AFSC Product Divisions, the Air Force user community, and other DOD and non-DOD agencies. Rome Laboratory maintains technical competence and research programs in areas including, but not limited to, communications, command and control, battle management, intelligence information processing, computational sciences and software producibility, wide area surveillance/sensors, signal processing, solid state sciences, photonics, electromagnetic technology, superconductivity, and electronic reliability/maintainability and testability.